Old Dominion University
ODU Digital Commons

Spring 2018

Study of ABC Membrane Transporters in Single Live Cells

Preeyaporn Songkiatisak
Old Dominion University

STUDY OF ABC MEMBRANE TRANSPORTERS IN SINGLE LIVE CELLS

by

Preeyaporn Songkiatisak
B.S. March 2002, Chulalongkorn University, Thailand
M.S. December 2009, James Madison University

A Dissertation Submitted to the Faculty of
Old Dominion University in Partial Fulfillment of the
Requirements for the Degree of

DOCTOR OF PHILOSOPHY

BIOMEDICAL SCIENCES

OLD DOMINION UNIVERSITY
May 2018

Approved by:

Xiao-Hong Nancy Xu (Director)

James Lee (Member)

Christopher Osgood (Member)

Guijun Wang (Member)

ABSTRACT

STUDY OF ABC MEMBRANE TRANSPORTERS IN SINGLE LIVE CELLS

Preeyaporn Songkiatisak
Old Dominion University, 2018
Director: Dr. Xiao-Hong Nancy Xu

The multidrug ATP-binding cassette (ABC) membrane transporters (efflux pumps) are found in both prokaryotes and eukaryotes and they can extrude diverse structurally unrelated substrates, such as antibiotics and chemotherapeutic agents out of the cells. The efflux pumps are responsible for multidrug resistance (MDR) and the failure of numerous treatments in infections and cancers. All ABC membrane transporters share a common modular topology containing two transmembrane domains (TMDs) and two nucleotide binding domains (NBDs). The underlying molecular mechanisms regarding how the similar structural ABC membrane transporters could selectively extrude a wide variety of substrates and cause MDR, are not yet fully understood. Radioisotopes and fluorophores have been widely used as probes to study efflux kinetics of multidrug membrane transporters in bulk cells which could have masked interesting rare events from individual cells. Moreover, radioisotopes and fluorophores do not process size-dependent physicochemical properties, making them unsuitable to serve as various sized substrates for the study of efflux function of the ABC transporter. In this dissertation, we focus on the development of three different sized single silver nanoparticles (Ag NPs) to serve as both drug nanocarriers and imaging probes to study size-dependent efflux function of ABC membrane transporters in single live cells (e.g., *Escherichia coli*) *in situ* in real time. We synthesized and characterized Ag NPs with diameters of 2.4 ± 0.7, 13.0 ± 3.1, and 92.6 ± 4.4 nm, functionalized them with a monolayer of 11-amino-1-undecanethiol (AUT) to prepare AgMUNH$_2$ NPs (control nanocarriers). We then covalently linked the AgMUNH$_2$ NPs with ofloxacin (Oflx) to prepare AgMUNH-Oflx NPs (antibiotic drug nanocarriers) with conjugation ratios of 8.6x10^2, 9.4x10^3, and 6.5x10^5 Oflx molecules per NP, respectively. We studied inhibitory effects of these antibiotic drug nanocarriers against *E. coli* and found size-dependent inhibitory effects in which the same amount of Oflx carried by the

largest nanocarriers exhibited the highest inhibitory effects, and the smallest nanocarriers exhibited the lowest inhibitory effects. The AgMUNH$_2$ NPs did not show significant inhibitory effects on cell growth. Furthermore, we used Ag NP-based nanocarriers as imaging probes to study efflux function of multidrug ABC membrane transporters in single live *E. coli* cells, because Ag NPs process distinctive size-dependent photostable plasmonic optical properties. We found that the accumulation rates of nanocarriers highly depended on the NP concentration, the presence of ATPase pump inhibitor, and the types and sizes of nanocarriers. Interestingly, the ABC membrane transporters extrude AgMUNH-Oflx NPs more effectively and rapidly than AgMUNH$_2$ NPs indicating that efflux pumps could be equipped with a sensing machinery to detect, recognize and extrude toxic substrates (e.g., antibiotics). Notably, the cells could extrude the smaller nanocarriers more effectively, leading to the least inhibitory effects. Therefore, the smaller drug nanocarriers could serve as excellent imaging probes to study the efflux function while the larger nanocarriers serve as powerful drug delivery vehicles. This study demonstrates the possibility of developing optimal-sized nanocarriers to achieve the maximum drug efficacy and potentially avoiding MDR.

This dissertation is dedicated to my parents Mr. Virat and Mrs. Noi Songkiatisak who always support me with their unconditional loves.

ACKNOWLEDGEMENT

There are many people who have worked and made this dissertation completed. First and foremost, I would like to express my deep sense of gratitude to my mentor, Dr. X. Nancy Xu for her valuable time and dedicated and insightful guidance and mentorship throughout my Ph.D. study at Old Dominion University. I would not complete this dissertation without her practical guidance, intellectual encouragement, critical feedback, and support. She has given me opportunities to explore, design and conduct interdisciplinary scientific research. I have learned new scientific techniques and more importantly research integrity. I value and cherish her vast expertise in cutting-edge scientific research, her great knowledge, inspiration and her belief and confidence in me to complete research projects. She is always available to discuss and give her valuable advice on any research project. Her weekly meetings and efforts to gel the graduate students together really create a good working environment and move our group towards the same direction.

I would like to extend my thanks to the members of my dissertation committee, Drs. James Lee, Christopher Osgood and Guijun Wang for their helpful advices and support through my graduate study. Moreover, I would like to acknowledge my fellow colleagues in Xulab, Drs. Prakash Nallathamby, Kerry Lee, Lauren Browning, Tao Huang, especially Drs. Feng Ding and Pavan Cherukuri for their dedication and contribution to this dissertation.

For the study in Chapter II, Dr. Huang synthesized 2 nm Ag NPs and Dr. Cherukuri synthesized 13 and 92 nm Ag NPs. Dr. Huang functionalized and characterized all three different sized drug nanocarriers. Dr. Ding did the stability study of the nanocarriers in the LB mediums. Dr. Cherukuri determined the conjugation ratios of ofloxacin molecules on each single NP. Dr. Ding, Dr. Cherukuri and I equally did the experiment to study inhibitory effects of drug nanocarriers on the cell growth. I studied cell growth and efflux function of the cells. I prepared figures and the manuscript.

For the studies in Chapter III-V, Dr. Cherukuri and I equally did all experiments and data analysis. I combined data, prepared figures, and wrote the manuscripts.

I am grateful for the encouragement and support from my family, friends and Xu lab group members during my graduate study.

NOMENCLATURE

ε	Extinction coefficient
ΔABM	*Pseudomonas aeruginosa* mutant strain with no expression of MexAB-OprM pumps
λ_{max}	Peak wavelength
°C	Degree Celsius
µm	Micrometer
µM	Micromolar
µL	Microliter
ABC	ATP-binding cassette
Ag NPs	Silver Nanoparticles
Ag	Silver
AgMUNH$_2$	Silver nanoparticle functionalized with 11-amino undecanethiol
AgMUNH-Oflx	Silver nanoparticle functionalized with 11-amino undecanethiol and conjugated with ofloxacin
ATP	Adenosine triphosphate
Au	Gold
AUT	11-amino-1-undecanethiol hydrochloride
C	Concentration
^{14}C	Radioactive isotope of carbon
CCD	Charged coupled device
Cryo-EM	Cryo-electron microscopy
DSB	Double-strand break
DFOMS	Dark-field optical microscopy and spectroscopy
DI	De-ionized

DLS	Dynamic light scattering
DNA	Deoxyribonucleic acid
EDC	1-Ethyl-3-[3-dimethylaminopropyl] carbodiimide hydrochloride
FWHM	Full-width-at-half-maximum
h	Hour
^{3}H	Tritium, a radioactive isotope of hydrogen
H_2O_2	Hydrogen peroxide
HRTEM	High-resolution transmission electron microscopy
LB	Luria broth
LPS	Lipopolysaccharide
LSPR	Localized surface plasmonic resonance
$M\Omega$	Megaohms
min	Minutes
mL	Milliliter
ms	Millisecond
MIC_{50}	Minimum inhibitory concentration at 50%
MDR	Multidrug resistance
nM	Nanomolar
nm	Nanometer
ns	Nanosecond
$NaBH_4$	Sodium borohydride
s-NHS	N-hydroxysulfosuccinimide
NBD	Nucleotide binding domain
NPs	Nanoparticles
OD	Optical Density

Oflx	Ofloxacin
p	Probability value
pM	Picomolar
PBS	Phosphate buffer saline
Pgp	P-glycoprotein
PI	Propidium iodide
PVP	Polyvinyl pyrrolidine
rcf	relative centrifugal force
R	Ratio
rpm	Revolutions per minute
s	Seconds
SMNOBS	Single molecular nanoparticle optical biosensor
TEM	Transmission electron microscopy
TMD	Transmembrane domain
UV-vis	Ultraviolet-visible
WT	Wild type

TABLE OF CONTENTS

LIST OF TABLES

LIST OF FIGURES

CHAPTER I

OVERVIEW

The ATP-binding cassette (ABC) membrane transporters are highly conserved proteins found in both prokaryotes and eukaryotes.[1-3] They use the energy of ATP binding and hydrolysis to translocate a large number of structurally and functionally unrelated substrates across biological membrane.[1-3] Multidrug ABC transporters (efflux pumps) can extrude antibiotics out of bacterial cells and chemotherapeutic agents from cancer cells resulting in multidrug resistance (MDR) and the failure of numerous treatments of infections and cancers.[2-4] MDR is responsible for the creation of superbugs and an urgent need of better drugs against pathogenic bacteria.[5-6] Multidrug membrane transporters have been extensively studied as a target aiming to overcome MDR and improve the efficacy of therapeutic drugs.[7]

All ABC transporters share a similar modular topology including two transmembrane domain (TMD) and two nucleotide binding domain (NBD).[1, 3, 7-8] In spite of extensive studies over decades, the molecular basis of MDR and efflux mechanisms of multidrug membrane transporters, for example how the similar structural membrane transporters could extrude diverse structurally unrelated substrates, remain not yet fully understood.[5] Conventional methods for the study of transport efflux kinetics in bulk bacterial cells include the use of radioisotopes (^{14}C and ^{3}H) or fluorophores (ethidium bromide and Hoechst dye) as probes to measure accumulations of substrates in the cells.[9-12] Study of the accumulation kinetics of bulk cells could have masked crucial rare events as individual cells act differently and their efflux kinetics are unsynchronized, emphasizing the importance of probing efflux kinetics of individual membrane transporters in single live cells in real time.[13-14] Moreover, single radioisotope or fluorophore are unable to measure sizes of substrates and membrane transporters as they lack distinctive size-dependent physicochemical properties. Thus, these conventional probes are not suitable to serve as various size-dependent pump

substrates for the study of efflux function of single membrane transporter in single live cells in real time.

The technological leap of nanomaterials provides the most promising strategies to overcome MDR and circumvent many side effects and toxicity from high doses of antibiotics.[15-17] Nanomaterials process unique physiochemical properties, particularly minuscule sizes and high surface-to-volume ratios.[18-19] These distinctive features make nanomaterials outstanding among other candidates as drug delivery vehicles to increase the drug payloads and enhance local drug doses resulting in therapeutic improvement.[20-21] Among nanomaterials, noble metal nanoparticles (e.g., Ag NPs and Au NPs) are the most interesting due to their unique plasmonic optical and surface properties.[17, 22]

Nobel metal nanoparticles (e.g., Ag NPs) process distinctive plasmonic properties, which highly depend on their sizes, shapes, dielectric constant, and surrounding environments.[23-24] Single Ag NPs have high Rayleigh scattering enables us to image and characterize them under illumination of halogen lamps using dark-field optical microscopy and spectroscopy (DFOMS).[14, 25-27] We have demonstrated that we can use superior size-dependent LSPR and photostable single Ag NPs as optical probes to study the size-dependent efflux kinetics of multidrug membrane transporters in single live cells in real time.[9, 13-14, 28-29] We have systematically studied the dependence of the accumulation of substrates and efflux function on the sizes, charges, chemicals, and bacterial strains of Gram-positive bacteria (BmrA in *Bacillus subtilis*)[9, 13, 29-30] and Gram-negative bacteria (MexAB-OprM in *Pseudomonas aeruginosa*)[14, 31-33] using bare and surface-functionalized NPs to mimic various sizes of antibiotics (drugs) with different surface properties (drug functional groups).

In this dissertation, we firstly used Ag NPs as powerful drug delivery vehicles because of their small sizes and high surface-to-volume ratio properties. We synthesized and characterized three different sized Ag NP-based antibiotic nanocarriers, aiming to study the dependence of the therapeutic effects of antibiotics (e.g., ofloxacin, Oflx) on the size of nanocarriers in a bacterial model (*Escherichia coli*).

We further used single antibiotic drug nanocarriers as excellent imaging probes to study efflux function of multidrug ABC membrane transporters. These studies would offer new insights into the mechanisms of MDR of multidrug ABC membrane transporters and the rational design of nanocarriers to improve drug efficacy and evade MDR.

This dissertation contains six chapters. In Chapter I, we provide a brief overview of the research background and significant findings of this dissertation research, and an outline the contents of each individual chapter.

In Chapter II, we developed antibiotic drug nanocarriers from different sized bare Ag NPs and then studied the dependence of their inhibitory effects against bacterial cells upon the dose of antibiotics and the size of nanocarriers. We aimed to (i) design antibiotic drug nanocarriers to achieve high efficacy, importantly to combat MDR and (ii) rationally develop biocompatible antibiotic drug nanocarriers to study efflux function of single multidrug membrane transporters in live bacterial cells. In this study, we synthesized and characterized three different sized bare Ag NPs (2.4 ± 0.7, 13.0 ± 3.1, and 92.6 ± 4.4 nm) and functionalized these NPs with a monolayer of 11-amino-1-undecanethiol hydrochloride (AUT) to prepare AgMUNH$_2$ NPs (control nanocarriers), and then covalently conjugated the amine group of the AgMUNH$_2$ NPs with the carboxyl group of an antibiotic (ofloxacin, Oflx) to produce antibiotic drug nanocarriers (AgMUNH-Oflx NPs). We determined the amount of conjugated Oflx molecules on each single NP (the conjugation ratios) of 2.4 ± 0.7, 13.0 ± 3.1, and 92.6 ± 4.4 nm as 8.6×10^2, 9.4×10^3, and 6.5×10^5 Oflx molecules/NP, respectively. We studied the dependence of inhibitory effects of free Oflx and conjugated Oflx attached on the surface of the nanocarriers on the dose of Oflx and the size of nanocarriers in *E. coli* and found that the inhibitory effects Oflx significantly depend on the dose of Oflx and the size of nanocarriers. The equal amount of Oflx carried by the large nanocarriers (13.0 ± 3.1 and 92.6 ± 4.4 nm) are much more toxic than free Oflx inhibiting cell growth and causing extensive cellular filamentation whereas surprisingly those delivered by the smaller nanocarriers are less toxic than free Oflx, as illustrated in Figure 1. The MIC$_{50}$ of free Oflx and the antibiotic nanocarriers with a diameter of 2.4 ± 0.7, 13.0 ± 3.1, and 92.6 ± 4.4 nm are 0.144, 0.314, 0.081 and 0.026 µM, respectively. Moreover, our control

experiments showed that the AgMUNH$_2$ NPs (control nanocarriers) are biocompatible and do not exhibit significant inhibitory effects on the cell growth. Thus, the results suggest that an optimal size of the nanocarriers is required to create maximum inhibitory effects against pathogenic bacteria in which the same amount of Oflx generates a substantially higher bactericidal potency when it is carried and delivered by the larger nanocarriers.
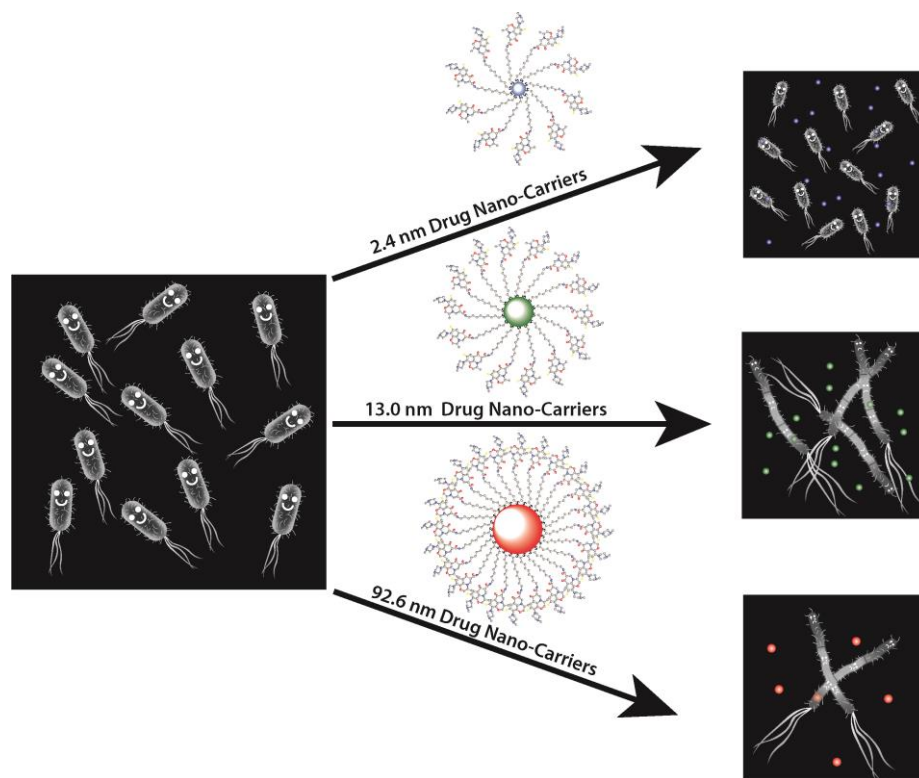
Figure 1. Schematic illustration of size-dependent inhibitory effects of antibiotic drug nanocarriers against *E. coli* using DFOMS.[34]

The inhibitory effects of free Oflx and conjugated Oflx attached on the surface of the nanocarriers depend on the dose of Oflx and the size of nanocarriers in *E. coli*. The largest antibiotic drug nanocarriers (92.6 ± 4.4 nm) show the highest inhibitory effects with the lowest MIC_{50} (0.026 ± 0.003 μM) of Oflx while the smallest antibiotic drug nanocarriers (2.4 ± 0.7 nm) exhibit the lowest bactericidal inhibitory with the highest MIC_{50} (0.314 ± 0.010 μM) of Oflx against *E. coli*. The larger antibiotic drug nanocarriers demonstrate higher efficacy of ofloxacin to target DNA gyrase during cell replication as the cells treated with conjugated Oflx carried by the larger nanocarriers show less numbers of cells and extensive cellular filamentation. The densely loaded Oflx molecules (multivalence) could enhance their binding affinity to the targets and the higher drug payload could raise local drug concentrations and their bactericidal effects.

In Chapter III, we used we used 2.4 ± 0.7 nm AgMUNH-Oflx NPs (the smallest antibiotic drug nanocarriers) and the same sized $AgMUNH_2$ NPs (control nanocarriers) to probe efflux kinetics of ABC (MsbA) membrane transporters of single live *E coli* cells. We demonstrate that we can use LSPR spectra of single AgMUNH-Oflx NPs and $AgMUNH_2$ NPs to identify and track transports of single NPs in and out of single cells over time using DFOMS. We found the high dependence of the accumulation of intracellular AgMUNH-Oflx NPs and $AgMUNH_2$ NPs upon a presence of a pump (ATPase) inhibitor (25 μM orthovanadate) and the concentration of NPs (0.7 and 1.4 nM), suggesting that the NPs enter the cells via passive diffusion which are driven by concentration gradient across the cellular membrane and are extruded out by multidrug ABC membrane transporter. Interestingly, we found that the accumulation of $AgMUNH_2$ NPs is higher than those of AgMUNH-Oflx NPs in single live cells, suggesting the efflux pumps can extrude noxious substrates (e.g., conjugated Oflx) more effectively and rapidly out of the cells as illustrated in Figure 2. This provides powerful evidence that multidrug membrane transporters could have a sensing machinery to selectively detect, recognize toxic substances (e.g., antibiotics and anticancer drugs), and then extrude them out as cellular defense mechanisms.
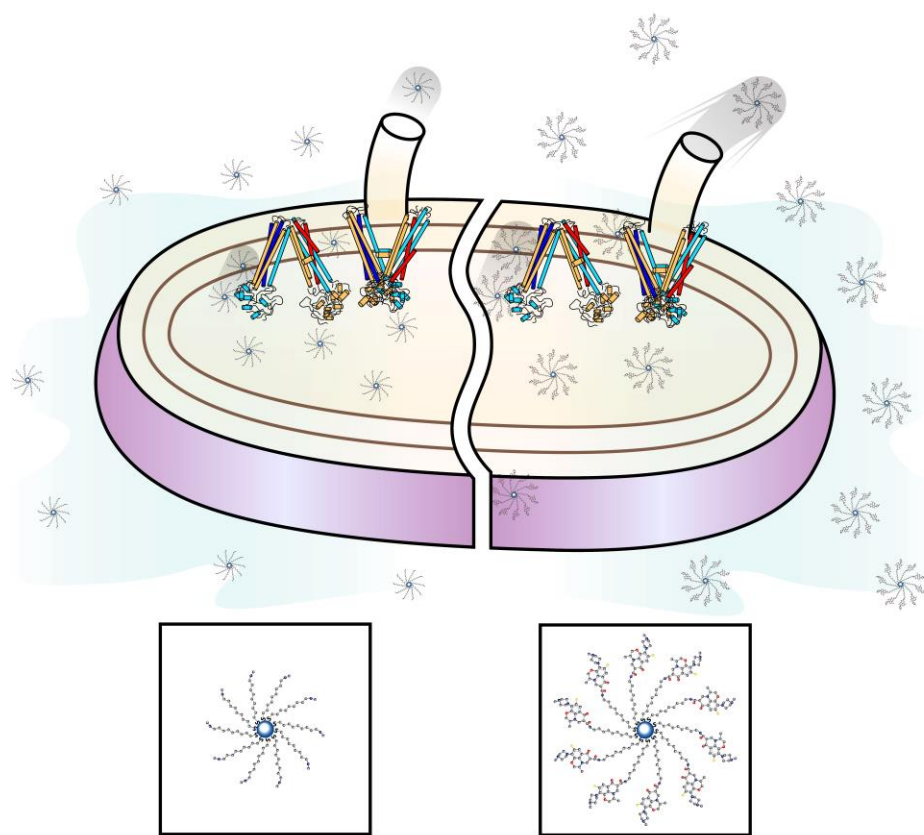
Figure 2. Schematic illustration of study of substrate-dependent efflux function of multidrug ABC (MsbA) membrane transporters in single live *E. coli* cells using 2.4 ± 0.7 nm drug nanocarrier optical probes.[35]

The accumulation of intracellular AgMUNH-Oflx NPs and $AgMUNH_2$ NPs depend upon a presence of a pump (ATPase) inhibitor (25 μM orthovanadate), the concentration of NPs and the type of NPs. The accumulation of the $AgMUNH_2$ NPs is twice higher than those of the AgMUNH-Oflx NPs in single live cells, suggesting substrate-dependent efflux kinetics of MsbA. The efflux pumps can extrude noxious substrates (e.g., AgMUNH-Oflx NPs) more effectively and rapidly out of the cells than biocompatible substrates (e.g., $AgMUNH_2$ NPs). This provides evidence that the multidrug ABC membrane transporters might have a sensing machinery to selectively detect, recognize toxic substances (e.g., antibiotics and anticancer drugs), and then extrude them out as cellular defense mechanisms.

In Chapter IV, we used 13.0 ± 3.1 nm AgMUNH-Oflx NPs (the slightly larger antibiotic drug nanocarriers) and AgMUNH$_2$ NPs (control nanocarriers) to probe efflux kinetics of ABC (MsbA) membrane transporters of single live *E coli* cells under dark-field microscopy. We found that the accumulation rates increase with the NP concentrations, suggesting passive diffusion could be the primary mechanism for the NPs enter into the cells. Interestingly, we found that the number of intracellular AgMUNH$_2$ NPs are far more than those of AgMUNH-Oflx NPs as presented in Figure 3. The pump inhibitor can only cause an increase of the accumulation rate of intracellular AgMUNH-Oflx NPs but not AgMUNH$_2$ NPs. These results confirm the dependence of efflux function of MsbA membrane transporters on types of substrates and the efflux pumps effectively extrude harmful substances, as reported previously in Chapter III.
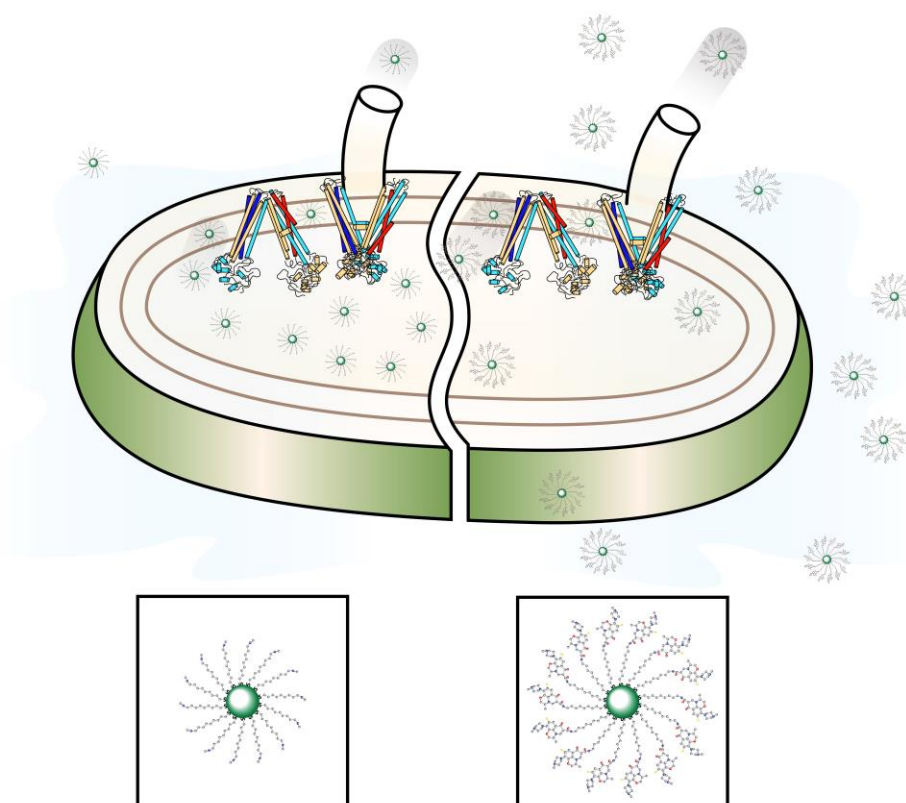
Figure 3. Schematic illustration of study of efflux mechanisms of multidrug ABC (MsbA) membrane transporters in single live *E. coli* cells using 13.0 ± 3.1 nm size-dependent plasmonic drug nanocarrier optical probes.[36]

The accumulation of intracellular AgMUNH-Oflx NPs and $AgMUNH_2$ NPs depend upon a presence of a pump (ATPase) inhibitor (25 μM orthovanadate), the concentration of NPs and the type of NPs. The NPs enter the cells through passive diffusion and are extruded out of the cells by the multidrug ABC membrane transporters. The accumulation of the $AgMUNH_2$ NPs is 24 times higher than those of the AgMUNH-Oflx NPs in single live cells, suggesting substrate-dependent efflux kinetics of MsbA and the efflux pumps can effectively extrude harmful substances.

In Chapter V, we studied efflux kinetics of ABC (MsbA) membrane transporters of single live *E coli* cells using the largest antibiotic drug nanocarriers (92.6 ± 4.4 nm AgMUNH-Oflx NPs) and the same sized control nanocarriers (AgMUNH$_2$ NPs). We found that the accumulation rates of intracellular NPs and efflux kinetics of MsbA membrane transporters highly depend on the concentration of NPs, suggesting that such large NPs could passively diffuse into the cells. Moreover, orthovanadate could interrupt efflux function of MsbA membrane transporters leading to the increase of accumulation rates of intracellular AgMUNH-Oflx NPs and AgMUNH$_2$ NPs. Interestingly, similar to the smaller drug nanocarriers (2.4 ± 0.7 and 13.0 ± 3.1 nm), we found that the accumulation rates of intracellular AgMUNH$_2$ NPs in the presence and absence of orthovanadate are higher than those of the AgMUNH-Oflx NPs, confirming that the efflux pump could detect conjugated Oflx molecules on the antibiotic drug nanocarriers and extrude them out more effectively than the control nanocarriers. Notably, we found size-dependent accumulation rates of intracellular AgMUNH-Oflx NPs. As illustrated in Figure 4, the number of intracellular NPs of the larger NPs (92.6 ± 4.4 nm) at 3.7 pM is lower than those of the smaller NPs (2.4 ± 0.7 nm and 13.0 ± 3.1 nm) at 1.4 nM possibly due to their low concentration gradient across the cellular membrane and/or their low membrane permeability. If we increase the concentration of the larger NPs (92.6 ± 4.4 nm) to 1.4 nM (378 times), the number of intracellular NPs and their accumulation rates could have been much higher than the smaller NPs, suggesting that they could be least effectively extruded out the cells.
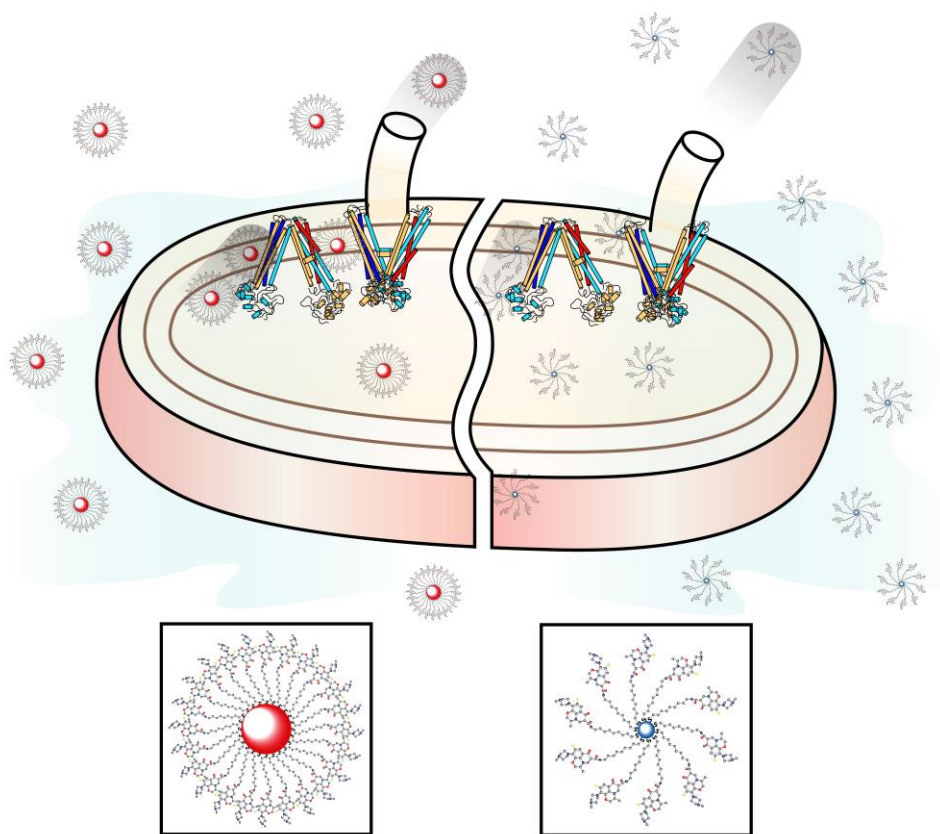
Figure 4. Schematic illustration of study of substrate- and size-dependent efflux function of multidrug ABC (MsbA) membrane transporters in single live *E. coli* cells using 92.6 ± 4.4 nm drug nanocarrier optical probes.[37]

The accumulation of intracellular AgMUNH-Oflx NPs and AgMUNH$_2$ NPs depend upon a presence of a pump (ATPase) inhibitor (25 μM orthovanadate), the concentration of NPs and the type of NPs. The NPs enter the cells through passive diffusion and are extruded out of the cells by the multidrug ABC membrane transporters. The accumulation of the AgMUNH$_2$ NPs is twice higher than those of the AgMUNH-Oflx NPs in single live cells, suggesting substrate-dependent efflux kinetics of MsbA and the efflux pumps can effectively extrude harmful substances. The smaller nanocarriers could be effectively extrude out of the cells by the multidrug ABC membrane transporters more effectively than the larger nanocarriers, and therefore, they are less toxic than the larger nanocarriers.

In Chapter VI, we summarized our research findings that previously described in the preceding chapters, underscored the significance of this research, and discussed the possible future research goals.

CHAPTER II

STUDY OF SIZE-DEPENDENT INHIBITORY EFFECTS OF ANTIBIOTIC DRUG NANOCARRIERS AGAINST *ESCHERICHIA COLI*

INTRODUCTION

Antibiotics have been used to treat infectious diseases for many years. Due to over-consumption and inappropriate use of these drugs, resistance to antibiotics has become increasingly widespread and posed significant challenges for infectious treatments.[15] MDR is responsible for the development of antibiotic resistance causing numerous impacts including higher doses of drugs, additional treatments and an urgent need of novel antibiotics.[15] The MDR phenomena are mainly associated with a robust array of membrane transporters of efflux pumps that extrude a wide variety of substrates including amino acids, ions, lipids and various drugs.[5-6] Multidrug membrane transporters have been extensively studied as a target aiming to overcome MDR and improve the efficacy of therapeutic drugs.[7] Unfortunately, molecular mechanisms of MDR and functions of membrane transporters remain ambiguous after decades of research.[5]

Escherichia coli (E. coli) is an opportunistic Gram-negative bacteria that can cause severe diarrhea, urinary tract infections and respiratory illness.[38-39] There are several membrane transporters associated with efflux systems in *E. coli*.[7] For instance, the MsbA is an essential ATP-binding cassette transporter protein for cell growth and is closely related to mammalian MDR proteins (Pgp, ABCB1, MDR1).[6, 40-41] In bacterial MsbA, a TMD is fused to an NBD in a half-transporter that then homodimerizes to form the full transporter [5, 20] MsbA is a poly-specific transporter which can recognize and transport a wide spectrum of drug molecules.[1, 10, 41].

The use of nanomaterials provides the most promising strategies to overcome MDR and circumvent many side effects and toxicity from high doses of antibiotics.[15-17] Nanomaterials possess such unique physiochemical properties, particularly minuscule

sizes and high surface-to-volume ratios.[18-19] Reduction of the size of the nanomaterials leads to a dramatic increase in the surface area relative to their volume, giving facile surface functionalization with various biological and drug molecules.[18] Nanocarriers promote drug binding affinity and increase the local drug payload resulting in enhanced therapeutic efficacy.[20-21] Although various nanomaterials with different designs, sizes and shapes have been extensively used as drug nanocarriers[15-16], systematical studies to understand their dependence of therapeutic effects and underlying molecular mechanisms upon their physiochemical properties, such as sizes are still elusive. Furthermore, recent studies mainly use biodegradable nanoparticles, such as liposome but only few studies focus on using noble metal NPs as nanocarriers to treat bacterial infection.[16]

Noble metal NPs (e.g. Ag and Au) have been proven to be versatile and widely used materials in biomedical applications, such as drug delivery and nanobiosensors[26, 42-43] In addition to a large surface-to-volume ratio, Ag NPs possess distinctive size-dependent photostable plasmonic optical properties enable us to image and determine the sizes of single NPs at the nanometer (nm) resolution in real time using dark-field optical microscopy and spectroscopy (DFOMS).[25] We have used the size-dependent localized surface plasma resonance (LSPR) spectra (color) of single NPs to study the sizes of NPs as they transported in and out of single live cells and thus determine the pore sizes of the membrane transporters.[9, 14] Moreover, We have developed single molecule nanoparticle optical biosensors (SMNOBS) from Ag NPs to probe important molecular events, such as cell apoptosis at a single cell resolution in real time.[26, 42]

In this study, we have synthesized, purified and characterized three different sized stable Ag NPs nanocarriers (2.4 ± 0.7, 13.0 ± 3.1 and 92.6 ± 4.4 nm). We have quantitatively studied dose and size dependent bactericidal effects of these antibiotic drug nanocarriers against *E. coli*, aiming to determine the dependence of the inhibitory effects of conjugated Oflx upon the size of nanocarriers. Single Ag NPs can serve as powerful drug delivery vehicles and excellent imaging probes, which allow us to investigate roles of different sized nanocarriers not only in boosting drug efficacy but also in efflux function of multidrug membrane transporters. These will guide us to the

rational design of optimally sized nanocarriers that can enhance drug binding affinity and increase the local drug payload concentrations at the target sites to achieve the highest drug efficacy and, more importantly overcome MDR.

RESULTS AND DISCUSSION

Synthesis and Characterization of Three Different Sized Ag NPs

We have synthesized and purified three different sized Ag NPs, as described in Methods and as we reported previously.[25-26, 43-45] Representative TEM images (Figure 5A: a-c) and histograms of size distribution (Figure 5B: a-c) of three different NP samples show nearly spherical shaped NPs with diameters of (2.4 ± 0.7), (13.0 ± 3.1) and (92.6 ± 4.4) nm, respectively.[46] Notably, the shapes of the smallest NPs are the closest to the spherical. In contrast, the shapes of the largest NPs are polygonal (the least spherical). The diameters of oval and irregular shaped NPs are determined by averaging the length and width of the NPs.

We characterized the plasmonic absorption and scattering of Ag NP solutions using UV-vis absorption spectroscopy.[46] UV-vis absorption spectra of three different sized NPs with diameters of (2.4 ± 0.7), (13.0 ± 3.1) and (92.6 ± 4.4) nm show the peak wavelength with full width at half maximum, λ_{max} (FWHM), at 392 (57), 395 (59) and 450 (182) nm, respectively. We did not observe any shoulder peak for NPs with diameters of either (2.4 ± 0.7) or (13.0 ± 3.1) nm, further demonstrating that they are nearly spherical. In contrast, we observed one shoulder peak wavelengths at 390 nm for the diameter of NPs of (92.6 ± 4.4) nm, which are most likely attributed to the in-plane quadrupole resonance of the NPs generated by transverse collective oscillation of the surface electrons between edges of the NPs. Notably, the TEM images of the NPs (Figure 5A: c) indeed show that they are polygonal with sharp edges.[46]
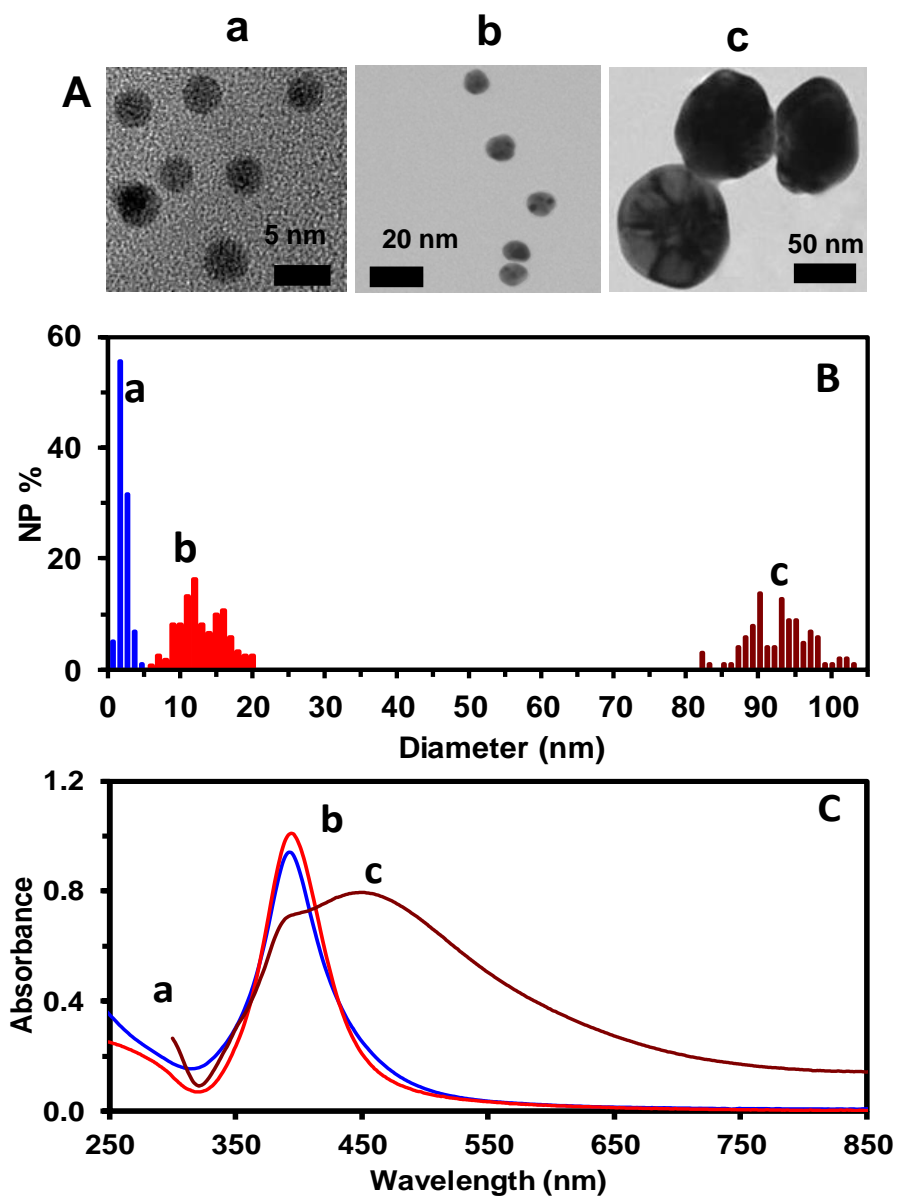
Figure 5. Characterization of sizes, shapes and plasmonic optical properties of three different sized Ag NPs.[46]

(A) HRTEM images of single Ag NPs and (B) histograms of their size distributions show nearly spherical shaped NPs with average diameters of (a) 2.4 ± 0.7, (b) 13.0 ± 3.1 and (c) 92.6 ± 4.4 nm. (C) UV-vis spectra of the NPs in DI water show the peak absorption (full width at half maximum), λ_{max} (FWHM), at: (a) 392 (57), (b) 395 (59), and (c) 450 nm with a shoulder peak of 390 nm, respectively.

Synthesis and Characterization of Antibiotic Nanocarriers (AgMUNH-Oflx NPs)

We functionalized the well purified and characterized Ag NPs with a monolayer of 11-amino-1-undecanethiol (AUT) by replacing citrate molecules electrostatically adsorbed on the surface of the NPs with AUT via the interaction of thiol groups of AUT with the NPs, to prepare AgMUNH$_2$ NPs, as presented in Material and Method and Figure 6. We washed the AgMUNH$_2$ NPs thoroughly with nanopure water to remove excess AUT using centrifugation. We then covalently conjugated the amine groups of each sized AgMUNH$_2$ NPs with the carboxyl group of ofloxacin (Oflx) via a peptide bond using a two-step method via EDC and s-NHS as mediators to prepare antibiotic nanocarriers (AgMUNH-Oflx NPs), as illustrated in Figure 6.[46]

We purified the drug nanocarriers (AgMUNH-Oflx NPs) by thoroughly washing them with deionized (DI) water, and characterized the conjugation ratios of Oflx molecules to the NPs using UV-vis absorption spectroscopy, as shown in Figure 7 and Table 1.[46] The absorption spectrum of 2.4 ± 0.7 nm Ag NPs (Figure 7A: a) shows a plasmonic absorption peak wavelength of 390 nm with a FWHM of 55 nm. After the surface of the NPs was functionalized with a monolayer of AUT, the refractivity of the NPs decreased and their dielectric constant increased, leading to a red-shifted and broader plasmonic absorption spectrum. Thus, the plasmonic absorption spectrum of AgMUNH$_2$ NPs (Figure 7A: b) shows a peak wavelength of 413 nm and a FWHM of 132 nm. Upon conjugation of Oflx with the AgMUNH$_2$ NPs, we observed both the distinctive absorption peak wavelengths of Oflx at 288 and 331 nm and the plasmonic peak absorption of the NPs at 416 nm for the nanocarriers (AgMUNH-Oflx NPs). We subtracted the absorption spectrum of AgMUNH$_2$ NPs from that of AgMUNH-Oflx NPs and determined the concentration of Oflx covalently attached onto the nanocarriers using the absorbance at 288 nm. We used the plasmonic peak absorbance of NPs in the same nanocarriers to determine the concentration of NPs. We divided the Oflx concentration of the nanocarrier by the NP concentration of the same nanocarrier
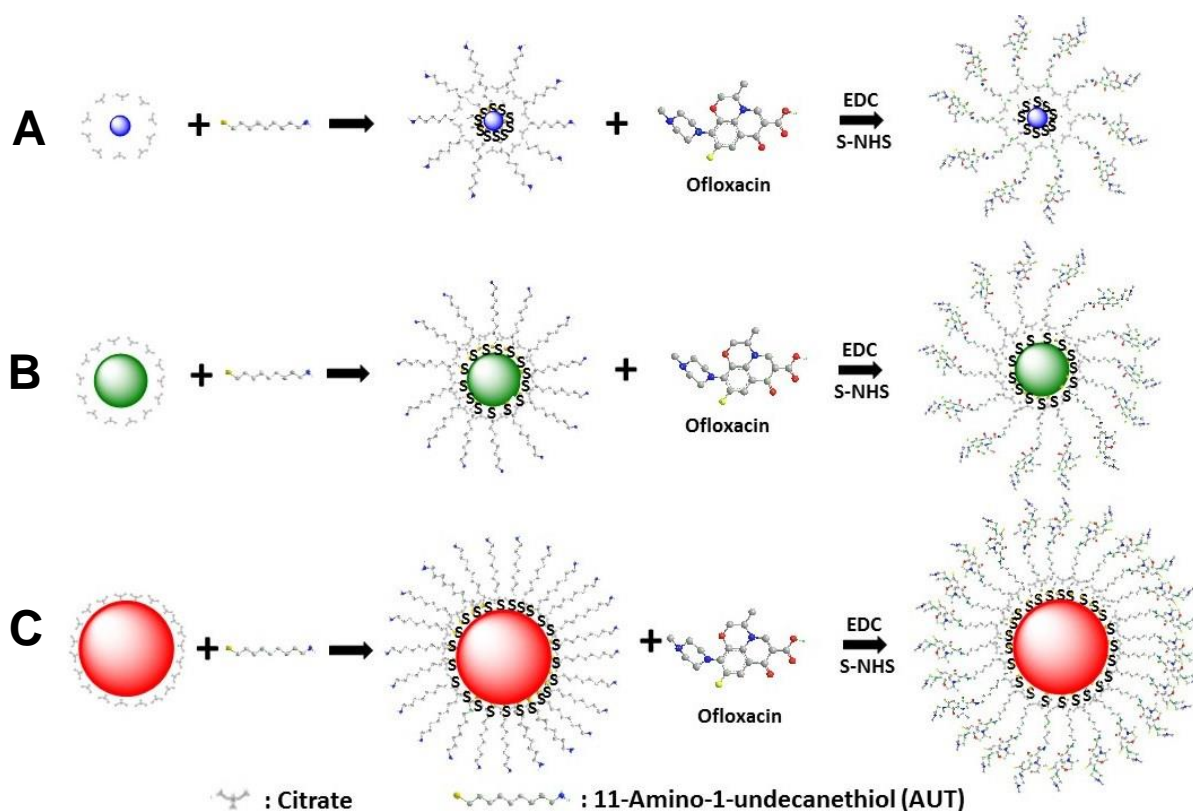
Figure 6. Schematic illustration of synthesis of three different sized antibiotic drug nanocarriers (Adapted from Ref 46).[46]

Functionalizing Ag NPs with monolayer of 11-amino-1-undecanethiol using interaction of its thiol groups (-SH) with the surface of Ag NPs with diameters of (A) 2.4 ± 0.7, (B) 13.0 ± 3.1 and (C) 92.6 ± 4.4 nm to synthesize AgMUNH$_2$ NPs. The amine groups of AgMUNH$_2$ conjugate with the carboxyl groups of ofloxacin via a peptide bond using EDC and sulfo-NHS as mediators to prepare AgMUNH-Oflx NPs called as antibiotic drug nanocarriers.
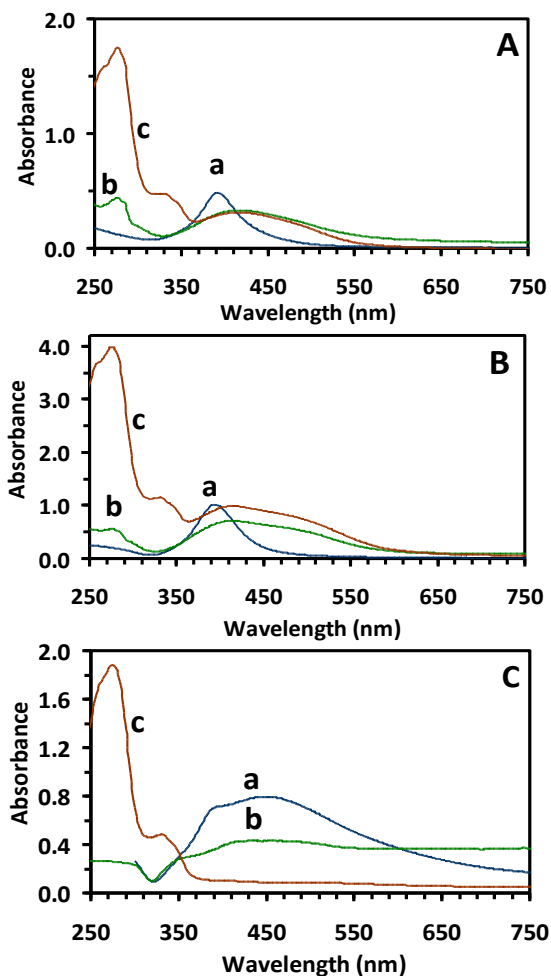
Figure 7. Characterization of conjugation ratios of Oflx molecules with NPs for three different sized Ag NPs using UV-vis absorption spectroscopy.[46]

(A) UV-vis absorption spectra of: (a) 2.4 ± 0.7 nm Ag NPs, (b) AgMUNH$_2$ NPs and (c) AgMUNH-Oflx NPs show the plasmonic absorption peak wavelength (λ_{max}) of NPs at 392, 413 and 416 nm, respectively. (B) UV-vis absorption spectra of: (a) 13.0 ± 3.1 nm Ag NPs, (b) AgMUNH$_2$ NPs and (c) AgMUNH-Oflx NPs show the plasmonic absorption λ_{max} of NPs at 394, 414 and 418 nm, respectively. (C) UV-vis absorption spectra of: (a) 92.6 ± 4.4 nm Ag NPs, (b) AgMUNH$_2$ NPs and (c) AgMUNH-Oflx NPs show the plasmonic absorption λ_{max} of NPs at 450, 453 and 486 nm, respectively. Note that Oflx signature absorption λ_{max} at 288 and 331 nm were observed in (c) only for all three sized nanocarriers in (A-C), showing the conjugation of Oflx with the NPs.

solution to quantitatively characterize the conjugation ratio of Oflx molecules to NPs, showing 8.6×10^2 Oflx molecules/NP for the 2.4 ± 0.7 nm Ag NPs. Using a close-packed model with the footprint of each AUT molecule of 0.214×0.214 nm^2 on the surface of the NP,[43] we found that the smooth surface area of a perfectly spherical NP with a diameter of 2.4 nm could only accommodate 395 Oflx molecules/NP. The 2-fold higher payload of 8.6×10^2 Oflx molecules/NP could be attributed to the rough surface and irregular shape of the NPs.[46]

The absorption spectrum of the 13.0 ± 3.1 nm Ag NPs (Figure 7B: a) shows a plasmonic absorption peak wavelength at 399 nm and a FWHM of 58 nm. After their surface was functionalized with a monolayer of AUT, their plasmonic absorption spectrum (Figure 7B: b) red-shifted and showed a peak wavelength of 413 nm and a FWHM of 132 nm. After the AgMUNH$_2$ NPs were conjugated with Oflx, the plasmonic absorption spectrum of AgMUNH-Oflx NPs (nanocarriers) exhibited both the distinctive absorption peak wavelengths of Oflx at 288 and 331 nm as well as the plasmonic peak absorption of NPs at 418 nm for the nanocarriers (AgMUNH-Oflx NPs). Using the same approaches as described above, we quantitatively characterized the conjugation ratio of Oflx molecules to NPs as 9.4×10^3 Oflx molecules/NP for the 13.0 ± 3.1 nm NPs, which is nearly equal to the maximum number of AUT molecules (1.2×10^4 molecules) that could be closely packed on the surface of a spherical NP with a diameter of 13 nm, as determined by the close-packed model.[46]

The absorption spectrum of the 92.6 ± 4.4 nm Ag NPs (Figure 7C: a) shows a plasmonic absorption peak wavelength at 450 nm. After their surface was functionalized with a monolayer of AUT, the peak wavelength of the plasmonic absorption spectrum red-shifted to 453 nm (Figure 7C: b). Upon conjugation of the AgMUNH$_2$ NPs with Oflx, the plasmonic absorption spectrum of AgMUNH-Oflx NPs exhibited both the distinctive absorption peak wavelengths of Oflx at 288 and 331 nm as well as a further red-shifted plasmonic peak absorption of the NPs to 500 nm. Using the same approaches described above, we quantitatively characterized the conjugation ratio of Oflx to the NPs

as 6.5×10^5 Oflx molecules/NP for the 92.6 ± 4.4 nm NPs, which is approximately equal to the maximum number of AUT molecules (5.9×10^5 molecules) that could be closely packed on the surface of a perfectly spherical NP with a diameter of 92.6 nm, as determined by the close-packed model.[46]

Table 1. Determination of Conjugation Ratios of Ofloxacin (Oflx) Molecules per NP for Three Different Sized Drug Nanocarriers. [46]

Diameter of NPs (nm)	C_{NPs}^a (nM)	C_{Oflx}^b (μM)	$R_{Oflx\ per\ NP}^c$
2.4 ± 0.7	50	43.2	8.6×10^2
13.0 ± 3.1	3.3	31.1	9.4×10^3
92.6 ± 4.4	0.030	19.4	6.5×10^5

[a] Plasmonic absorbance of drug nanocarriers (AgMUNH-Oflx NPs) at λ_{max} of 416, 418, 486 nm was used to determine the concentration of 2.4 ± 0.7; 13.0 ± 3.1 and 92.6 ± 4.4 nm NPs, respectively.

[b] C_{Oflx} was determined by subtracting UV-vis spectra of AgMUNH$_2$ NPs from that of AgMUNH-Oflx NPs, and dividing the peak absorbance of the subtracted UV-vis spectra at 288 nm by molar absorptivity ($\varepsilon_{288\ nm}$) of Oflx, 7.8×10^3 M^{-1} cm^{-1}

[c] Conjugation ratio of the number of Oflx molecules per NP was calculated by dividing the concentration of Oflx with concentration of NPs for the same solution of AgMUNH-Oflx NPs for 2.4 ± 0.7; 13.0 ± 3.1 and 92.6 ± 4.4 nm NPs, respectively.

Study of Stability of Drug Nanocarriers (AgMUNH-Oflx NPs) in Cell Culture Medium

In order to study the dependence of the inhibitory effects of these antibiotic nanocarriers against *E. coli* on the sizes of NPs and doses of antibiotic, it is crucial that the nanocarriers remain stable (non-aggregated) in cell culture medium and that their sizes and doses remain unchanged over the entire duration of the cell culture experiment. If the nanocarriers aggregate in the cell culture medium, then their sizes and doses would change over time, making a study of their size and dose dependent inhibitory effects unreliable.

Therefore, we first characterized the stability (non-aggregation) of each size of drug nanocarriers (AgMUNH-Oflx NPs) in a commonly used standard LB medium (1% tryptone, 0.5% yeast extract, and 0.5% NaCl in DI water, pH = 7.2) over 24 h using UV−vis absorption spectra. Unfortunately, none of the nanocarriers at the desired concentration were stable in this standard medium.[46]

We then reduced the concentration of NaCl to 0.1% and characterized the stability (non-aggregation) of the drug nanocarriers in the modified medium (1% tryptone, 0.5% yeast extract, and 0.1% NaCl in DI water, pH = 7.2) over 24 h using UV−vis absorption spectroscopy. The results in Figure 8 show that the absorption spectra of the nanocarriers remain unchanged over 24 h, indicating that the nanocarriers with Ag NP diameters of 2.4 ± 0.7, 13.0 ± 3.1, and 92.6 ± 4.4 nm and concentrations of 6.0 nM, 0.8 nM, and 7 pM were stable (non-aggregated) in the modified medium over 24 h, respectively.[46]
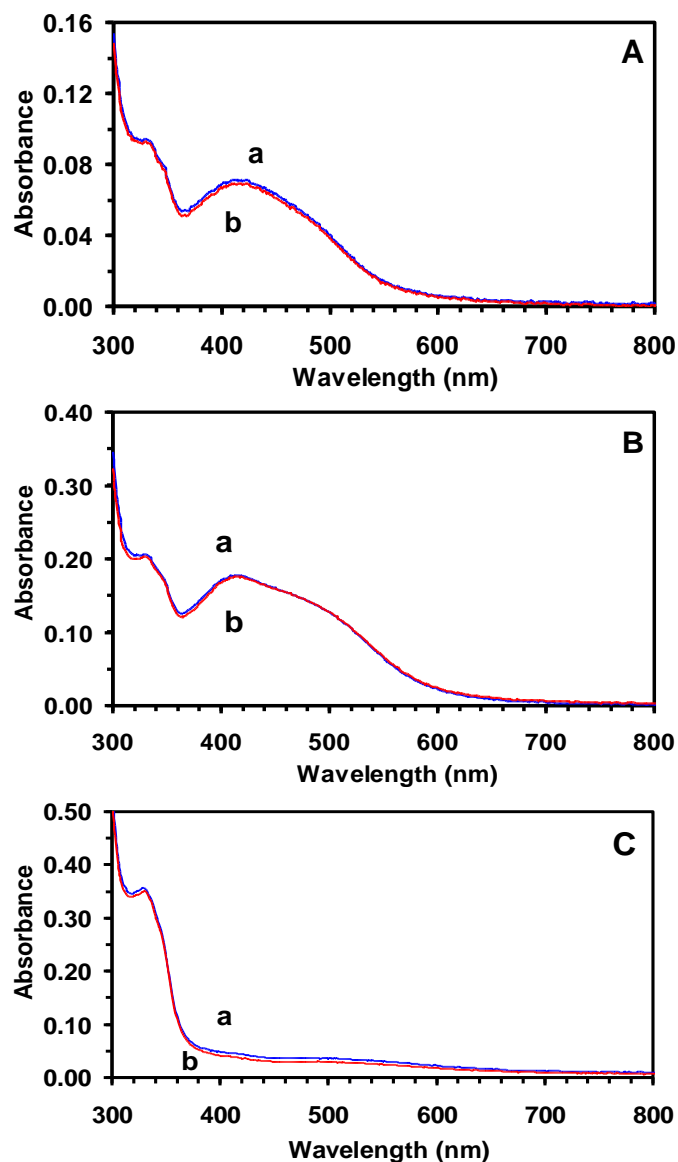
Figure 8. Characterization of the stability (non-aggregation) of three sized antibiotic nanocarriers (AgMUNH-Oflx NPs) in the modified LB medium using UV-vis absorption spectroscopy.[46]

The UV-vis absorption spectra of 6 nM, 0.8 nM and 7 pM of AgMUNH-Oflx NPs for the Ag NPs with diameters of: (A) 2.4 ± 0.7, (B) 13.0 ± 3.1 and (C) 92.6 ± 4.4 nm, in the modified LB medium at (a) 0 and (b) 24 h, remain essentially unchanged over time, which indicates that the nanocarriers were stable (non-aggregated) in the medium over 24 h, respectively.

Characterization of Suitability of the Modified LB Medium for Cell Culture

We previously found that the antibiotic drug nanocarriers were unstable in the standard LB medium (1% tryptone, 0.5% yeast extract and 0.5% NaCl in DI water, pH = 7.2) but they were stable (non-aggregation) in the modified LB medium (1% tryptone, 0.5% yeast extract and 0.1% NaCl in DI water, pH = 7.2).[46] Therefore, we studied cell growth of *E. coli* (MsbA) strain in the modified LB medium to ensure that it was suitable for culturing healthy cells as the standard LB medium. We pre-cultured the cells in the standard LB medium for 12 h. We then cultured the pre-culture cells in the standard and the modified LB and measure the cell growth over time by measuring optical density at 600 nm ($OD_{600\ nm}$) every hour. The growth curves of the cells cultured in the standard LB medium (Figure 9A) and the cells cultured in the modified LB medium (Figure 9B) are similar indicating that the modified LB medium is well suited to culture the cells.

We then characterized the viability of cells cultured in the standard and the modified medium over 16 h via LIVE/DEAD *Bac*Light assay. Representative images of the cells cultured in the standard LB medium (Figure 10A) and the modified LB medium (Figure 10B) show SYTO9 green fluorescence (Figure 10A, B: b) but not propidium iodide (PI) red fluorescence demonstrating that cells are viable. As the cells cultured in the modified LB medium show more than 99% viability (Figure 10C), the modified LB medium can be used to culture the cells.
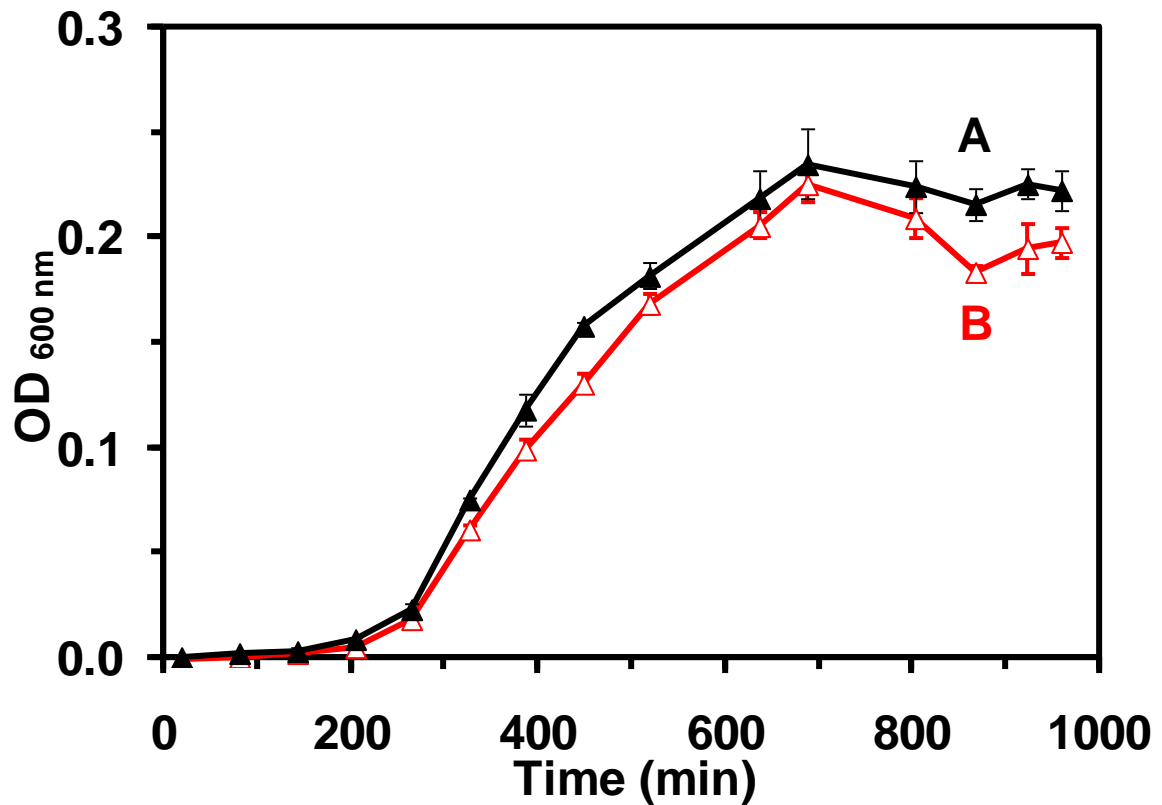
Figure 9. Characterization of growth kinetics of the live cells cultured in standard and modified LB medium.

The cellular growth curves of *E. coli* (MsbA) in **(A)** standard and **(B)** modified LB medium over time show that the growth rates of the cells in either medium are nearly identical, which indicates that the modified LB medium is well suited to culture the cells.
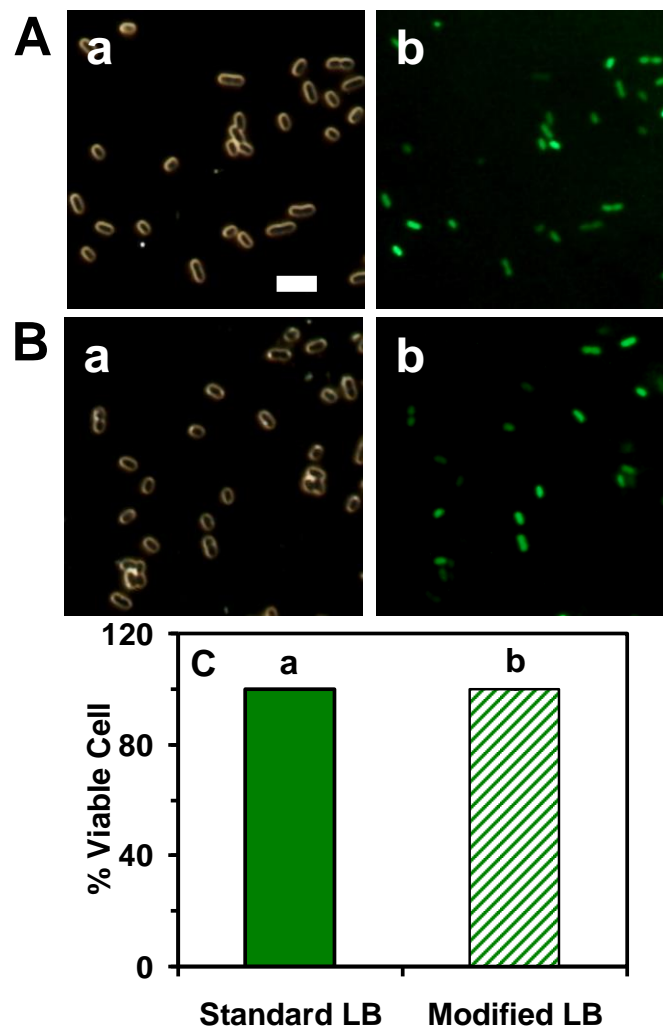
Figure 10. Characterization of viability of *E. coli* (MsbA) cells cultured in standard and modified LB medium using LIVE/DEAD *Bac*Light assay.

Optical image (a) and fluorescence images (b) of single *E. coli* (MsbA) cultured in medium over 16 h, and suspended in the PBS buffer and assayed using LIVE/DEAD *Bac*Light assay. The cells emitted the green fluorescence (λ_{max} = 525 nm) of SYTO9 indicating viable cells (C) Plot of the percent of the live cells (live cells divided by the total number of cells) cultured in (a) standard and (b) modified LB medium show that more than 99% of the cells (MsbA) are viable, which further indicates that the modified LB medium is well suitable to culture the cells. Minimum 900 cells were assayed. The scale bar in (A) is 5 μm.

In addition, we characterized the efflux pump function of MsbA in live cells by probing the dependent accumulation of intracellular fluorescence dye (Hoechst 33342) using time-course fluorescence intensity. The Hoechst 33342 dye is a well-known substrate of MsbA (ABC) membrane transporters and has been used to for efflux function studies.[10-11] The dye emits weak fluorescence intensity in aqueous solution but its intensity dramatically increases (up to 10 times) once it internalizes into the cells and intercalates with DNA.[47] Therefore, Hoechst 33342 dye is suitable for monitoring intracellular accumulation of the dye and for characterization of the efflux function of multidrug membrane transporters of live cells in real time. The results in Figure 11 demonstrated the fluorescence intensity of Hoechst 33342 dye (0.5 µM) incubated with the cells cultured in the standard LB medium (Figure 11C) and the modified LB medium (Figure 11D) gradually increased and remain stable over time. We further studied effects of a pump (ATPase) inhibitor, orthovanadate,[48-49] on the efflux pump function. The cells cultured in the standard LB medium (Figure 11A) and the modified LB medium (Figure 11B) with a presence of orthovanadate (25 µM) showed higher accumulation rates of the dye than in their absence. Altogether, the cells cultured in modified LB medium exhibited relatively the same efflux pump function of MsbA as those in the standard LB medium demonstrating that the modified LB medium well suited to culture healthy cells.
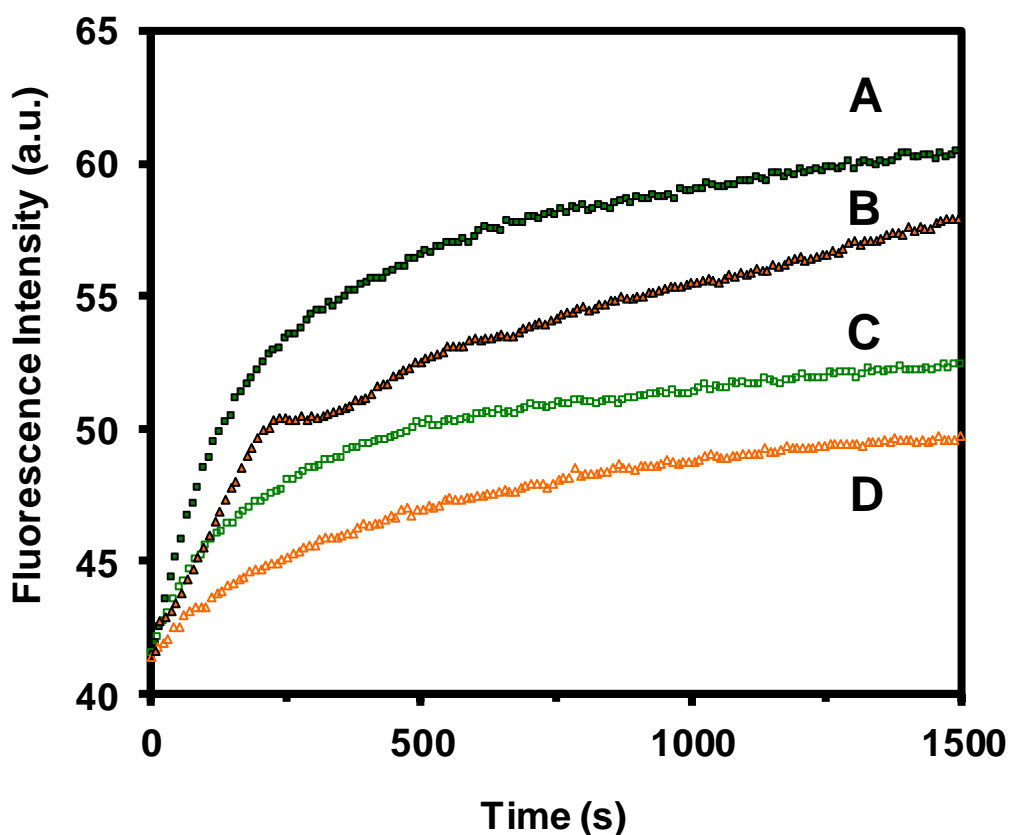
Figure 11. Characterization of accumulations and efflux kinetics of the Hoechst 33342 for live cells cultured in standard and modified LB medium.

Time-dependent fluorescence intensity of Hoechst 33342 (0.5 µM) incubated with the cells (OD $_{600\ nm}$ = 0.1 in PBS buffer, pH 7.2): MsbA cells cultured in standard (A) and modified (B) LB medium in the presence of 25 µM orthovanadate and MsbA cells cultured in standard (C) and modified (D) LB medium in the absence of orthovanadate. The cells cultured in standard (A and C) and modified (B and D) LB medium show similar accumulation and efflux kinetics, which demonstrates that the modified LB medium is well suitable to culture the cells for the study of accumulation and efflux kinetics of MsbA.

Study of Size and Dose Dependence of Inhibitory Effects of Antibiotic Drug Nanocarriers

We cultured the cells (10^4 pre-cultured cells) in the modified LB medium containing a dilution series of free drug Oflx, each given sized antibiotic drug nanocarriers (AgMUNH-Oflx NPs) and the corresponding size of AgMUNH$_2$ NPs (no conjugated Oflx, control experiment) in test tubes. We then incubated the cells with vigorous shaking (200 rpm, 37 ^{o}C) over 18 h.

The dilution series consist of 0, 0.045, 0.09, 0.18, 0.38 and 0.68 µM of free drug Oflx (Figure 12A: a-f) or the conjugated Oflx from the antibiotic drug nanocarriers (Figure 12B-D: a-e), which corresponded to the concentrations of antibiotic drug nanocarriers (NP concentrations): (Figure 12B: a-e) 5.21×10^{-2}, 0.104, 0.209, 0.440, and 0.788 nM of NPs with a diameter of 2.4 ± 0.7 nm using the ratio of 8.6×10^2 Oflx molecules per NP; (Figure 12C: a-e) 4.77×10^{-3}, 9.54×10^{-3}, 1.91×10^{-2}, 4.03×10^{-2} and 7.21×10^{-2} nM for NPs with a diameter of 13.0 ± 3.1 nm using the ratio of 9.4×10^3 Oflx molecules per NP; (Figure 12D: a-e) 6.89×10^{-2}, 0.138, 0.276, 0.582 and 1.04 pM for NPs with a diameter of 92.6 ± 4.4 nm using the ratio of 6.5×10^5 Oflx molecules per NP. Moreover, control experiments included the modified LB medium alone (No cells) and the cells that were cultured at the same time and under the same conditions as samples, incubated with the modified LB medium containing 0.788 nM, 7.21×10^{-2} nM and 1.04 pM AgMUNH$_2$ NPs (in the absence of Oflx) with a diameter of Ag NPs of 2.4 ± 0.7, 13.0 ± 3.1 and 92.6 ± 4.4 nm, respectively (Figure 12B-D: f).

We sampled the cell solutions every 6 h and quantitatively determined the bacterial cell concentration by measuring OD$_{600 \text{ nm}}$ in a 96-well plate using a plate reader (BioTek SynergyHT) equipped with an UV-vis absorption spectral detector. We subtracted OD$_{600 \text{ nm}}$ of the NPs or the antibiotic drug nanocarriers from the cell samples with the NPs or the antibiotic drug nanocarriers to determine the OD$_{600 \text{ nm}}$ of the cell concentrations. We plotted OD$_{600 \text{ nm}}$ of the cell suspension over time and determined 18h as the duration for the cells in the medium alone (control) required to reach
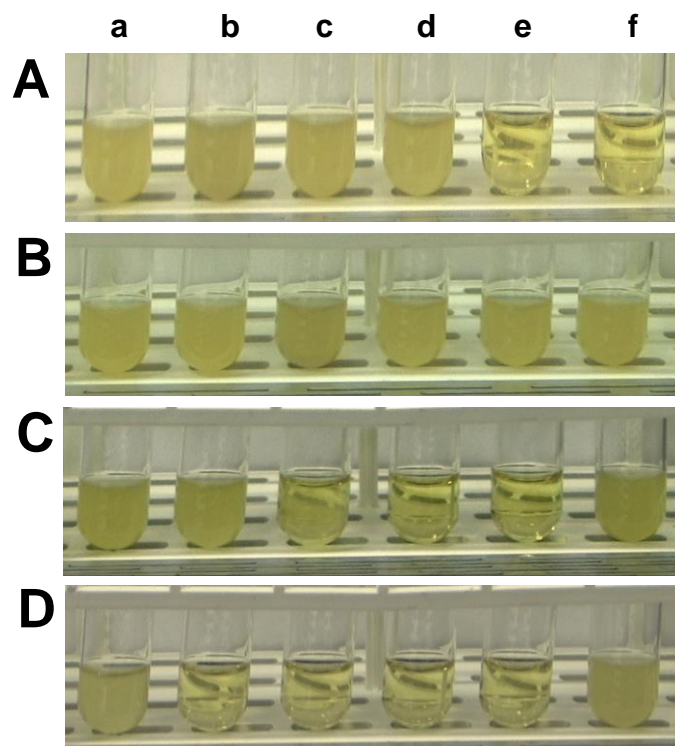
Figure 12. Study of the concentration and size dependent inhibitory effects of antibiotic drug nanocarriers (AgMUNH-Oflx NPs) upon the growth of *E. coli* (MsbA) cells.

Images of the modified LB-medium cultured with the MsbA cells containing: (A) free drug Oflx alone at 0, 0.045, 0.09, 0.18, 0.38 and 0.68 µM (a-f); (B) the conjugated Oflx from antibiotic drug nanocarriers with a diameter of 2.4 ± 0.7 nm at 0.045, 0.09, 0.18, 0.38 and 0.68 µM (a-e); (C) the conjugated Oflx from antibiotic drug nanocarriers with a diameter of 13.0 ± 3.1 nm at 0.045, 0.09, 0.18, 0.38 and 0.68 µM (a-e); (D) the conjugated Oflx from antibiotic drug nanocarriers with a diameter of 92.6 ± 4.4 nm at 0.045, 0.09, 0.18, 0.38 and 0.68 µM (a-e). The concentrations of Oflx conjugated onto the NPs are determined based upon their conjugation ratios. The concentrations of AgMUNH$_2$ NPs in (f) containing the same concentration of the NPs as those in (e) for each type of NPs in (B-D) but without carrying Oflx (control experiments for the study of effects of NPs), respectively.

confluence and for the cells in the medium with Oflx or drug nanocarriers or NPs to reach their equilibriums. We used the $OD_{600\,nm}$ of each cell suspension at 18 h to determine the inhibitory effects of the free drug Oflx and conjugated Oflx as described in the following.

The plot of normalized $OD_{600\,nm}$ of the cells suspension cultured with free drug Oflx and the conjugated Oflx with a given sized antibiotic drug nanocarrier at 18 h (Figure 13) indicates that the inhibitory effects of Oflx significantly depend upon the dose of Oflx and the size of the antibiotic drug nanocarriers. The control experiments (Figure 13A-C) of the cells incubated with each size of $AgMUNH_2$ NPs (absence of Oflx, 2.4 ± 0.7, 13.0 ± 3.1 or 92.6 ± 4.4 nm) which consisted of the same concentration of NPs as those of the highest concentration of the given sized nanocarrier, gave the same $OD_{600\,nm}$ as those cultured in the medium alone. These findings indicate that the $AgMUNH_2$ NPs do not significantly contribute to inhibitory effects on the growth of MsbA cells.

On the contrary, the $OD_{600\,nm}$ of the cell suspension incubated with Oflx alone show the high dose-dependent inhibitory effects of Oflx on the growth. As the concentration of Oflx increases, $OD_{600\,nm}$ of the cell suspension decreases, indicating that the number of the cells decreases. By fitting the plot (Figure 13D), we determined the concentration of Oflx that reduced the cell growth to half and defined it as minimum inhibitory concentration (MIC_{50}) of Oflx. The MIC_{50} of free Oflx is 0.144 ± 0.008 μM (Table 2). Likewise, the results in Figure 13E-G show high dose-dependent inhibitory effects as the $OD_{600\,nm}$ of the cell suspension decreases when the concentration of conjugated Oflx increases. Interestingly, the $OD_{600\,nm}$ of the cell suspension incubated with 2.4 ± 0.7 nm drug nanocarriers with the conjugation ratio of 8.6×10^2 Oflx molecules/NP decreases less rapidly than those of free Oflx and the other two larger nanocarriers, giving the MIC_{50} of 0.314 ± 0.010 μM Oflx (Figure 13E). The MIC_{50} of 13.0 ± 3.1 nm drug nanocarriers with the conjugation ratio of 9.4×10^3 Oflx molecules/NP is 0.081 ± 0.002 μM Oflx (Figure 13F) which is lower than the MIC_{50} of free Oflx and 2.4 ± 0.7 nm drug nanocarriers. Notably, the MIC_{50} of 92.6 ± 4.4 nm drug nanocarriers with
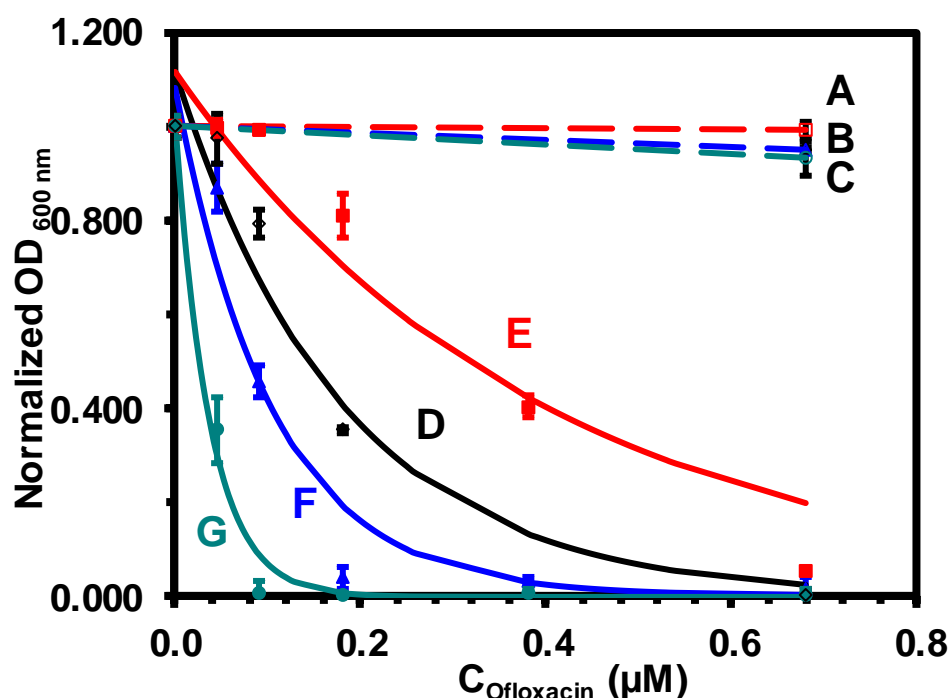
Figure 13. Study of dose and size dependent inhibitory effects of antibiotic drug nanocarriers (AgMUNH-Oflx NPs) in *E. coli* (MsbA) using UV-vis spectroscopy.

Plots of normalized $OD_{600\ nm}$ of the cells cultured for 18 h in the modified LB-medium containing (A-C) $AgMUNH_2$ NPs (absence of Oflx, control), (D) free drug Oflx, and (E-G) the conjugated Oflx from antibiotic drug nanocarriers with a diameters of NPs (E) 2.4 ± 0.7, (F) 13.0 ± 3.1 and (G) 92.6 ± 4.4 nm, respectively. The concentrations of $AgMUNH_2$ NPs in (A-C) containing the same concentration of the NPs as those carried the highest Oflx concentrations in (E-G) for each type of NPs but without carrying Oflx (control experiments for the study of effects of NPs), respectively. The points are experimental data and a solid line is generated by fitting of the experimental data with an equation ($y = a*e^{-bx}$) as followings: (D) $y = 1.12\ e^{-5.57x}$, $R^2 = 0.944$; (E) $y = 1.12\ e^{-2.56x}$, $R^2 = 0.928$; (F) $y = 1.08\ e^{-9.58x}$, $R^2 = 0.941$; (G) $y = 1.01e^{-26.7x}$, $R^2 = 0.988$. Concentrations of Oflx (MIC_{50}) for free Oflx and Oflx conjugated on a given sized nanocarrier were determined using the exponential fitting equation at the half of the maximum of the normalized $OD_{600\ nm}$ for each curve, respectively.

Table 2. Study of Dependence of the MIC of Oflx upon the Size of Nanocarriers against *E. coli* (MsbA-WT)

Samples	MIC$_{50}$ of Oflx (µM) *
Free Oflx alone	0.144 ± 0.008
Nanocarriers (2.4 ± 0.7 nm)	0.314 ± 0.010
Nanocarriers (13.0 ± 3.1 nm)	0.081 ± 0.002
Nanocarriers (92.6 ± 4.4 nm)	0.026 ± 0.003

* The MIC of Oflx for each sample was determined by fitting the experimental data with the exponential decay ($y = a*e^{-bx}$, inhibitory effects upon the exponential cell growth) to determine the parameters (a and b) of a fitting equation with a regression. The equation was then used to determine the concentration of Oflx at which the cell growth was inhibited to the half of the cell growth of the blank control experiment, as described in Figure 13 caption.

the conjugation ratio of 6.5×10^5 Oflx molecules/NP is 0.026 ± 0.003 µM Oflx (Figure 13G), showing the lowest MIC$_{50}$ and the highest inhibitory effects among the nanocarriers and free Oflx. We summarize MIC$_{50}$ of free Oflx and drug nanocarriers in Table 2. The results show the significant dependence of inhibitory effects of Oflx upon the dose of Oflx and the size of nanocarriers.

It is noteworthy that the MIC$_{50}$ of conjugated Oflx show significant size dependence. The largest size (92.6 ± 4.4 nm) nanocarriers exhibit the lowest MIC$_{50}$ and

the highest inhibitory effects among the nanocarriers and free drug Oflx. In other words, the same amount of Oflx molecules loaded and delivered via the largest NPs (92.6 ± 4.4 nm) is the most potent, followed by 13.0 ± 3.1 nm nanocarriers, free Oflx and 2.4 ± 0.7 nm nanocarriers (Table 2). The MIC_{50} of conjugated Oflx of 2.4 ± 0.7 nm nanocarriers is 2.2 times higher than that of free drug Oflx. In contrast, the MIC_{50} of conjugated Oflx of 13.0 ± 3.1 nm and 92.6 ± 4.4 nm nanocarriers are 1.8 times and 5.5 times lower than that of free Oflx. These findings suggest that the densely loaded Oflx on the larger nanocarriers could enhance binding affinity with the target (multivalence) and contribute to higher local drug concentration compared with those Oflx molecules on the smaller nanocarriers. Notably, the MIC_{50} of free Oflx and conjugated Oflx in Table 2 indicates that the inhibitory effects of drug nanocarriers significantly depend on their sizes but not in a linear manner, which suggests the tradeoff between the distribution of the same amount of the drugs throughout the cells (pharmacodynamics) and localization of the same amount of loaded on individual nanocarriers (high affinity) could contribute to their inhibitory effects. Free drug Oflx and conjugated Oflx on the smaller nanocarriers (2.4 ± 0.7 nm) possibly distribute inside the cells better than the drugs loaded with the larger nanocarriers (13.0 ± 3.1 nm and 92.6 ± 4.4 nm) while the larger nanocarriers offer the higher local drug concentration and the better drug binding affinity with the target sites than the smaller nanocarriers. Considering the combination of drug distribution and multivalence factors, a critical size of nanocarriers is required to enhance and maximize antibiotic potency against pathogenic bacterial cells.

Interestingly, the inhibitory effects of free drug ofloxacin and conjugated Oflx in antibiotic drug nanocarriers against *E. coli* cells follow the same trend as those against *P. aeruginosa* (WT and ΔABM).[46] We previously reported that the MIC_{50} of free drug Oflx and conjugated Oflx on 2.4 ± 0.7, 13.0 ± 3.1 and 92.6 ± 4.4 nm nanocarriers against were 0.59 ± 0.16, 1.00 ± 0.07, 0.40 ± 0.06 and 0.11 ± 0.01 μM, respectively.[46] For the same amount of Oflx molecules carried and delivered by the largest NPs (92.6 ± 4.4 nm) are the most potent, followed by 13.0 ± 3.1 nm nanocarriers, free drug Oflx, and 2.4 ± 0.7 nm nanocarrier. The MIC_{50} of Oflx varies in different bacterial strains because Oflx antibiotic potency could depend upon several factors including the membrane

permeability of the drug and the ability of the cells to extrude the drug out of the cells.[16, 50] Notably, we have studied efflux function of multidrug ABC (MsbA) membrane transporters using these three-sized drug nanocarriers as imaging probes and found that the efflux pumps could extrude all the sized nanocarriers. [35-37] The cells could extrude the smaller nanocarriers more effectively, leading to the least inhibitory effects. In contrast, the cells could not extrude the largest nanocarriers out of single live cells as effectively as smaller NPs. The extrusion of conjugated Oflx of the largest nanocarriers could affect the MIC_{50} of the largest nanocarriers the most similar to results from our previous study.[46] These observations emphasize that the inhibitory effects could be attributed to the interplay among various factors, including multivalence effects, drug distribution, and extrusion of Oflx molecules.

Filamentation Induced by Ofloxacin in *E. coli*

Ofloxacin is a broad-spectrum antibiotic in the fluoroquinolone family commonly used to treat infections of the skin, bladder and urinary tract.[51] The molecular target is DNA gyrase (topoisomerase II) which is a crucial bacterial enzyme catalyzing the negative supercoiling of double stranded DNA during cell replication resulting in DNA double-strand breaks (DBSs).[51] Processing of DBSs induces the SOS response (DNA repair mechanism) in *E. coli*, leading to a cascade of events such as filamentation.[52-54] Generally, β-lactam antibiotics are reported to induce filamentous cells initiation by inhibiting penicillin-binding protein which terminate the formation of the peptidoglycan network in the bacterial cell wall.[52, 55] The fluoroquinolones possibly induce peptidoglycan degradation causing filamentous cells by partially inactivating D-alanine carboxypeptidases, enzymes that are suggested to regulate the extent of peptide side-chain cross-linking in peptidoglycan.[52, 56]

In addition to measuring $OD_{600\ nm}$, we sampled the cells incubated with a series of free drug Oflx, each given sized antibiotic drug nanocarriers (AgMUNH-Oflx NPs) and the same size of AgMUNH2 NPs (no conjugated Oflx, control experiment) in test tubes to image using dark-field microscopy. Representative images of the cells incubated with
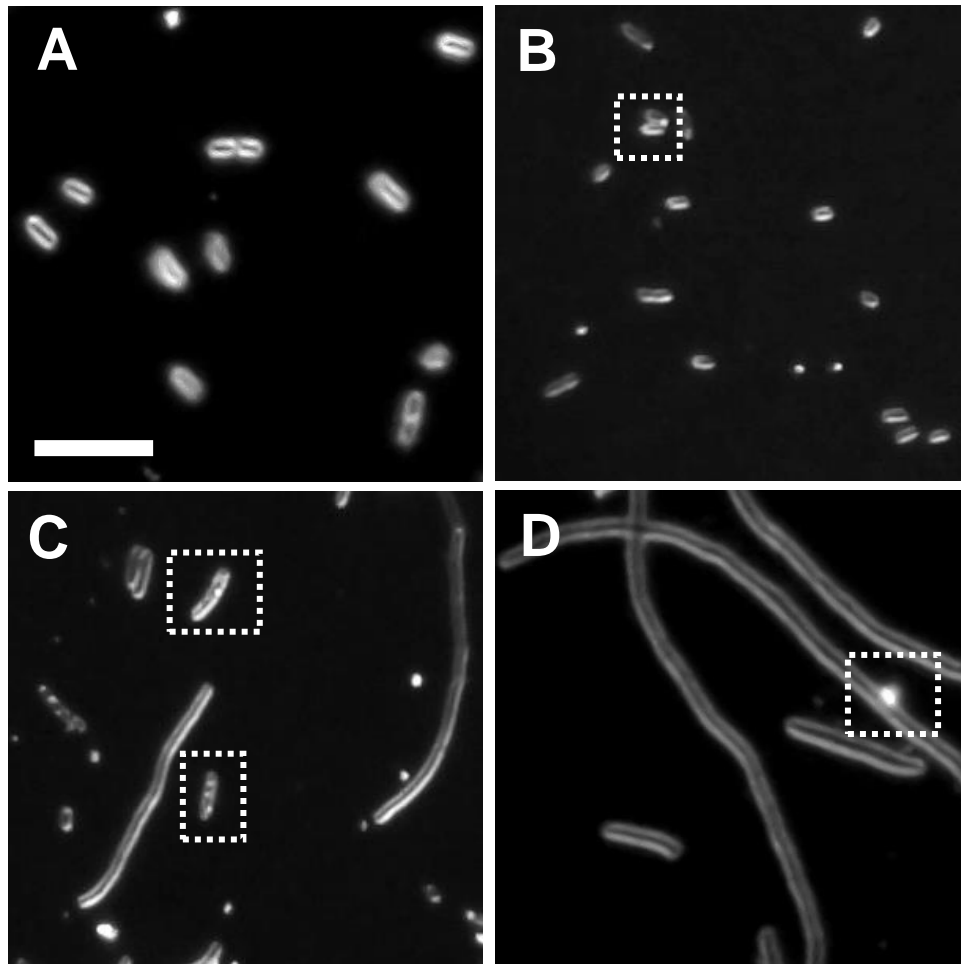
Figure 14. Study of cellular filamentation induced by ofloxacin in single *E. coli* (MsbA) cells.

Dark-field optical images of single *E. coli* (MsbA) cells cultured for 18 h in the modified LB medium containing (A) 0 and (B-D) 0.045 µM Oflx in antibiotic drug nanocarriers with diameters of NPs (B) 2.4 ± 0.7, (C) 13.0 ± 3.1 and (D) 92.6 ± 4.4 nm, show that the inhibitory effects of the antibiotic drug nanocarriers depends upon the sizes of the nanocarriers. Antibiotic drug nanocarriers attach to the cells and the larger size of the antibiotic drug nanocarriers demonstrate higher efficacy of ofloxacin to target DNA gyrase during cell replication as the cells treated with conjugated Oflx carried by the larger nanocarriers (C and D) showed less numbers of cells and extensive cellular filamentation. The scale bar is 10 µm.

(Figure 14A) 0 (control) and (Figure 14B-D) 0.045 µM conjugated Oflx from antibiotic drug nanocarriers with diameters of NPs (b) 2.4 ± 0.7, (c) 13.0 ± 3.1 and (d) 92.6 ± 4.4 nm, respectively showed that the inhibitory effects of the antibiotic drug nanocarriers upon the growth of *E. coli* (MsbA) cells are associated with the sizes of the nanocarriers. The same amount of Oflx delivered into the cells using the largest nanocarriers is the most potent since the cells exposed 92.6 ± 4.4 nm antibiotic drug nanocarriers, vice versa (Figure 14) demonstrate cellular filamentation indicating the inhibitory action of Oflx.

SUMMARY

We have successfully synthesized, purified and characterized three different sized Ag NPs with a diameter of 2.4 ± 0.7, 13.0 ± 3.1 and 92.6 ± 4.4 nm, then functionalized them with a monolayer of $MUNH_2$ to prepare $AgMUNH_2$ NPs and then covalently conjugated with Oflx molecules to prepare antibiotic drug nanocarriers (AgMUNH-Oflx NPs). The antibiotic drug nanocarriers at desired concentrations are stable (non-aggregation) in a modified LB medium over time of cell culturing. We have studied the dependence of bacterial inhibitory effects of free drug Oflx and conjugated Oflx on the dose of Oflx and the size of nanocarriers against *E. coli*. Notably, we have found that the MIC_{50} of free drug Oflx and conjugated Oflx significantly depend on the dose of Oflx and the size of nanocarriers. The largest nanocarriers (92.6 ± 4.4 nm) show the highest inhibitory effects with the lowest MIC_{50} (0.026 ± 0.003 µM) while the smallest nanocarriers (2.4 ± 0.7 nm) exhibit the lowest bactericidal inhibitory with the highest MIC_{50} (0.314 ± 0.010 µM) against *E. coli*. These results demonstrate that inhibitory potency of the same amount of Oflx molecules could substantially elevate when they are carried and delivered via the larger nanocarriers, suggesting that the densely loaded Oflx molecules (multivalence) augment membrane binding affinity and increase local drug concentrations. Interestingly, the inhibitory effects of drug nanocarriers are dose dependent but not linearly proportional to their sizes indicating that the tradeoff between the multivalence effects and their intracellular distribution (pharmacodynamics) could contribute to their inhibitory effects. In addition, we have

found that Oflx molecules can cause cellular filamentation resulting from the unsuccessful cell division. Conjugated Oflx delivered by the largest nanocarriers effectively induce filamentous cells confirming that the largest nanocarriers significantly increase drug efficacy. Moreover, the MICs of free drug Oflx and conjugated Oflx in antibiotic drug nanocarriers are size-dependent in both *E. coli* and *P. aeruginosa* (WT) which for the same amount of Oflx molecules carried and delivered by the largest NPs (92.6 ± 4.4 nm) are the most potent, followed by 13.0 ± 3.1 nm nanocarriers, free drug Oflx, and 2.4 ± 0.7 nm nanocarriers. Altogether, inhibitory effects of Oflx exhibit high dependence on the dose of Oflx and the sizes of nanocarriers. Thus, these new findings provide the potentials to design optimal drug nanocarriers to achieve the maximum antibiotic potency and overcome MDR in pathogenic bacterial infections.

MATERIALS AND METHODS

Reagents and Cell Line

We purchased silver nitrate (99.9%, Sigma-Aldrich), sodium citrate dehydrate (99%, Sigma-Aldrich), sodium borohydride (98%, Sigma-Aldrich), hydrogen peroxide (30%, Sigma-Aldrich), polyvinylpyrrolidone (PVP, Sigma-Aldrich), 2-mercaptoethanol (99%, Sigma-Aldrich), 11-amino-1-undecanethiol hydrochloride (AUT, 99%, Sigma-Aldrich), ofloxacin powder (99%, Sigma-Aldrich), sodium chloride, sodium phosphate (Sigma-Aldrich), sodium phosphate monobasic monohydrate (Sigma-Aldrich), bacto-tryptone and bacto yeast extract (Sigma-Aldrich). We purchased 1-Ethyl-3-[3-dimethylaminopropyl]-carbodiimide hydrochloride (EDC, 99%, Pierce) and N-hydroxysulfosuccinimide (Sulfo-NHS, 98.5%, Pierce). We purchased silver perchlorate monohydrate (99%, Alfa Aesar), Live/dead backlight viability assay (Life Technologies) and Hoechst 33342 (Life Technologies). We used all reagents as received. We used the nanopure deionized (DI) water (18 MΩ water, Barnstead) to rinse glassware and prepare all solutions including standard LB medium (1% tryptone peptone, 0.5% yeast extract, and 0.5% NaCl, pH = 7.2) and modified LB medium (1% tryptone peptone, 0.5% yeast extract, and 0.1% NaCl, pH = 7.2). We purchased cell line of *Escherichia coli*, WT w3110 (MsbA) from Coli Genetic Stock Center (CGSC).

Synthesis and Characterization of Ag NPs

We had synthesized, purified and characterized three different sized Ag NPs with diameters of (2.4 ± 0.7), (13.0 ± 3.1) and (92.6 ± 4.4) nm, as we reported previously.[25-26, 42-45, 57] Briefly, we synthesized Ag NPs with diameters of 2.4 ± 0.7 nm by adding $NaBH_4$ (150 μL, 100 mM) into a stirring mixture (42.3 mL) of silver nitrate (0.11 mM), sodium citrate (1.91 mM), PVP (0.052 mM), and hydrogen peroxide (25.0 mM) that were freshly prepared using nanopure water.[43] We stirred the solution at room temperature for another 3 h and filtered the solution using 0.2 μm membrane filters. We prepared Ag NPs with diameters of 13.0 ± 3.1 nm by rapidly adding ice-cold $AgClO_4$ (2.5 Ml, 10 mM) into a stirring ice-cold mixture (247.5 mL) of sodium citrate (3 mM) and $NaBH_4$ (10 mM).[27, 58] We stirred the solution at room temperature for 4 h, and filtered it using 0.2 μm filter. We synthesized (92.6 ± 4.4) nm Ag NPs by adding sodium citrate (10 mL, 34 mM) into a refluxing (100°C) aqueous solution of 3.98 mM $AgNO_3$ (500 mL).[25, 59] We stirred the mixtures at 325 rpm for 35 min, and cooled the solution to room temperature. We then added additional 2.5 mM sodium citrate as a stabilizer into the solution, and filtered the solution using 0.2 μm filter.[46]

We purified each NP solution by thoroughly washing the NPs three times with the DI water using centrifugation immediately after the synthesis. We characterized the NP concentrations, the LSPR images and spectra of single NPs, and sizes of single NPs using UV-vis spectroscopy (Hitachi U-2010), dark-field optical microscopy and spectroscopy (DFOMS), high-resolution transmission electron microscopy (HRTEM) (JEOL, JEM-2100F), and dynamic light scattering (DLS) (Nicomp 380ZLS particle sizing system), respectively.[46] We have fully described our DFOMS in our previous studies.[9, 12, 14, 26-28, 31, 43, 58, 60-62] In this study, the DFOMS is equipped with a dark-field optical microscope with a dark-field condenser (oil 1.43–1.20, Nikon) and a 100× objective (Nikon Plan fluor 100× oil, iris, SL. N.A. 0.5–1.3, W.D. 0.20 mm), a CCD camera (Micromax, Roper Scientific) and a Multispectral Imaging System (Nuance, CRI).[43, 62]

Synthesis and Characterization of Drug Nanocarriers (AgMUNH-Oflx NPs)

We added AUT (1 mL, 100 mM, in ethanol) into the freshly prepared Ag NPs (100 mL, 50 nM, 3.3 nM and 30 pM) of three different sized Ag NPs (2.4 ± 0.7, 13.0 ± 3.1 and 92.6 ± 4.4 nm), respectively. We stirred the mixtures for 24 h to attach AUT onto the surface of NPs via the interaction of thiol groups with the NPs to prepare functional $AgMUNH_2$ NPs (Figure 2). We washed the $AgMUNH_2$ NPs thoroughly three times with nanopure water to remove excess AUT using centrifugation (Beckman Optima L90k, 4°C). After each washing and re-suspension step, we immediately characterized the concentrations, optical properties and sizes of each $AgMUNH_2$ NP solution using UV-vis spectroscopy, DFOMS and DLS, respectively. Note that the $AgMUNH_2$ NPs were suspended in DI water for the storage, and only suspended in the respective buffer right before the experiment.

We suspended the half of purified $AgMUNH_2$ NPs solution (50 mL) in the PBS buffer (pH 7.0) right before control experiment. We suspended the other half of $AgMUNH_2$ NPs solution (50 mL) in the MES buffer (50 mM, pH 5.0) right before conjugating them with Oflx. We conjugated the amine groups of each sized $AgMUNH_2$ NPs (50 mL) with the carboxyl group of Oflx via peptide bonds using a two-step method with EDC and s-NHS as mediators (Figure 6), as described in the following. We first dissolved Oflx in 0.5 M HCl (1 mL) and then diluted it using MES buffer (pH 5.0). We added the EDC (100 μL, 100 mM) and s-NHS (100 μL, 500 mM) into the Oflx solution (3 mL, 50 mM), and stirred it at room temperature for 40 min, to form Oflx-s-NHS esters. We added 2-mercaptoethanol to quench the excess EDC. We added the Oflx-s-NHS esters to the $AgMUNH_2$ NPs in the MES buffer (pH 5.0) and well mixed the solution using a rotary shaker at room temperature for 3 h, to synthesize the AgMUNH-Oflx NPs (nanocarriers).

We purified the drug nanocarriers (AgMUNH-Oflx NPs) by washing them with DI water three times, and stored them at 4°C for the future use. After each washing, we immediately characterized the concentrations, optical properties and sizes of $AgMUNH_2$ NPs using UV-vis spectroscopy, DFOMS and DLS, respectively. We measured the UV-

vis absorbance spectra of various concentrations of nanocarriers (AgMUNH-Oflx NPs), and plotted the peak absorbance of the nanocarriers versus their concentration to construct a calibration curve and determine their molar absorptivity.

We measured the UV-vis absorbance spectra of various concentration of Oflx alone (absence of NPs) in the solution, and plotted the peak absorbance at 288 nm versus Oflx concentration to construct a calibration curve and determine its molar absorptivity ($\varepsilon_{288\ nm} = 7.8 \times 10^3$ $M^{-1}cm^{-1}$ and $\varepsilon_{330\ nm} = 2.4 \times 10^3$ $M^{-1}cm^{-1}$). We subtracted UV-vis absorption spectra of AgMUNH$_2$ NPs from that of the same sized and concentration of AgMUNH-Oflx NPs to obtain UV-vis absorption spectra of Oflx conjugated with the AgMUNH$_2$ NPs and used molar absorptivity of Oflx to determine its concentration. We also determine the NP concentration based upon the peak absorbance of the plasmonic absorption spectra of the NPs. By dividing the concentration of Oflx with concentration of NPs in the same AgMUNH-Oflx NPs solution using UV-vis absorption spectroscopy, we determined conjugation ratios of Oflx molecules with the NPs for each sized drug nanocarrier.

Study of Stability of Drug Nanocarriers (AgMUNH-Oflx NPs) in Cell Culture Medium

We characterized the stability (non-aggregation) of AgMUNH-Oflx NPs in the commonly used standard LB medium (1% tryptone, 0.5% yeast extract and 0.5% NaCl in DI water, pH = 7.2) and the modified medium (1% tryptone, 0.5% yeast extract and 0.1% NaCl in DI water, pH = 7.2) over 24 h using UV-vis absorption spectroscopy. We found that the nanocarriers with the diameters of Ag NPs of (2.4 ± 0.7, 13.0 ± 3.1 and 92.6 ± 4.4 nm) at a desired concentration (6.0 nM, 0.8 nM and 7 pM) are stable (non-aggregated) in the modified medium over 24 h, but they are unstable (aggregated) in the standard medium, respectively.

Cell Line, Cell Culture Medium, Cell Culture and Characterization

Gram-negative *E. coli* (MsbA) strain was cultured in the standard and the modified LB medium and the cell growth was studied. We first pre-cultured the cells in a standard LB medium in an incubated floor shaker (Thermo Scientific, MaxQ5000) (160 rpm, 37 °C) for 12 h. We then cultured the cells in either the standard LB medium or the modified LB mediums in the incubated floor shaker (160 rpm, 37 °C) for another 8 h. We followed the cell growth in each medium over time and characterized the cell growth curves by measuring $OD_{600\ nm}$ of cell suspension in every 30 min for over 8 h. Furthermore, we studied viability of the cultured cells at the end of the experiment at a single cell resolution using LIVE/DEAD *Bac*Light viability and counting assay.[63] We imaged cells in the micro-chamber using dark-field optical microscopy and epi-fluorescence microscopy and counted the green fluorescence cells (peak wavelength of fluorescence spectra of SYTO9, λ_{max} = 520 nm) and the red fluorescence cells (peak wavelength of fluorescence spectra of propidium iodide, λ_{max} = 610 nm) as live and dead cells, respectively.

By the end of the cell culture, we studied cell efflux function using time course of fluorescence dye accumulation in intact cells overtime. We harvested the cells using centrifugation (Beckman Model J2-21 Centrifuge, JA-14 rotor, at 7500 rpm, 23 °C, 10 min), washed the cells with the PBS buffer (0.5 mM phosphate buffer, 1.5 mM NaCl, pH 7.2) for three times, and finally re-suspended the cells in the buffer. The final concentration of the cells was adjusted to $OD_{600\ nm}$ = 0.1.[9, 28, 31, 60, 64] Time-dependent fluorescence intensity of Hoechst 33342 (0.5 µM) incubated with cells with a presence and an absence of orthovanadate (25 µM) was measured at a 10-s data acquisition interval in real time using a fluorescence spectrometer (Cary Eclipse). The excitation and emission wavelengths were 354 and 478 nm, respectively.

Study of Inhibitory Effects of Drug Nanocarriers (AgMUNH-Oflx NPs)

We cultured the cells (10^4 pre-cultured cells) in the modified LB medium (2.5 mL) containing a dilution series of ofloxacin alone and a conjugated ofloxacin from given

sized antibiotics drug nanocarriers and incubated the cells in an incubated floor shaker (Thermo Scientific, MaxQ5000) with vigorous shaking (200 rpm, 37ºC) over 18 h.

The dilution series consist of 0, 0.045, 0.09, 0.18, 0.38 and 0.68 µM of free drug Oflx or conjugated Oflx from the nanocarriers, which is corresponded to the concentrations of nanocarriers (NP concentrations): (i) 5.21×10^{-2}, 0.104, 0.209, 0.440, and 0.788 nM for NPs with a diameter of 2.4 ± 0.7 nm with the ratio of 8.6×10^2 Oflx molecules per NP; (ii) 4.77×10^{-3}, 9.54×10^{-3}, 1.91×10^{-2}, 4.03×10^{-2} and 7.21×10^{-2} nM for NPs with a diameter of 13.0 ± 3.1 nm with the ratio of 9.4×10^3 Oflx molecules per NP; (iii) 6.89×10^{-2}, 0.138, 0.276, 0.582 and 1.04 pM for NPs with a diameter of 92.6 ± 4.4 nm with the ratio of 6.5×10^5 Oflx molecules per NP. In addition, control experiments included the modified LB medium alone (No cells) and the cells, which were cultured at the same time and under the same conditions as samples, incubated with the modified LB medium containing 0.788 nM, 7.21×10^{-2} nM and 1.04 pM $AgMUNH_2$ NPs (in the absence of Oflx) with a diameter of Ag NPs of 2.4 ± 0.7, 13.0 ± 3.1 and 92.6 ± 4.4 nm, respectively.

The cell solutions were sampled every 6 h and quantitatively determined the bacterial cell concentration by measuring $OD_{600\ nm}$ in a 96-well plate using a plate reader (BioTek SynergyHT) equipped with an UV-vis absorption spectral detector. We plotted $OD_{600\ nm}$ of the cell suspension over time to determine the time (18 h) for the cells reached their confluence. Thus, we used the $OD_{600\ nm}$ of each cell suspension at 18 h to determine the inhibitory effects of the free drug Oflx and conjugated Oflx as described in the following.

The $OD_{600\ nm}$ of each cell suspension was normalized with the maximum $OD_{600\ nm}$ (the cells cultured in the medium alone, blank control) among the dilution series of the cell suspensions for each type of samples (e.g., free Oflx, each sized nanocarriers), respectively. We then plotted the normalized $OD_{600\ nm}$ of the cell suspension versus the concentration of free drug Oflx (Oflx alone) or concentration of Oflx conjugated with a given sized drug nanocarrier to determine the MIC_{50} of Oflx. We repeated each experiment three times and plotted the average of three experimental measurements for

each sample with a standard deviation of the normalized $OD_{600\ nm}$ of each cell suspension (points in Figure 13). We fitted the points using the exponential decay ($y = a*e^{-bx}$, inhibitory effects upon the exponential cell growth) to determine the parameters (***a, b***) of the equation with the highest possible regression. The equation was then used to determine the MIC_{50} (the concentration of Oflx at which the cell growth was inhibited to the half of the cell growth of the blank control experiment), as described in Figure 13 caption. The points in Figure 13 are experimental data and a solid line is generated by fitting the experimental data with an equation ($y = a*e^{-bx}$) as followings: (D) $y = 1.12\ e^{-5.57x}$, $R^2 = 0.944$; (D) $y = 1.12\ e^{-2.56x}$, $R^2 = 0.928$; (F) $y = 1.08\ e^{-9.58x}$, $R^2 = 0.941$; (G) $y = 1.01e^{-26.7x}$, $R^2 = 0.988$. Concentrations of Oflx (MIC, IC_{50}) for free Oflx and Oflx conjugated with a given sized nanocarrier were determined using the exponential fitting equation at the half of the maximum normalized $OD_{600\ nm}$ for each curve, respectively. The "a" and "b" in the equation for each sample were determined based upon the best fitting (the highest regression with the lowest error). As a control experiment, we also plotted the normalized $OD_{600\ nm}$ of the cell suspension at 18 h versus the concentration of $AgMUNH_2$ NPs (absence of Oflx) that is the same as the highest concentration of the given nanocarrier for each cell strain.

In addition to measuring $OD_{600\ nm}$, we sampled the cell solutions every 6 h and prepare cells in a micro chamber for imaging using DF microscope to observe cell morphologies. We took five representative locations of each sample.

Data Analysis and Statistics

We characterized sizes and shapes of Ag NPs using TEM, and LSPR spectra of single Ag, $AgMUNH_2$, and AgMUNH-Oflx NPs using DFOMS.[46] We imaged at least 100 NPs for each size and type of NPs per measurement and repeated each experiment three times for each individual size. Therefore, a minimal of 300 NPs was characterized using TEM and DFOMS.[46] We ran experiments including the study of stability of NPs in the medium, cell growth curves, and determination of drug inhibitory effects three times on each concentration and for each size of antibiotic drug nanocarriers. We used average of three measurements with standard deviations for each study.

CHAPTER III

SINGLE ANTIBIOTIC NANOCARRIER OPTICAL PROBES FOR STUDY OF SUBSTRATE-DEPENDENT EFFLUX FUNCTION OF MULTIDRUG ABC MEMBRANE TRANSPORTERS IN SINGLE LIVE *ESCHERICHIA COLI* CELLS

INTRODUCTION

The ATP-binding cassette (ABC) membrane transporters (efflux pumps) are highly conserved proteins existing in a variety of prokaryotes and eukaryotes.[1-3] They use the energy of ATP binding and hydrolysis to transport a large number of structurally and functionally unrelated substrates across biological membranes.[1-3] Multidrug ABC transporters can extrude antibiotics out of bacterial cells and chemotherapeutic agents from cancer cells (e.g., P-glycoproteins, Pgp) resulting in multidrug resistance (MDR) and the failure of numerous treatments of infections and cancers.[2-4] All ABC transporters share a similar modular topology including two transmembrane domain (TMD) and two nucleotide binding domain (NBD).[1, 3, 7-8] The TMDs, which contain the large diversity of selective substrate binding sites, form the transmembrane channel for substrates to cross the membrane whereas the NBDs, which are a hallmark of this transporter and more highly conserved, couple conformational changes induced by ATP hydrolysis leading to the extrusion of the substrates out of the cells against concentration gradients across the cellular membrane.[1, 3, 7-8] This process is called as efflux function.

MsbA, an essential homodimeric (2 x 65 kDa) ABC membrane transporters in Gram-negative bacteria (e.g., *Escherichia coli*), shares structural and functional similarities and is the most closely to Pgp which is a multidrug ABC membrane transporter found in cancer cells.[1, 5] Its primary function is translocation of lipid A and lipopolysaccharide (LPS) from the cytoplasmic leaflet (inward-facing) to the periplasmic leaflet (outward-facing) of bacterial inner membrane using ATP hydrolysis as an energy source.[1-2, 5, 8, 40] Functional studied have also shown that MsbA can recognize and extrude a wide variety of drug spectrums and confers resistance to certain antibiotics.[1,

[10, 65] MsbA is an ATPase which is stimulated by substrates, such as lipid A, LPS and multiple drugs, and it is inhibited by orthovanadate (Na$_3$VO$_4$).[40] Adenosine diphosphate (ADP) is stably trapped in the active site, with orthovanadate occupying the position of the gamma phosphate. The orthovanadate appears to interact with five oxygen mimicking the gamma phosphate during the transition state for ATP hydrolysis.[66-67] Notably, ATPases are involved in various cellular processes, such as intracellular transports and DNA replication making them attractive targets for drug discovery. Currently, a number of ATPase inhibitors are in clinical trials. For example, Tariquidar (XR9576) is a Pgp inhibitor that is administrated in a combination with chemotherapeutic agents such as doxorubicin, docetaxel or vinorelbine.[68-69]

Despite the increasing number of available crystal and cryo-EM structures of ABC transporters, many questions related to the molecular basis of the transport mechanisms involving in substrate recognition, translocation and coupling to ATP hydrolysis are still elusive. [1-2, 7-8] One of the most interesting questions is how ABC transporters extrude numerous structurally unrelated hydrophobic and amphipathic compounds out of the cells. The identification of the drug-binding sites in Pgp found at the interface between the TMDs, suggests a large and flexible drug-binding cavity that can accommodate multiple substrates via interactions with aromatic and hydrophobic residues.[3, 70] We hypothesize that individual efflux pumps might process a substrate sensing machinery which can specifically recognize a given noxious pump substrate (e.g., antibiotics and chemotherapeutic agents) and extrude it out of the cells, underscoring the importance of characterization of efflux function in single live cells in real time. Although X-ray crystallography and cryo-EM are the primary techniques to depict the structures of membrane transporters at the atomic resolution,[2, 71-73] unfortunately they cannot provide real-time dynamic insights into how the efflux pumps selectively recognize and interact with structurally unrelated substrates and then translocate membrane transporters to extrude the substrates out of the cells.[2, 71-73]

Conventional methods for the study of transport efflux kinetics in bulk bacterial cells include the use of radioisotopes (^{14}C and ^{3}H) or fluorophores (ethidium bromide and Hoechst dye) as probes to measure accumulation of substrates in the cells.[9-12]

Study of the accumulation kinetics of bulk could have masked rare interesting events as individual cells act differently and their efflux kinetics are unsynchronized.[13-14] Therefore, it is important to probe efflux kinetics of individual membrane transporters in single live cells in real time.[13-14] Moreover, radioisotopes or fluorophores are unable to measure sizes of substrates and membrane transporters as they lack of distinctive size-dependent physicochemical properties. Thus, these conventional probes are not suitable to serve as various size-dependent pump substrates for the study of efflux function of single membrane transporter in single live cells in real time.

Noble metal nanoparticles (e.g., silver nanoparticles, Ag NPs) possess distinctive size-dependent photostable plasmonic optical properties which highly depend on their sizes, shapes, dielectric constants and surrounding environments.[23-24, 74] These features enable us to image and determine the sizes of single NPs at the nanometer (nm) resolution in real time using dark-field optical microscopy and spectroscopy (DFOMS).[9, 13-14, 29, 43, 58-59, 61-62, 75-77] Furthermore, we have demonstrated that we can use size-dependent localized surface plasmon resonance (LSPR) spectra and size-dependent scattering intensity of single Ag NPs as photostable optical probes which mimic various sizes of antibiotics to study the size-dependent efflux kinetics of multidrug membrane transporters in single live cells in real time.[9, 13-14, 29] Moreover, we have functionalized Ag NPs with biocompatible peptides and studied the dependence of efflux function of single BmrA membrane transporters in *Bacillus subtilis* (Gram-positive bacteria) upon charged substrates.[13]

We synthesized, purified and characterized antibiotic drug nanocarriers (2.4 ± 0.7 nm AgMUNH-Oflx NPs) by functionalizing nanocarriers (AgMUNH$_2$ NPs) with antibiotics (Ofloxacin, Oflx) to have 8.6×10^2 Oflx molecules per NP, as described previously.[46] We found that the AgMUNH-Oflx NPs exhibited inhibitory effects whereas the AgMUNH$_2$ NPs did not show significant inhibitory effects on the cell growth.[46] In this study, due to distinctive LSPR spectra of Ag NPs (color), we used the AgMUNH-Oflx NPs (antibiotic drug nanocarriers) and the AgMUNH$_2$ NPs (control nanocarriers without drug) as powerful imaging probes aiming to study substrate-dependent efflux function of single MsbA membrane transporters in single live *E. coli* cells to observe whether

curtain types of substrates play a key role in the selective extrusion of efflux pumps and to determine the pore size of the transporters. This study offers a possibility to address how the structurally similar membrane transporters could selectively extrude a plethora of structurally unrelated substrates. To our knowledge, study of efflux function of MsbA transporters in single live *E. coli* cells using such small sized drug nanocarriers has not yet been reported. It remains elusive whether the MsbA possesses substrate-dependent efflux function. Better understanding of efflux mechanisms of multidrug membrane transporters could provide new insights into rational designs of drugs or drug carriers to improve drug efficacy and avoid MDR.

RESULTS AND DISCUSSION

Real-time Probing of Efflux Kinetics of Membrane Transporters Using Single Antibiotic Drug Nanocarriers

We suspended the cells in a PBS buffer (0.5 mM phosphate buffer saline with 1.5 mM NaCl, pH = 7.0) rather than in cell culture medium. The cells grow and divide in the cell culture medium leading to the change of cell concentration and cellular growth stages over time. This makes results incomparable with other experiments.[9, 13-14, 29-30] Consequently, we incubated bacterial cells in the PBS buffer at a given concentration and a certain growth stage with given concentrations of pump substrates (e.g. fluorescence dyes or Ag NPs) to determine the dependence of substrate accumulations and efflux kinetics of membrane transporters in a given cell strain.[9, 13-14, 29-30] We incubated the cells ($OD_{600 \text{ nm}}$ = 0.7) with 2.4 ± 0.7 nm AgMUNH-Oflx NPs (antibiotic drug nanocarriers) or the $AgMUNH_2$ NPs (control nanocarriers without drug) and then tracked single nanocarriers in and out of single live cells in real time using DFOMS. Representative dark-field optical images of the single live *E. coli* cells (MsbA-WT) (Figure 15, 16: A) with single intracellular and extracellular nanocarriers as boxed show cross-sections of single rod-shaped bacterial cells with 2 μm in length and 0.5 μm in width. As described previously, [9, 12-14, 29-30, 75] the cell membranes above and below the focal plane (190 nm depth of field) become invisible under dark-field illumination because they are out of the focal plane of the dark-field microscope, allowing us to

image thin-layer cross sections of single bacterial cells and track single nanocarriers on the thin-layer membrane section.

The illumination of dark-field microscopy requires to pass into the cellular membrane to radiate the intracellular NPs and scattering of intracellular NPs must be transmitted through the membrane to reach the detector. The cellular membrane absorb photon causing a dimmer intensity of intracellular NPs (Figure 15B, 16B: a). Moreover, as intracellular NPs are located inside the cell membrane, they are out of the focus plane and appear blurry. On the other hand, scattering of extracellular NPs is a combination of the scattering intensity of NPs and the cell membrane leading to a higher scattering intensity and brighter images (Figure 15B, 16B: b). We have shown that these distinctive properties and scattering intensity of NPs are practical to distinguish intracellular NPs and extracellular NPs in the study of efflux function of multidrug membrane transporters in real time.[9, 13-14, 28-30] In this study, we use this validated approach to determine intracellular and extracellular NPs. Intracellular AgMUNH-Oflx NPs (Figure 15B: a) and AgMUNH$_2$ NPs (Figure 16B: a) are dimmer, blurry and exhibit a lower scattering intensity than extracellular AgMUNH-Oflx NPs (Figure 15B: b) and AgMUNH$_2$ NPs (Figure 16B: b). The representative LSPR spectra of single AgMUNH-Oflx NPs (i – iii) in Figure 15C show the peak wavelength and full-width-at-half-maximum (FWHM) at 524 (85), 535 (101), and 550 (123) nm, respectively. In addition, the representative LSPR spectra of single AgMUNH$_2$ NPs (i – iii) in Figure 16C show the peak wavelength and FWHM at 531 (109), 551 (109), and 538 (104) nm, respectively. These distinctive LSPR spectra of single NPs (Figure 15, 16: C) enable us to effectively identify NPs from other cellular debris and other substances which lack of plasmonic properties, therefore they appear white under dark-field illumination.[9, 13-14, 29-30] Notably, individual Ag NPs process unique LSPR spectra depending on their sizes, shapes and surrounding environment enable us to use single Ag NPs as individual imaging probes.[23-24, 43]
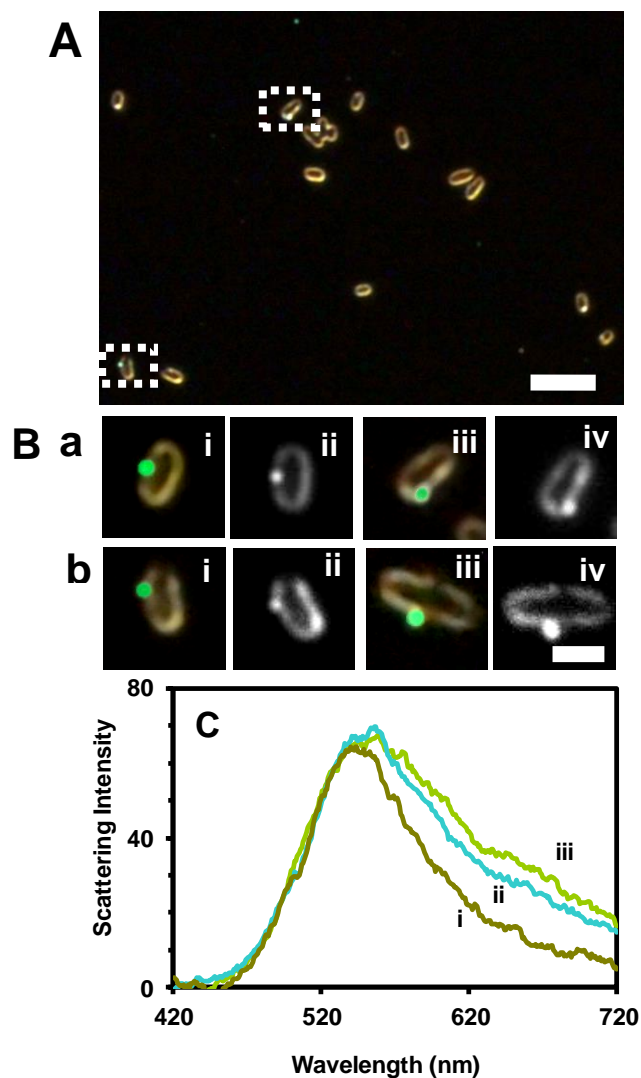
Figure 15. Imaging of single intracellular and extracellular 2.4 ± 0.7 nm AgMUNH-Oflx NPs in single living bacterial cells using DFOMS.

(A) The representative optical image of bacterial cells incubated with 1.4 nM AgMUNH-Oflx NPs showing intracellular and extracellular NPs as squared. (B) Zoom in optical color (i and iii) and CCD (ii and iv) images of single cells show (a) intracellular and (b) extracellular NPs which are pseudo colored in color images. The scale bar in A and B are 10 and 2 μm, respectively. (C) LSPR spectra of representative single 2.4 ± 0.7 nm AgMUNH-Oflx NPs (i-iii) show peak wavelengths and full width at half maximum (FWHM) at 524 (85), 535 (101), and 550 (123) nm, respectively.
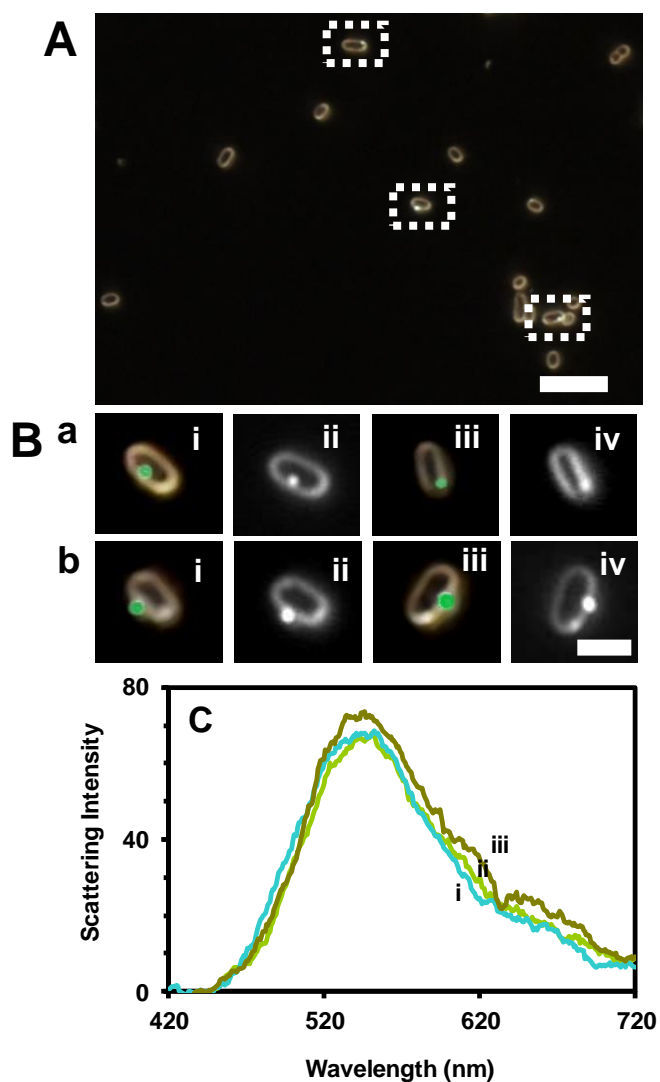
Figure 16. Imaging of single intracellular and extracellular 2.4 ± 0.7 nm AgMUNH$_2$ NPs in single living *E. coli* cells using DFOMS.

(A) The representative optical image of bacterial cells incubated with 1.4 nM AgMUNH$_2$ NPs showing intracellular and extracellular NPs as squared. (B) Zoom optical color (i and iii) and CCD (ii and iv) images of single cells show (a) intracellular and (b) extracellular NPs which are pseudo colored in color images. The scale bar in A and B are 10 and 2 μm, respectively. (C) LSPR spectra of representative single 2.4 ± 0.7 nm AgMUNH$_2$ NPs (i-iii) show peak wavelengths and full width at half maximum (FWHM) at 531 (109), 551 (109), and 538 (104) nm, respectively.

We found that the peak wavelength of the $AgMUNH_2$ NPs are at the longer wavelength than those of the AgMUNH-Oflx NPs. This might be due to size distribution of the NPs (range 1- 5 nm)[46] where the sizes of these individual $AgMUNH_2$ NPs could be larger than these individual AgMUNH-Oflx NPs. Moreover, we determined the sizes of NPs and tracked the stability (non-aggregation) and transports of single NPs inside and outside the membrane of single live cells *in situ* in real time. For example, if individual NPs aggregated and became the larger NPs, we would have observed the huge red-shifted of LSPR spectra and color change of the NPs. We did not observe such a phenomenon during each experiment (2 h) indicating that the NPs are stable (non-aggregated) in the PBS buffer and inside the cells over time. In short, we used plasmonic features of the Ag NP-based antibiotic drug nanocarriers (AgMUNH-Oflx NPs) and the control nanocarriers ($AgMUNH_2$ NPs) to characterize the number of nanocarriers and monitor them *in situ* in real time as they transported in and out the cellular membrane over time using the same approach described previously.[9, 13-14, 29-30] Single Ag NPs are photostable, unlike fluorescence probes, which enable us to probe efflux function of multidrug membrane transporters using antibiotic drug nanocarriers over time.[9, 13-14, 29-30, 43]

Insights into Pump Substrates and Effects of Pump Inhibitor on Accumulation Rates of Antibiotic Drug Nanocarriers in Single Live Cells

Differently from eukaryotes, prokaryotes (bacterial cells, such as *E. coli*) do not have endocytosis pinocytosis and exocytosis. Therefore, these cellular processes are not responsible for the transport of NPs in and out the live bacterial cells. We studied the accumulation rates of the antibiotic drug nanocarriers (AgMUNH-Oflx NPs) and the control nanocarriers ($AgMUNH_2$ NPs) in MsbA (WT) living cells to determine whether the NPs are substrates of MsbA. The results in Figure 17A, B: b and Table 3 show that the cells accumulate the intracellular NPs over time. The accumulation rates of intracellular AgMUNH-Oflx NPs and $AgMUNH_2$ NPs during their incubation with 1.4 nM NPs over 41.5 min are 1.03 and 2.16 intracellular NPs/min, respectively (Table 3). We further study the effects of a pump (ATPase) inhibitor, orthovanadate (Na_3VO_4) to

determine whether MsbA membrane transporters are specifically responsible for the efflux of the nanocarriers. Note that MsbA is an ATPase which is stimulated by substrates such as lipid A, lipopolysaccharide (LPS) and multiple drugs, and it is inhibited by orthovanadate.[40] The results in Figure 17A, B: b and Table 3 show that the cells accumulate the intracellular AgMUNH-Oflx NPs and AgMUNH$_2$ NPs much more rapidly in the presence of orthovanadate. The accumulation rates of intracellular AgMUNH-Oflx NPs and AgMUNH$_2$ NPs during their incubation with 1.4 nM NPs over 41.5 min in the presence of orthovanadate are 3.61 and 4.52 intracellular NPs/min, respectively (Table 3). We found that the numbers of intracellular AgMUNH-Oflx NPs and AgMUNH$_2$ NPs significantly increased when the cells were incubated with orthovanadate ($p < 0.0005$). These findings suggest the high dependence of accumulation rates of intracellular AgMUNH-Oflx NPs and AgMUNH$_2$ NPs upon the pump function of MsbA in the presence of the inhibitor. Taken together, the results in Figure 17 and Table 3 indicate that MsbA (WT) is indeed responsible for the extrusion of the intracellular NPs out of the cells and the pump function is hindered by the inhibitor leading to an increase of the accumulation of intracellular NPs in the absence of the inhibitor.

The size of antibiotic drug nanocarriers are order of magnitude larger than those of conventional antibiotics. It seems almost impossible that these nanocarriers can permeate into the cells and be extruded out by the efflux pumps. To determine whether the antibiotic drug nanocarriers cause any possible steric effects to efflux pumps and they are suitable substrates for probing the efflux function, we used a fluorescence dye (Hoechst 33342) to study the dependence of accumulation kinetics probing the efflux function of MsbA (WT) in the presence and its absence of orthovanadate. The Hoechst dye is a well-known substrate of MsbA (ABC) membrane transporters and has been commonly used in studies of efflux function.[10-11] Fluorescence intensity of the dye is weak in aqueous solution but it dramatically increases when the dye internalizes into the cells and intercalates with DNA.[47] The cells incubated with orthovanadate (Figure 17C: a) accumulated more amount of intracellular dye molecules with the higher rate of accumulation (slopes of the curves) than those were not incubated with orthovanadate
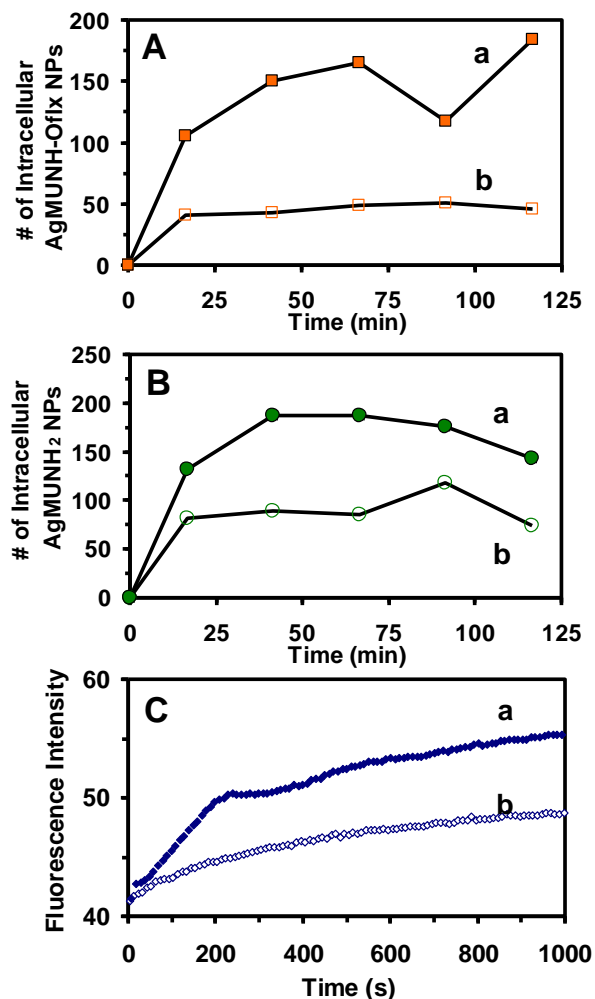
Figure 17. Study of effects of a pump (ATPase) inhibitor, orthovanadate on the accumulations of single 2.4 ± 0.7 nm AgMUNH-Oflx NPs, AgMUNH$_2$ NPs, and fluorescence dye (Hoechst 33342) molecules.

(A) Plots of number of intracellular AgMUNH-Oflx NPs (A) and AgMUNH$_2$ NPs (B) and plots of the fluorescence intensity of Hoechst 33342 dye (C) over time in the presence (a, solid) and absence (b, empty) of the inhibitor (25 µM). In (A) and (B), the points represent the experimental measurements and the lines are added to guide the trend. At each time point (25 min), 900 cells were analyzed. In (A) and (B), the p values of data in (a) and (b) are less than 0.0005 (<0.0005), indicating statistically significant difference of intracellular NPs in the presence (a) and absence (b) of orthovanadate, and the dependence of accumulation kinetics of the NPs on the pump inhibitor.

Table 3. Summary of Accumulation Rates and Numbers of Intracellular Single 2.4 ± 0.7 nm NPs in Single Living *E. coli* Cells

Types of NPs	$C_{Ag\ NPs}$ (nM)	Inhibitor [a] (µM)	Accumulation rate (NPs min^{-1}) [b]	Numbers of intracellular NPs [c]
AgMUNH-Oflx	0.7	0	0.59	25
	1.4	0	1.03	43
	1.4	25	3.61	150
AgMUNH$_2$	0.7	0	1.38	57
	1.4	0	2.16	90
	1.4	25	4.52	188

[a] Orthovanadate;

[b] Accumulation rates (slopes of the plots) at the 41.5 min incubation;

[c] Numbers of intracellular NPs accumulated in 900 live cells at the 41.5 min incubation.

(Figure 17C: b). The results in Figure 17C are similar to those observed using the AgMUNH-Oflx NPs (Figure 17A) and the AgMUNH$_2$ NPs (Figure 17B) indicating that the AgMUNH-Oflx NPs and the AgMUNH$_2$ NPs are substrates of MsbA membrane transporter and well suited as small fluorescence molecules for the study of efflux kinetics of single MsbA membrane transporter in single live cells. Unlike fluorescence probes, LSPR of plasmonic single NPs provide information regarding the sizes of pump substrates and the pore sizes of membrane transporters which enable us to determine the size-dependent efflux kinetics of multidrug membrane transporters. Taken together, we demonstrate that the efflux pumps can extrude the small sized drug nanocarriers out of the cells and we can track them to study efflux function of MsbA in single cells in real time.

Study of Concentration Dependence on Accumulation Rates of Antibiotic Drug Nanocarriers in Single Living Cells

We further studied how the antibiotic drug nanocarriers (AgMUNH-Oflx NPs) and the control nanocarriers (AgMUNH$_2$ NPs) enter the cells and whether they passively diffuse into the cells as same as those conventional pump substrates, such as antibiotics. Thus, we determined the accumulation rates of single AgMUNH-Oflx NPs and AgMUNH$_2$ NPs upon their concentrations (0.7 and 1.4 nM). The results in Figure 18 show that the number of intracellular of both AgMUNH-Oflx NPs (Figure 18A) and AgMUNH$_2$ NPs (Figure 18B) significantly depends on the NP concentration (AgMUNH-Oflx NPs, $p < 0.0005$ and AgMUNH$_2$ NPs, $p < 0.0005$), and the number of intracellular NPs increases as the NP concentration increases at any given incubation time. As the NP concentration increases from 0.7 to 1.4 nM, the number of intracellular AgMUNH-Oflx NPs accumulated in single live cells increases from 25 to 43 within 41.5 min at the rates of 0.59 and 1.03 NPs/min, respectively, and similarly the number of intracellular AgMUNH$_2$ NPs accumulated in single live cells increases from 57 to 90 within 41.5 min at the rates of 1.38 and 2.16 NPs/min, respectively.

Likewise, we found the concentration dependence of the accumulation of fluorescence dye (Hoechst 33342) where the dye at a higher concentration (Figure 18C:

a) passively entered the cells more rapidly and accumulated inside the cells more than that at the lower concentration (Figure 18C: b). These findings suggest that both AgMUNH-Oflx NPs and AgMUNH$_2$ NPs most likely passively diffuse into the cells and be extruded out of the cells by MsbA transporters similarly to conventional antibiotics. The diffusion rates of AgMUNH-Oflx NPs and AgMUNH$_2$ NPs show high dependence on the concentration gradients of the NPs across the cellular membrane of single cells and the diffusion rates increase as the NP concentration gradients increase and vice versa. In contrast, the efflux of substrates (e.g., AgMUNH-Oflx NPs and AgMUNH$_2$ NPs) out of the cells against concentration gradients is an active transport process which requires ATP energy and depends on substrate selectivity. Thus, the efflux rates of the AgMUNH-Oflx NPs and AgMUNH$_2$ NPs are not proportional to the NP concentration and interestingly the accumulation of intracellular AgMUNH$_2$ NPs rises more rapidly than those of the AgMUNH-Oflx NPs as NP concentration increases.
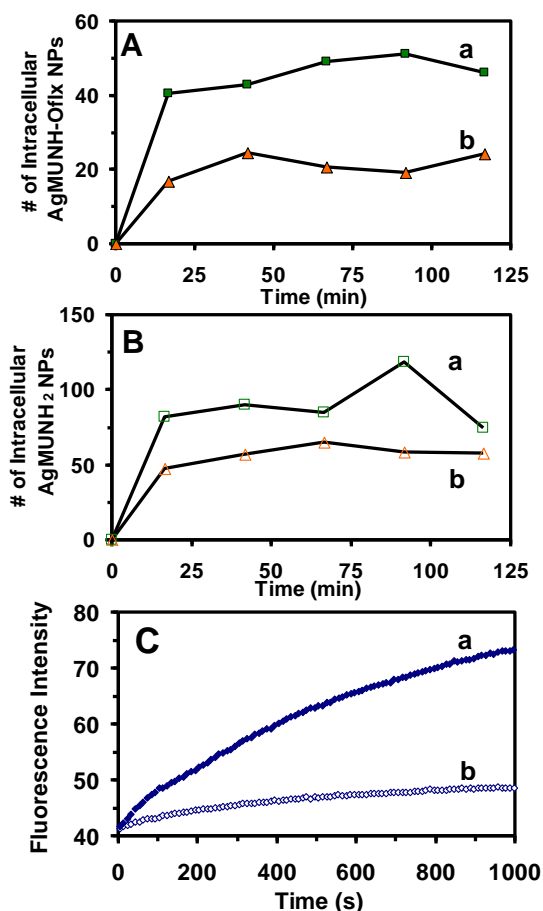
Figure 18. Study of the concentration dependent accumulations of 2.4 ± 0.7 nm AgMUNH-Oflx NPs, AgMUNH₂ NPs, and fluorescence dye (Hoechst 33342) molecules in living *E. coli* cells.

(A) Plots of number of intracellular AgMUNH-Oflx NPs in *E. coli* incubated with 1.4 nM (a) and 0.7 nM (b) of AgMUNH-Oflx NPs versus time. (B) Plots of number of intracellular AgMUNH₂ NPs in MsbA incubated with 1.4 nM (a) and 0.7 nM (b) of AgMUNH₂ NPs versus time. (C) Plots of fluorescence intensity of Hoechst 33342 dye at 1 µM (a) and 0.5 µM (b) versus time. In (A) and (B), the points represent the experimental measurements and the lines are added for trend projection. Note that 900 cells were analyzed at each point (every 25 min). The p values of data in (a) and (b) are less than 0.0005 (<0.0005), indicating statistically significant difference of intracellular NPs in the cell incubated with (a) 1.4 nM and (b) 0.7 nM at 95% confidential level, and concentration dependent efflux functions of MsbA.

Study of Substrate-Dependent Accumulation Rates of Single Drug Nanocarriers in Single Live Cells

It is worth noting that the accumulation of intracellular AgMUNH-Oflx NPs and AgMUNH$_2$ NPs in single live cells in the presence and its absence of orthovanadate strongly suggest the dependence on types of substrates. The number of intracellular AgMUNH$_2$ NPs are significantly higher than the number of intracellular AgMUNH-Oflx NPs in both 0.7 nM ($p < 0.0005$) and 1.4 nM ($p < 0.0005$) concentrations (Figure 18). We observed twice higher accumulation rates of AgMUNH$_2$ NPs in single live cells than those of AgMUNH-Oflx NPs over 41.5 min. Interestingly, the number of intracellular AgMUNH$_2$ NPs is only significantly higher than those of AgMUNH-Oflx NPs in single live cells in the absence of orthovanadate ($p < 0.0005$) but it is not in its presence of orthovanadate. These findings suggest that MsbA extrudes the AgMUNH-Oflx NPs more effectively than the AgMUNH$_2$ NPs because the intracellular AgMUNH-Oflx NPs increase much greater than the AgMUNH$_2$ NPs when the inhibitor disrupts efflux function. As the AgMUNH-Oflx NPs differ from the AgMUNH$_2$ NPs with regards to their multiple conjugated Oflx molecules which exhibit inhibitory effects, the plausible explanation why the cells extrude the AgMUNH-Oflx NPs more effectively is that they could selectively extrude noxious molecules as cellular defense mechanisms. This could lead to further studies to address how multidrug membrane transporters can selectively extrude a large number of chemically and functionally unrelated substances out of the cells and how MDR occurs.

Quantitative accumulation rates of intracellular AgMUNH-Oflx NPs and AgMUNH$_2$ NPs in single living cells (Figure 17 and 18) are summarized in Table 3. We demonstrate that both the AgMUNH-Oflx NPs and AgMUNH$_2$ NPs are substrates of MsbA membrane transporters and they are suitable optical probes to study efflux function of MsbA membrane transporters in single live cells. These results indicate the dependence of accumulation kinetics of single NPs in single live cells on types of substrates, the pump inhibitor and the concentration of NPs.

Characterization of the Viability of Single Cells

We have reported that antibiotic drug nanocarriers with a diameter of 2.4 ± 0.7 nm inhibited bacterial growth in a dose-dependent manner.[46] Therefore, we characterized the viability of the cells MsbA (WT) to ensure that the doses of the antibiotic drug nanocarriers (AgMUNH-Oflx NPs), the control nanocarriers (AgMUNH$_2$ NPs) and the pump inhibitor that we used to probe efflux function of *E. coli* did not cause cell death and interfere with their pump function. We characterized viability of the cells incubated with the antibiotic drug nanocarriers (AgMUNH-Oflx NPs) or the control nanocarriers (AgMUNH$_2$ NPs) throughout the duration of the experiment over 2 h using LIVE/DEAD *Bac*Light assay. The green SYTO9 fluorescence dye (λ_{max} = 520 nm) stains cellular nucleic acids which identify the live cells while the red PI fluorescence dye (λ_{max} = 610 nm) penetrates into only the cells with disintegrated membrane which detect the dead cells.[63]

Representative optical images of the cells incubated with AgMUNH-Oflx NPs (1.4 nM) in the presence (Figure 19A: a) and absence (Figure 19B: a) of orthovanadate (25 µM) over 2 h show the cells with and without NPs. Their fluorescence images illustrate the green fluorescence but not the red fluorescence indicating that the cells are viable (Figure 19A, B: b). We determined percentage of live and dead cells by dividing the number of viable cells by the total number of cells. We found that 99 % of the cells incubated with 1.4 nM AgMUNH-Oflx NPs in the presence and absence of orthovanadate (25 µM) (Figure 19C) were viable. Similarly, representative optical images of the cells incubated with AgMUNH$_2$ NPs (1.4 nM) in the presence (Figure 20A: a) and absence (Figure 20B: a) of orthovanadate (25 µM) over 2 h show the cells with and without NPs. The cells emitted green fluorescence but not red fluorescence suggesting that they were viable (Figure 20A, B: b). The results show that 99 % of the cells are alive (Figure 20C). As the cells with the NPs and orthovanadate are all alive, the accumulation rates of the NPs in single live cells are associated with NP passive diffusion and efflux function of the membrane transporters but not the compromised membrane integrity due to the cell death. The findings further demonstrate that the doses (0.7 and 1.4 nM) of the AgMUNH-Oflx NPs are suitable to use in study MDR and
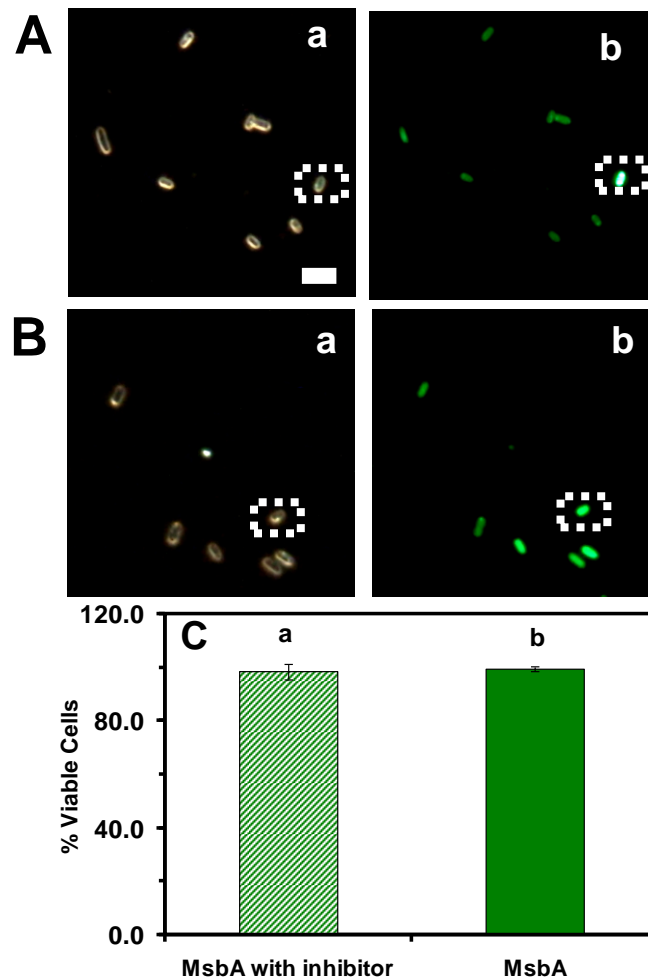
Figure 19. Characterization of viability of single bacterial cells incubated with 2.4 ± 0.7 nm AgMUNH-Oflx NPs using LIVE/DEAD *Bac*Light viability and counting assay.

In (A) and (B), representative dark field optical image (a) and fluorescence image (b) of single bacterial cells (MsbA), incubated with 1.4 nM AgMUNH-Oflx in the presence (A) and absence (B) of the inhibitor (25 μM) over the duration of each experiment for 2 h, show that the cells with intracellular NPs (as squared) or without NPs emit the green fluorescence (λ_{max} = 520 nm) of SYTO9, indicating that cells are viable. (C) Plots of percentage of viable cells (a) and dead cells (b) of MsbA incubated with 1.4 nM AgMUNH-Oflx with and without the inhibitor, indicate that 99 % of the cells are alive. Minimum 300 cells were assayed and analyzed. The scale bar is 5 μm.

Figure 20. Characterization of viability of single bacterial cells incubated with 2.4 ± 0.7 nm AgMUNH₂ NPs using LIVE/DEAD *Bac*Light viability and counting assay.

In (A) and (B), representative dark field optical image (a) and fluorescence image (b) of single bacterial cells (MsbA), incubated with 1.4 nM AgMUNH₂ in the presence (A) and absence (B) of the inhibitor (25 µM) over the duration of each experiment for 2 h, show that the cells with intracellular NPs (as squared) or without NPs emit the green fluorescence (λ_{max} = 520 nm) of SYTO9, indicating that cells are viable. (C) Plots of percentage of viable cells (a) and dead cells (b) of MsbA incubated with 1.4 nM AgMUNH₂ with and without the inhibitor, indicate that 99 % of the cells are alive. Minimum 300 cells were assayed and analyzed. The scale bar is 5 µm.

efflux function of multidrug membrane transporter of antibiotic drug nanocarriers in bacteria.

SUMMARY

We synthesized, purified and characterized Ag NP-based antibiotic drug nanocarriers (AgMUNH-Oflx NPs) with a diameter of 2.4 ± 0.7 nm containing 8.6×10^2 Oflx molecules per NP.[46] The NPs up to 1.4 nM are stable (non-aggregated) in the PBS buffer and biocompatible with the cells (MsbA WT) over the experimental period (2 h). Due to distinctive features of Ag NPs, we are able to image and track such small single antibiotic drug nanocarriers as they transport in and out live single bacterial cells and use LSPR spectra of single AgMUNH-Oflx NPs and $AgMUNH_2$ NPs (absence of Oflx, control nanocarriers) study efflux function of MsbA membrane transporters in single live cells. We found that the accumulation rates of both AgMUNH-Oflx NPs and $AgMUNH_2$ NPs highly depend on the concentration of NPs and a pump inhibitor (orthovanadate), similar to those observed using a well-known substrate (Hoechst dye 33342) of MsbA membrane transporters, suggesting that the AgMUNH-Oflx NPs and $AgMUNH_2$ NPs are substrates of MsbA membrane transporters and they passively diffuse into the cells. Interestingly, we observed twice higher accumulation rates of $AgMUNH_2$ NPs in single live cells than those of AgMUNH-Oflx NPs, suggesting substrate-dependent efflux kinetics of MsbA (WT) membrane transporters in single live cells and their potential capabilities to detect, recognize and extrude toxic substrates (e.g., antibiotics or anticancer drugs) efficiently. These findings agree with our previous study that the AgMUNH-Oflx NPs exhibit inhibitory effects while the $AgMUNH_2$ NPs are biocompatible with the cells.[46] These results provide a new evidence that multidrug membrane transporter might have a sensing machinery to detect and recognize toxic substrates, which lead to further studies to address molecular basis of efflux mechanisms about how multidrug membrane transporters can selectively extrude a large number of chemically and functionally unrelated substances out of the cells.

MATERIALS AND METHODS

Reagents and Cell Line

We purchased sodium chloride, sodium phosphate (Sigma-Aldrich), sodium phosphate monobasic monohydrate (Sigma-Aldrich), bacto-tryptone and yeast extract (Sigma-Aldrich), orthovanadate (Sigma-Aldrich). We purchased Live/dead backlight viability assay (Life Technologies) and Hoechst 33342 (Life Technologies). We used all reagents as received. We used the nanopure deionized (DI) water (18 MΩ water, Barnstead) to rinse glassware and prepare all solutions including standard LB medium (1% tryptone peptone, 0.5% yeast extract, and 0.5% NaCl, pH = 7.2). We purchased cell line of *Escherichia coli*, WT w3110 (MsbA) from Coli Genetic Stock Center (CGSC).

Cell Culture and Preparation

Gram-negative *E. coli* (MsbA) strain cells were cultured in an Erlenmeyer flask containing 10 mL of L-Broth (LB) medium (1% tryptone peptone, 0.5% yeast extract, and 0.5% NaCl, pH = 7.2) in an incubated floor shaker (Thermo Scientific, MaxQ5000; 160 rpm, 37 °C). After 12 h incubation, we inoculated 3 mL of pre-cultured cells into 10 mL of the LB medium in an Erlenmeyer flask. We then incubated the flask in the shaker (160 rpm, 37 °C) for another 8 h. We harvested the cultured cells using centrifugation (Beckman Model J2-21 Centrifuge, JA-14 rotor, at 7500 rpm, 23 °C, 10 min), washed the cells with the PBS buffer (0.5 mM phosphate buffer, 1.5 mM NaCl, pH 7.0) three times, and finally re-suspended the cells in the buffer. The final concentration of the cells was adjusted to $OD_{600\ nm}$ = 0.7 and used for the entire study.

Imaging of Single NPs in Single Living Cells

We prepared the cell suspension ($OD_{600\ nm}$ = 0.7) containing 0.7 nM and 1.4 nM AgMUNH-Oflx NPs or $AgMUNH_2$ NPs (control NPs without ofloxacin) in the presence and absence of orthovanadate (25 µM). The timer was started to record the incubation time as NPs were added into the cell suspension.

We sampled the mixture (1 µL) into a freshly prepared micro-chamber created by nail polish and imaged the cells on 18 representative locations using DFOMS equipped with a CCD camera and a digital color camera every 25 min (7 min for the slide preparation and 18 min for imaging). We acquired LSPR spectra of single intracellular and extracellular NPs in real time, which enabled us to identify and locate positions of single NPs simultaneously.

The design and construction is fully explained in our previous studies.[9, 12-14, 25, 28-30, 42-43, 58-59, 61-62, 75, 78] In particular, our dark-field optical microscope was equipped with a dark-field condenser (oil 1.43-1.20, Nikon), a 100x objective (Nikon Plan fluor 100x oil, iris SL N.A. 0.5-1.3, W.D.0.20 mm), a charge coupled device (CCD) camera (Micromax, Roper Scientific), a digital color camera (Handycam, Sony) and a multispectral imaging system (Nuance, Cambridge Research Inc.).[42-43] We have achieved high temporal resolution up to 5 ms to continuingly image of transport of single NPs in and out of single living cells.[9, 14] However, we acquired images in every 1 min as we found that the transport of single NPs in and out of single living cells was not a rapid process.[9, 14] Thus, a temporal resolution of minutes was sufficient to study transport of single NPs in real time.

We prepared a fresh micro-chamber every 25 min and imaged single cells for 18 representative locations. This approach allowed us to study transport of single NPs in massive numbers of cells (1500 cells) for each sample to make data adequate for probing accumulation rates of bulk cells at a single cell resolution. We quantified intracellular NPs and plotted them versus incubation time and determined the accumulation rates (slopes of the plots) of single NPs in the cells over time.

Real-time Imaging of Viability of Single Cells

At the end of each experiment (2 h), we characterized the viability of the cells at a single cell resolution using live/dead *Bac*Light viability and counting assay. We imaged cells in a micro-chamber using dark-field optical microscopy and epi-fluorescence microscopy and counted the green fluorescence cells (peak wavelength of

fluorescence spectra of SYTO9, λ_{max} = 520 nm) and the red fluorescence cells (peak wavelength of fluorescence spectra of propidium iodide, λ_{max} = 610 nm) as live and dead cells, respectively.

Fluorescence Spectroscopy Measurement

The cells in the PBS buffer were incubated with Hoechst 33342 (0.5 µM and 1 µM) with the presence and absence of orthovanadate (25 µM). Time-course fluorescence intensity of the dye was measured at a 10-s data acquisition interval in real time using a fluorescence spectrometer (Cary Eclipse). The excitation and emission wavelengths were 354 and 478 nm, respectively.

Data Analysis and Statistics

We acquired eighteen representative locations of each cell suspension incubated with 0.7 nM and 1.4 nM NPs every 25 min over 2 h and 5 min. Approximately fifteen cells were acquired in a single CCD image simultaneously. Therefore, approximately 300 cells were imaged every 25 min and 1500 cells were studied over 2 h and 5 min for each measurement. We repeated each experiment three times. Thus, we studied 4500 cells for each sample allowing us to gain sufficient statistics to study efflux function of bulk cells at single cell resolution. We analyzed the numbers of intracellular NPs in 900 cells (300 cells per each measurement) at every 25 min and plotted them over time to determine the accumulation rates (slopes of the plots) of intracellular NPs of both AgMUNH-Oflx NPs and AgMUNH$_2$ NPs in the cells in the presence and absence of orthovanadate (25 µM) NPs at 41.5 min incubation. We performed statistical analysis (2-sample t-test) using SPSS to compare means of intracellular NPs in the treated cells.

A minimum of 150 cells incubated with each type of NPs after each experiment were studied cellular viability. We repeated each measurement three times. Therefore, 450 cells were assayed for each sample.

CHAPTER IV

PROBING OF EFFLUX MECHANISMS OF MULTIDRUG ABC MEMBRANE TRANSPORTERS IN SINGLE LIVE *ESCHERICHIA COLI* CELLS USING SIZE-DEPENDENT PLASMONIC ANTIBIOTIC DRUG NANOCARRIERS

INTRODUCTION

The ATP-binding cassette (ABC) transporters are highly conserved proteins found in both prokaryotes and eukaryotes.[3, 8, 20] These membrane proteins couple ATP hydrolysis to the active transport of various structurally and functionally unrelated substances (e.g., drugs, ions, sugars and lipids) against their concentration gradients across cell membrane.[5, 8, 20] The extrusion of a wide variety of drugs, such as antibiotics and chemotherapeutic agents leads to the ineffective treatments and multidrug resistance (MDR).[4, 79] These major impacts underscore an urgency of a better understanding of MDR mechanisms aiming to develop more effective drugs and avoid MDR.

The ABC transporters are commonly composed of four core structure domains: two transmembrane domains (TMDs) and two nucleotide-binding domains (NBDs).[3, 5, 7-8] The TMDs which contain predominantly structural divergence within the various subgroups of ABC transporters to define the large diversity of substrate specificity, form the transmembrane channel for substrates to cross the membrane. The NBDs is more highly conserved empower the transporters by coupling ATP hydrolysis leading to the extrusion of the substrates out of the cells against concentration gradients.[3, 5-8] This process is named as efflux function. The MsbA is an essential ABC transporter in Gram-negative bacteria such as *Escherichia coli* that transports lipid A and lipopolysaccharide.[5, 8, 10] In bacterial MsbA, a TMD is fused to an NBD in a half-transporter that then homodimerizes to form the full transporter.[5] MsbA is a poly-specific transporter which can recognize and transport a wide spectrum of drug molecules.[1, 10, 41] Interestingly, MsbA from *E. coli* shares significant protein sequence identity with

mammalian multidrug resistance proteins (Pgp, ABCB1, MDR1) that are essentially associated with resistance of anticancer drugs in human.[5]

A central question for ABC transporters to understand the underlying mechanisms how they can extrude a wide variety of structurally unrelated substrates is still unclear despite the increasing number of X-ray crystal and cryo-EM structures. The X-ray crystallography and cryo-EM are the primary techniques to depict the structures of membrane transporters at an atomic resolution; however, they cannot provide real-time dynamic information.[2, 71-73] For example, how do the efflux pumps sense such a wide range of diverse substrates? How quickly do the pumps recognize the substrates and extrude them out of the cells?

Radioisotopes and fluorescence dyes are widely used as substrates in the study of efflux kinetics of membrane transporters in bulk cells.[8-12] Though these methods can monitor the accumulation of substrates in real time, the results represent the average behavior of a massive number of bulk cells and could mask rare interesting events as individual cells have their independent efflux kinetics.[13, 32] Besides, radioisotopes and fluorophores do not process distinctive size-dependent physicochemical properties therefore they are incapable of providing size information of membrane transporters and are unsuitable to serve as various size-dependent pump substrates for the study of efflux function of single membrane transporter in single live cells in real time.

Noble metal nanoparticles (e.g., silver nanoparticles, Ag NPs) process distinctive size-dependent photostable plasmonic optical properties which show high dependence on their sizes, shapes, dielectric constants and surrounding environments.[23-24, 74] We have demonstrated that we can use superior size-dependent LSPR and photostable single Ag NPs as optical probes to study the size-dependent efflux kinetics of multidrug membrane transporters in single live cells in real time for any desired period using dark-field optical microscopy and spectroscopy (DFOMS).[9, 13-14, 29, 33, 59, 61, 76, 80-82] We have systematically studied the dependence of the accumulation of substrates and efflux function on the sizes, charges, chemicals, and bacterial strains of Gram-positive bacteria (BmrA in *Bacillus subtilis*) and Gram-negative bacteria (MexAB-OprM in

Pseudomonas aeruginosa) using bare and surface-functionalized NPs to mimic various sizes of antibiotics (drugs) with modified surface properties (drug functional groups).[9, 13-14, 29, 33, 59, 61, 76, 80-82]

In this study, we used size-dependent LSPR (color) AgMUNH-Oflx NPs containing 9.4×10^3 Oflx molecules/NP[46] and AgMUNH$_2$ NPs (control NPs without Oflx) with a diameter of 13.0 ± 3.1 nm to probe efflux function of single MsbA membrane transporters in single live cell *E. coli* aiming to study their substrate-dependent accumulation and efflux function. We previously reported substrate-dependent efflux function of MsbA on the smaller sized AgMUNH-Oflx NPs (2.4 ± 0.7 nm). Therefore, this study offers a possibility to compare efflux kinetics of MsbA membrane transporters responded to different sized antibiotic optical probes to investigate whether types and sizes of substrates play a pivotal role in the selective extrusion of efflux pumps. Insights into the molecular basis of multidrug membrane transporters could guide us to a better design of drugs that provide higher efficacy and more importantly can combat MDR.

RESULTS AND DISCUSSION

Real-time Imaging of Single NPs inside and outside Single Live Cells

We synthesized, purified and characterized antibiotic drug nanocarriers (AgMUNH-Oflx NPs) by functionalizing AgMUNH$_2$ NPs (13.0 ± 3.1 nm) with ofloxacin (Oflx) to have 9.4×10^3 Oflx molecules/NP, as previously described.[46] We used the distinctive LSPR spectra (color) of single Ag NP-based nanocarriers to probe efflux kinetics of MsbA multidrug membrane transporters as the cell membrane and debris do not process plasmonic properties and appear white under dark-field illumination. Furthermore, single Ag NPs are photostable,[43] unlike fluorescence probes, allowing us to probe efflux function of multidrug membrane transporters using antibiotic drug nanocarriers over time. We incubated the cells ($OD_{600\ nm} = 0.7$) with antibiotic drug nanocarriers (AgMUNH-Oflx NPs) or control nanocarriers (AgMUNH$_2$ NPs) and tracked single nanocarriers in and out of single living cells in real time using DFOMS. Representative dark-field optical images of the single live cells (WT) (Figure 21, 22: A)

with single intracellular (Figure 21B, 22B: a) and extracellular NPs (Figure 21B, 22B: b) show cross-sections of single rod-shaped bacterial cells with 2 µm in length and 0.5 µm in width. As explained previously, we can image the thin-layer section of single cells with single NPs using DFOMS because the membranes of single live cells above and below the focal plane (190 nm depth of field) are invisible under dark-field illumination.[9, 12-14, 28-29, 33]

As the dark-field illumination penetrates the cell membrane to radiate intracellular NPs, scattering of the NPs is required to transmit through the cell membrane to reach the detector. However, the cell membrane absorbs photons making the intracellular NPs blurry, dimmer and exhibit lower scattering intensity (Figure 21B, 22B: a). On the contrary, the extracellular NPs show higher scattering intensity as they include scattering intensity from both the NPs and the cell membrane. We have validated that these distinctive properties of NPs could be used to distinguish intracellular NPs and extracellular NPs to study efflux function of multidrug membrane transporters in single live cells in real time. We use this approach to determine the intracellular AgMUNH-Oflx NPs (Figure 21B: a) which are dimmer and exhibit lower scattering intensity than the extracellular AgMUNH-Oflx NPs (Figure 21B: b), the same as those observed in the AgMUNH$_2$ NPs (Figure 22B: a, b). The representative LSPR spectra of single AgMUNH-Oflx NPs (i – iii) in Figure 21C show the peak wavelength and full-width-at-half-maxima (FWHM) at 557 (128), 565 (126), and 578 (109) nm, respectively. In addition, the representative LSPR spectra of single AgMUNH$_2$ NPs (i – iii) in Figure 22C show the peak wavelength and FWHM at 554 (124), 557 (96), and 565 (101) nm, respectively. Note that the peak wavelengths of individual AgMUNH$_2$ NPs are possibly at the longer wavelength than those of the AgMUNH-Oflx NPs. This might be because of the size distribution of the NPs ranging from 6 to 20 nm[46] and the sizes of these individual AgMUNH$_2$ NPs could be larger than these individual AgMUNH-Oflx NPs. We observed multiple AgMUNH$_2$ NPs entered individual cells and they were not aggregated. We would have detected the huge red-shift of LSPR spectra (changed color) and a much higher of scattering intensity of the single NPs if the NPs became aggregated and their
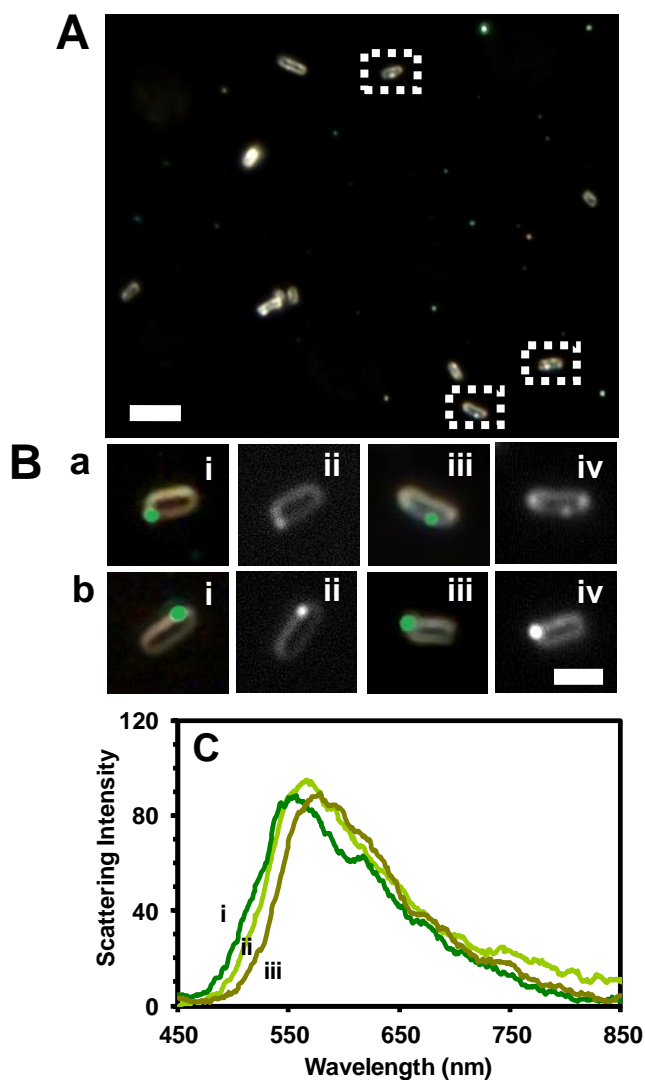
Figure 21. Imaging of single intracellular and extracellular 13.0 ± 3.1 nm AgMUNH-Oflx NPs in single living *E. coli* cells using DFOMS.

(A) The representative optical image of bacterial cells incubated with 1.4 nM AgMUNH-Oflx NPs showing intracellular and extracellular NPs as squared. (B) Zoom in optical color (i and iii) and CCD (ii and iv) images of single cells show (a) intracellular and (b) extracellular NPs which are pseudo colored in color images. The scale bar in A and B are 10 and 2 μm, respectively. (C) LSPR spectra of representative single 13.0 ± 3.1 nm AgMUNH-Oflx NPs (i-iii) show peak wavelengths and full width at half maximum (FWHM) at 557 (128), 565 (126), and 578 (109) nm, respectively.
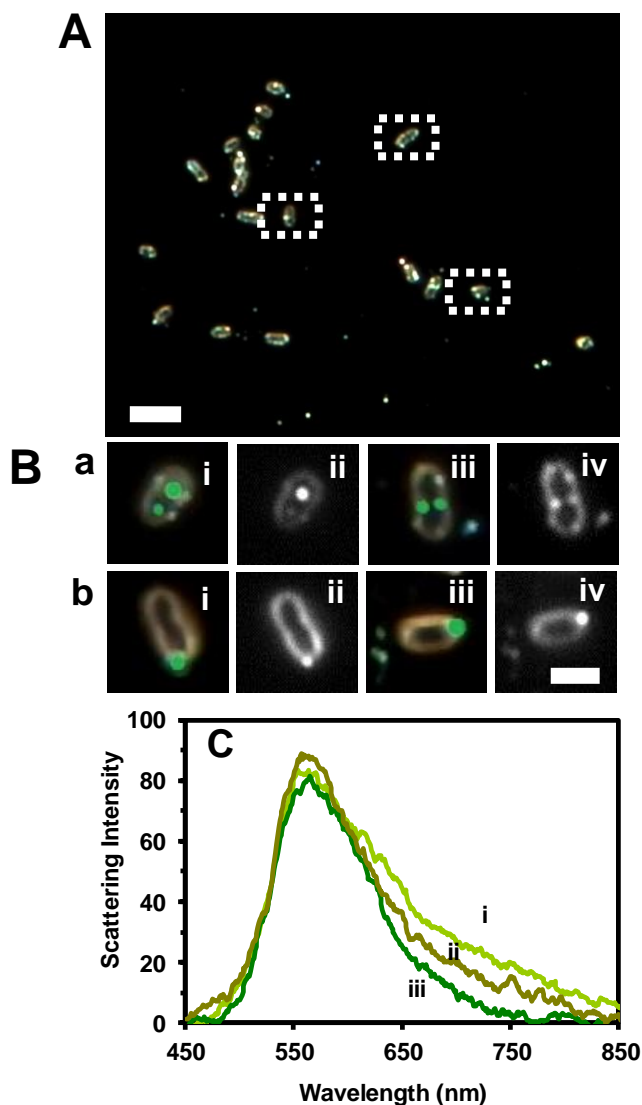
Figure 22. Imaging of single intracellular and extracellular 13.0 ± 3.1 nm AgMUNH$_2$ NPs in single living *E. coli* cells using DFOMS.

(A) The representative optical image of bacterial cells incubated with 1.4 nM AgMUNH$_2$ NPs showing intracellular and extracellular NPs as squared. (B) Zoom optical color (i and iii) and CCD (ii and iv) images of single cells show (a) intracellular and (b) extracellular NPs which are pseudo colored in color images. The scale bar in A and B are 10 and 2 μm, respectively. (C) LSPR spectra of representative single 13.0 ± 3.1 nm AgMUNH$_2$ NPs (i-iii) show peak wavelengths and full width at half maximum (FWHM) at 554 (124), 557 (96), and 565 (101) nm, respectively.

sizes were larger. Taken together, we have successfully used plasmonic features of Ag NP-based antibiotic drug nanocarriers (AgMUNH-Oflx NPs) and control nanocarriers (AgMUNH$_2$ NPs) to characterize single nanocarriers, determine their numbers, and monitor them *in situ* in real time as they transport in and out the cellular membrane over time.

The Dependence of Efflux Function of Single Live Cells on the Pump Inhibitor

We studied the accumulation rates of the antibiotic drug nanocarriers (AgMUNH-Oflx NPs) and the same sized control nanocarriers (AgMUNH$_2$ NPs) in live MsbA (WT) cells in the presence of a pump (ATPase) inhibitor, orthovanadate to determine whether the NPs are substrates of MsbA membrane transporters in which they are responsible for the efflux of the nanocarriers. The results in Figure 23A, B: b and Table 4 show that the cells accumulate the intracellular NPs over time. The accumulation rates of intracellular AgMUNH-Oflx NPs and AgMUNH$_2$ NPs during their incubation with 1.4 nM NPs over 41.5 min are 1.11 and 27.42 intracellular NPs/min, respectively (Table 4). We further study the effects of a pump (ATPase) inhibitor, orthovanadate on MsbA which is an ATPase[40] to determine whether MsbA membrane transporters are specifically responsible for the efflux of the nanocarriers. The results in Figure 23A and Table 4 show the accumulation rate of the AgMUNH-Oflx NPs in the cells increases much more rapidly from 1.11 to 2.09 NPs/min when orthovanadate is presence. The number of intracellular AgMUNH-Oflx NPs significantly increase after the MsbA pumps are inhibited ($p < 0.0005$). In contrast, the number of intracellular AgMUNH$_2$ NPs is insignificantly different in the presence and its absence of orthovanadate ($p = 0.636$) and the accumulation rates of intracellular AgMUNH$_2$ NPs remain essentially unchanged at 27.42 and 27.87 NPs/min, respectively (Figure 23B). The high dependence of accumulation rates of only intracellular AgMUNH-Oflx NPs not AgMUNH$_2$ NPs on the MsbA pump function in the presence of orthovanadate suggests that the AgMUNH-Oflx NPs are substrates of MsbA (WT) which is indeed responsible for the extrusion of the intracellular AgMUNH-Oflx NPs. Moreover, the results (Figure
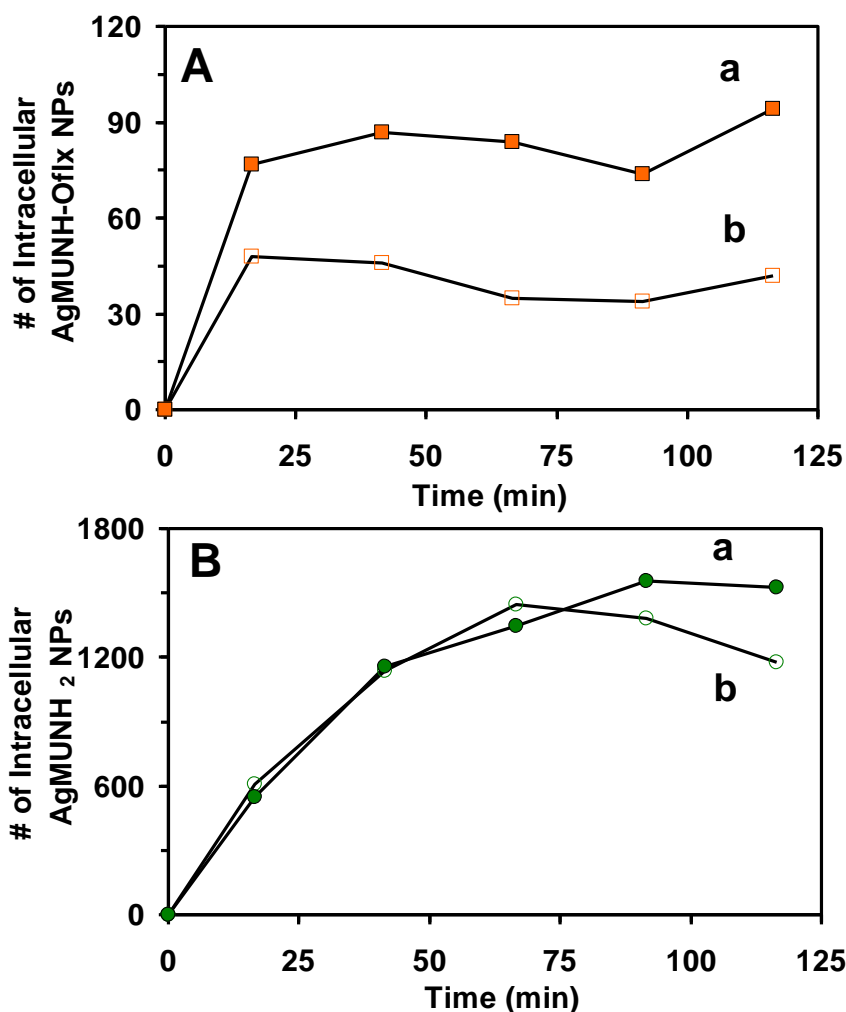
Figure 23. Study of effects of a pump (ATPase) inhibitor, orthovanadate on the accumulations of single 13.0 ± 3.1 nm AgMUNH-Oflx NPs and AgMUNH$_2$ NPs.

(A) Plots of number of intracellular AgMUNH-Oflx NPs (A) and AgMUNH$_2$ NPs (B) over time in the presence (a, solid) and absence (b, empty) of the inhibitor (25 µM). The points represent the experimental measurements and the lines are added to guide the trend. At each time point (25 min), 900 cells were analyzed. In (A), the p value of data (a) and (b) is less than 0.0005 (<0.0005), showing the significant difference of intracellular NPs in the presence (a) and absence (b) of orthovanadate with 95% confidential level, and the dependence of accumulation kinetics of AgMUNH-Oflx NPs on the pump inhibitor.

23B and Table 4) suggest that the AgMUNH$_2$ NPs ineffectively be extruded out of the cells by the MsbA membrane transporters. The efflux pumps could take long time to recognize and extrude the NPs out as the number of intracellular AgMUNH$_2$ NPs in the absence of orthovanadate start to decrease after 90 min (Figure 23B: b).

The size of antibiotic drug nanocarriers are order of magnitude larger than those of conventional antibiotics. However, the results in Figure 23A are similar to those observed using a fluorescence dye (Hoechst 33342) reported previously,[35] indicating that the AgMUNH-Oflx NPs did not cause steric effects and they are suitable substrates for probing efflux function of single MsbA membrane transporters in single live cells.

Table 4. Summary of Accumulation Rates and Numbers of Intracellular Single 13.0 ± 3.1 nm NPs in Single Living *E.coli* Cells.

Types of NPs	$C_{Ag\ NPs}$ (nM)	Inhibitor [a] (µM)	Accumulation rate (NPs min^{-1}) [b]	Numbers of intracellular NPs [c]
AgMUNH-Oflx	0.7	0	0.41	17
	1.4	0	1.11	46
	1.4	25	2.09	87
AgMUNH$_2$	0.7	0	12.23	508
	1.4	0	27.42	1138
	1.4	25	27.87	1156

[a] Orthovanadate;

[b] Accumulation rates (slopes of the plots) at the 41.5 min incubation;

[c] Numbers of intracellular NPs accumulated in 900 live cells at the 41.5 min incubation.

The Dependence of Efflux Function of NP Substrates on Their Type and Size in Single Live Cells

To further study how the ABC membrane transporters could extrude a wide variety of structurally and functionally unrelated substances, we studied the dependence of the accumulation of intracellular NPs in single live cells upon types and sizes of NPs. The numbers of intracellular AgMUNH$_2$ NPs is significantly higher than those of the AgMUNH-Oflx NPs in the absence and its absence of orthovanadate (p < 0.0005) (Figure 23 and Table 4). We observed much higher accumulation rates of the AgMUNH$_2$ NPs (27.42 NPs/min) in single live cells than those of the AgMUNH-Oflx NPs (1.11 NPs/min) over 41.5 min. These results suggest a strong dependence of efflux function on types of substrate which MsbA membrane transporters possibly be equipped with a sensing machinery for selectively detect and recognize noxious substrates (e.g., conjugated Oflx molecules) and then extrude them out of the cells. Interestingly, 13.0 ± 3.1 nm AgMUNH$_2$ NPs accumulate in the cells 12 times more rapidly than 2.4 ± 0.7 nm AgMUNH$_2$ NP, suggesting size-dependent efflux kinetics of AgMUNH$_2$ NPs and the ABC membrane transporters could extrude 13.0 ± 3.1 nm AgMUNH$_2$ NPs at their least efficiency.

Furthermore, we compare the number of intracellular AgMUNH-Oflx NPs with a diameter of 2.4 ± 0.7 nm with those of 13.0 ± 3.1 nm in the cells treated with 1.4 nM NPs to study the size-dependent accumulation of single nanocarriers in single live cells. Notably, the numbers of intracellular AgMUNH-Oflx NPs with a diameter of 2.4 ± 0.7 nm and 13.0 ± 3.1 nm are insignificantly different and their accumulation rates of intracellular AgMUNH-Oflx NPs are 1.03 and 1.11 NPs/min, respectively. When orthovanadate is absence, the number of intracellular NPs of both sized AgMUNH-Oflx NPs is not significantly different (0.7 nM, p = 0.29 and 1.4 nM, p = 0.738) but when orthovanadate is present, the number of intracellular NPs of the smaller AgMUNH-Oflx NPs is significantly higher than that of the larger sized AgMUNH-Oflx NPs (p = 0.004). These results suggest size-dependence of the efflux kinetics of single nanocarriers in MsbA in which efflux pumps extrude the small AgMUNH-Oflx NPs more effectively since

there are more numbers of the smaller NPs retain inside the cells when the pump function was inhibited.

We previously reported in Chapter II, that the MIC_{50} of the smaller nanocarriers is approximately 4 times higher than that of the larger nanocarriers. This observation could be attributed to the lower multivalent effects (higher binding affinity with the targets) of the smaller nanocarriers and the ability of the cells to effectively extrude the smaller nanocarriers out.

The Dependence of Efflux Function on NP Concentrations in Single Live Cells

We further studied the dependence of accumulation and efflux rates of antibiotic drug nanocarriers (13.0 ± 3.1 nm AgMUNH-Oflx NPs) and the control nanocarriers ($AgMUNH_2$ NPs) upon their concentrations (0.7 and 1.4 nM), aiming to determine how they enter the cells. The results in Figure 24 show that the number of intracellular of both AgMUNH-Oflx NPs (Figure 24A) and $AgMUNH_2$ NPs (Figure 24B) significantly depends on NP concentrations (AgMUNH-Oflx NPs, $p < 0.0005$ and $AgMUNH_2$ NPs, $p < 0.0005$). The accumulation rates of single AgMUNH-Oflx NPs and $AgMUNH_2$ NPs increase from 0.14 to 0.37 (2.6 times) and from 4.08 to 9.14 (2.2 times), respectively as the concentration of NPs increases from 0.7 to 1.4 nM. The results in Figure 24 suggest that NPs enter the cells via passive diffusion in which the NPs are driven by the concentration gradient across the membrane.

We summarize quantitative accumulation rates of intracellular AgMUNH-Oflx NPs and $AgMUNH_2$ NPs in single living cells (Figure 23, 24) in Table 4. The results demonstrate that AgMUNH-Oflx NPs and $AgMUNH_2$ NPs are substrates of MsbA membrane transporters and the cells accumulate intracellular $AgMUNH_2$ NPs at the highest rate. We found the dependence of the accumulation rates on the type of substrates, the pump inhibitor and the concentration of NPs.
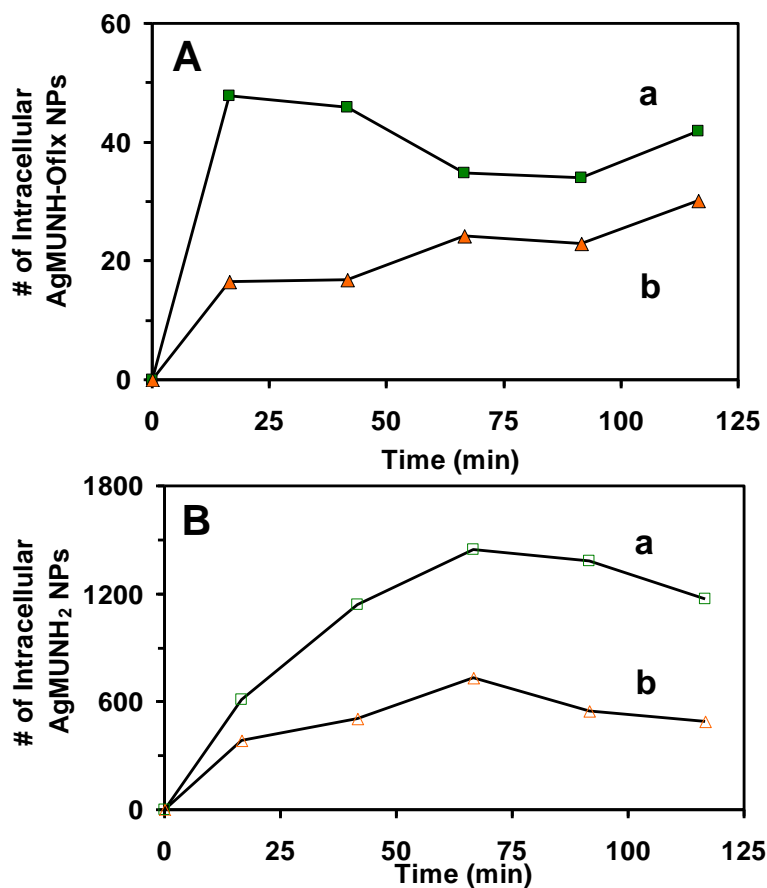
Figure 24. Study of the dependence of the accumulations of 13.0 ± 3.1 nm AgMUNH-Oflx NPs and AgMUNH$_2$ NPs on NP concentrations in living *E. coli* cells.

(A) Plots of number of intracellular AgMUNH-Oflx NPs in MsbA incubated with 1.4 nM (a) and 0.7 nM (b) of 13.0 ± 3.1 nm AgMUNH-Oflx NPs versus time. (B) Plots of number of intracellular AgMUNH$_2$ NPs in MsbA incubated with 1.4 nM (a) and 0.7 nM (b) of 13.0 ± 3.1 nm AgMUNH$_2$ NPs versus time. The points represent the experimental measurements and the lines are added for trend projection. Note that 900 cells were analyzed at each point (every 25 min). In (A) and (B), the p values of data in (a) and (b) are less than 0.0005 (<0.0005), indicating statistically significant difference of intracellular NPs in the cell incubated with (a) 1.4 nM and (b) 0.7 nM at 95% confidential level, and concentration dependent efflux functions of MsbA.

Characterization of Viability of Single Cells

We characterized the viability of the cells (MsbA WT) to ensure that the doses of the antibiotic drug nanocarriers (AgMUNH-Oflx NPs), the control nanocarriers (AgMUNH$_2$ NPs) and the pump inhibitor that we used to probe efflux function of *E. coli* did not kill the cells and interfere with their pump function. At the end of the experiment, we studied viability of the cells incubated with the antibiotic drug nanocarriers (AgMUNH-Oflx NPs) or the control nanocarriers (AgMUNH$_2$ NPs) with the presence and absence of orthovanadate throughout the duration of the experiment over 2 h using live/dead *Bac*Light assay. We acquired optical and fluorescence images of single cells using DFOMS and epifluorescence microscopy, respectively. We observed intracellular and extracellular NPs using DFOMS and assay cellular viability using fluorescence staining. The green SYTO9 fluorescence dye (λ_{max} = 520 nm) penetrates to the cells and stains cellular nucleic acids of the live cells while the red PI fluorescence dye (λ_{max} = 610 nm) enter only the dead with compromised cell membrane integrity.

Representative optical images of the cells incubated with 1.4 nM AgMUNH-Oflx NPs in the presence (Figure 25A: a) and absence (Figure 25B: a) of orthovanadate (25 µM) over 2 h show the cells with and without NPs. Viable cells emit green fluorescence but not the red fluorescence as illustrated in Figure 25A: b and Figure 25B: b. We determined the percentage of live and dead cells by dividing the number of viable cells by the total number of cells. The results show that 99 % of the cells incubated with 1.4 nM AgMUNH-Oflx NPs in the presence and absence of orthovanadate (25 µM) (Figure 25C) are alive. Similarly, representative optical images of the cells incubated with 1.4 nM AgMUNH$_2$ NPs in the presence (Figure 26A: a) and absence (Figure 26B: a) of orthovanadate (25 µM) over 2 h show the cells with and without NPs. The cells emit green fluorescence but not red fluorescence suggesting that they are alive (Figure 26A, B: b). The results show that 99 % of the cells are alive (Figure 26C). As most of the cells are alive, the accumulation rates of the NPs in single live cells are involved in the passive diffusion process of NPs and efflux function of the membrane transporters but not the compromised membrane integrity due to the cell death. The findings further demonstrate that the doses (0.7 and 1.4 nM) of the AgMUNH-Oflx NPs are
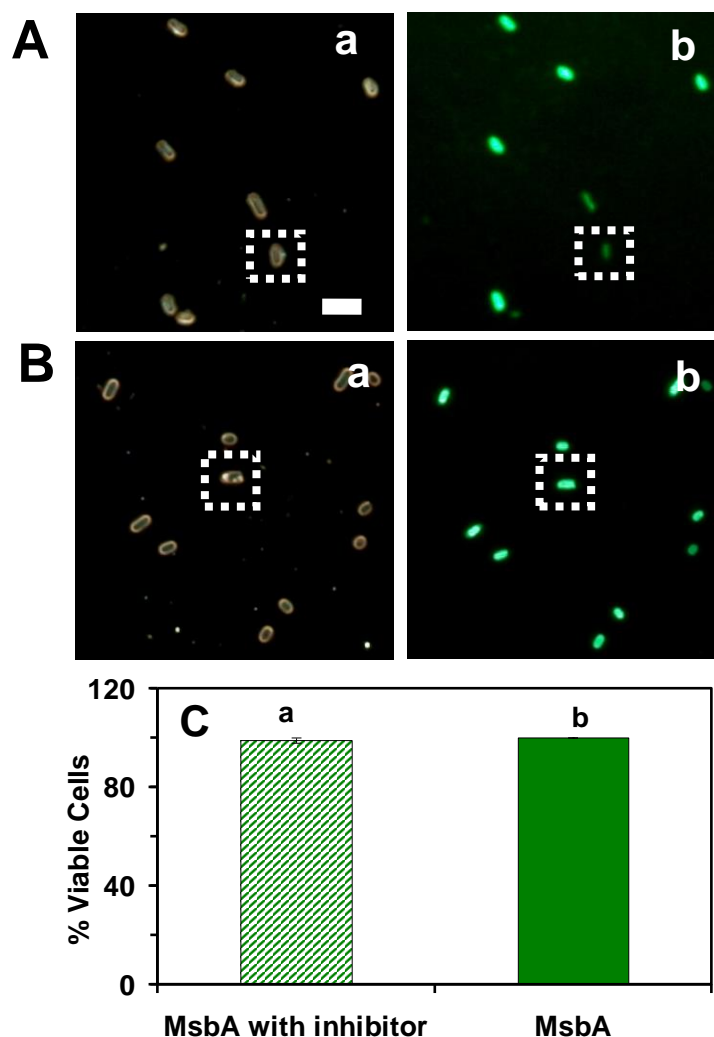
Figure 25. Characterization of viability of single bacterial cells incubated with 13.0 ± 3.1 nm AgMUNH-Oflx NPs using LIVE/DEAD *Bac*Light viability and counting assay.

In (A) and (B), representative dark field optical image (a) and fluorescence image (b) of single bacterial cells (MsbA), incubated with 1.4 nM AgMUNH-Oflx in the presence (A) and absence (B) of the inhibitor (25 µM) over the duration of each experiment for 2 h, show that the cells with intracellular NPs (as squared) or without NPs emit the green fluorescence (λ_{max} = 520 nm) of SYTO9, indicating that cells are viable. (C) Plots of percentage of viable cells (a) and dead cells (b) of MsbA incubated with 1.4 nM AgMUNH-Oflx with and without the inhibitor, indicate that 99 % of the cells are alive. Minimum 300 cells were assayed and analyzed. The scale bar is 5 µm.

Figure 26. Characterization of viability of single bacterial cells incubated with 13.0 ± 3.1 nm AgMUNH₂ NPs using LIVE/DEAD *Bac*Light viability and counting assay.

In (A) and (B), representative dark field optical image (a) and fluorescence image (b) of single bacterial cells (MsbA), incubated with 1.4 nM AgMUNH₂ in the presence (A) and absence (B) of the inhibitor (25 μM) over the duration of each experiment for 2 h, show that the cells with intracellular NPs (as squared) or without NPs emit the green fluorescence (λ_{max} = 520 nm) of SYTO9, indicating that cells are viable. (C) Plots of percentage of viable cells (a) and dead cells (b) of MsbA incubated with 1.4 nM AgMUNH₂ with and without the inhibitor, indicate that more than 99 % of the cells are alive. Minimum 300 cells were assayed and analyzed. The scale bar is 5 μm.

biocompatible and suitable for the study of mechanisms related to MDR and efflux function of multidrug membrane transporters in bacterial cells such as *E. coli*.

SUMMARY

We used LSPR spectra (color) of the AgMUNH$_2$ NPs (absence of Oflx) and the AgMUNH-Oflx NPs containing 9.4x10^3 of Oflx molecules per NP to identify and monitor single NPs in the study of efflux function and kinetics of MsbA (ABC) membrane transporters in single live cells in real time. The NPs up to 1.4 nM are biocompatible to the cells over 2 h of experimental duration. We found the concentration dependence of the accumulation rates of the AgMUNH-Oflx NPs and AgMUNH$_2$ NPs indicating that the passive diffusion driven by concentration gradients is the main mechanism for the NPs to transport into the cells. Interestingly, we found effects of the pump inhibitor (orthovanadate) only on the accumulation rate of AgMUNH-Oflx NPs which increases in the presence of the inhibitor. In contrast, the accumulation rates of AgMUNH$_2$ NPs in the presence and absence of orthovanadate are the same (9 NPs/min) and much higher than those of the AgMUNH-Oflx NPs. These results suggest that substrate-dependent efflux function of MsbA membrane transporters in which they could be equi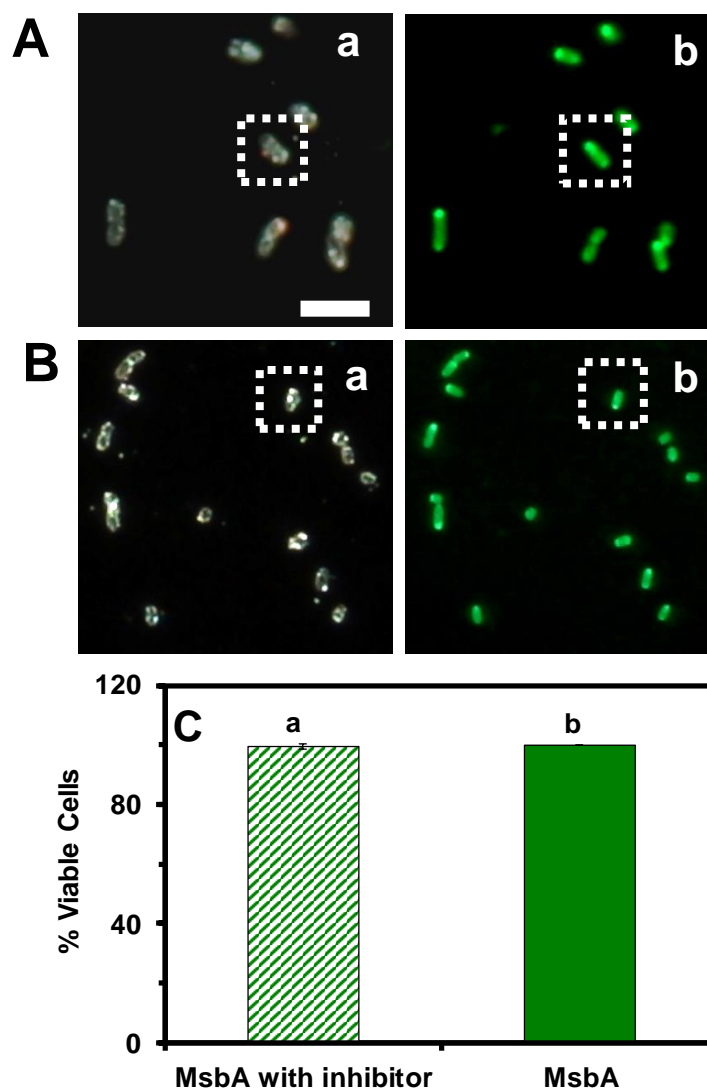pped with a sensing machinery to detect, recognize and extrude toxic substrates (e.g., antibiotics and chemotherapeutic agents). Notably, the efflux pumps ineffectively extrude the AgMUNH$_2$ NPs and this process starts after 90 min of incubation suggesting that the efflux pumps might take a long time to sense the AgMUNH$_2$ NPs. Moreover, we found size-dependent accumulation rates of intracellular AgMUNH-Oflx NPs with a diameter of 2.4 ± 0.7 nm and 13.0 ± 3.1 nm. The cells could extrude the smaller nanocarriers more effectively than the larger nanocarriers. Taken together, this study demonstrates that single AgMUNH-Oflx NPs and AgMUNH$_2$ NPs could be used as optical imaging probes for study of size- and substrate-dependent efflux function of MsbA (ABC) membrane transporters in bacterial cells because they process size-dependent LSPR spectra and contain conjugated drug molecules on the surface that exhibit bactericidal effects. Results from this study also suggest an evidence that multidrug membrane transporters could have a sensing machinery to screen for toxic substrates. Insights into the

molecular basis of efflux mechanisms how multidrug membrane transporters could extrude a wide variety of substrates will lead to better understandings and a feasibility of a design of better drugs that could potentially avoid MDR in pathogenic bacterial cells, such as *E. coli*.

MATERIALS AND METHODS

Reagents and Cell Line

We purchased sodium chloride, sodium phosphate (Sigma-Aldrich), sodium phosphate monobasic monohydrate (Sigma-Aldrich), bacto-tryptone and yeast extract (Sigma-Aldrich), orthovanadate (Sigma-Aldrich). We purchased Live/dead backlight viability assay (Life Technologies) and Hoechst 33342 (Life Technologies). We used all reagents as received. We used the nanopure deionized (DI) water (18 MΩ water, Barnstead) to rinse glassware and prepare all solutions including standard LB medium (1% tryptone peptone, 0.5% yeast extract, and 0.5% NaCl, pH = 7.2). We purchased cell line of *Escherichia coli*, wt w3110 (MsbA) from Coli Genetic Stock Center (CGSC).

Cell Culture and Preparation

Gram-negative *E. coli* (MsbA) strain cells were pre-cultured in an Erlenmeyer flask containing 10 mL of L-Broth (LB) medium (1% tryptone peptone, 0.5% yeast extract, and 0.5% NaCl, pH = 7.2) in an incubated floor shaker (Thermo Scientific, MaxQ5000; 160 rpm, 37 °C) for 12 h. We then inoculated 3 mL of pre-cultured cells into 10 mL of fresh LB medium in an Erlenmeyer flask. We then incubated the flask in the shaker (160 rpm, 37 °C) for an additional 8 h. We harvested the cultured cells using centrifugation (Beckman Model J2-21 Centrifuge, JA-14 rotor, at 7500 rpm, 23 °C, 10 min), washed the cells with the PBS buffer (0.5 mM phosphate buffer, 1.5 mM NaCl, pH 7.0) three times, and finally re-suspended the cells in the PBS buffer. The final concentration of the cells was adjusted to $OD_{600\,nm} = 0.7$ and used for the entire study.

The real-time study of efflux function of membrane transporters in bacterial cells has been always conducted in PBS buffer but not in cell culture medium which would lead to the cell growth and creation of the cells with different growth stages.[9, 12-14, 28-29, 33] It is crucial to study efflux function of membrane transporter at a constant cell concentration and a certain cellular stage in order to compare results among other experiments. Our previous studies have demonstrated that the cells suspended in the PBS buffer retain their efflux function over hours and they are suitable for the study of efflux function.[9, 12-14, 28-29, 33]

Real-time Imaging of Single NPs inside and outside Single Living Cells and Characterization of Cellular Viability

We prepared cell suspension ($OD_{600\ nm}$ = 0.7) containing 0.7 nM and 1.4 nM AgMUNH-Oflx NPs or $AgMUNH_2$ NPs (control NPs without ofloxacin) in the presence and absence of orthovanadate (25 µM). We started a timer simultaneously as we added NPs into the cell suspension.

After the sample prepared, we sampled the mixture (1 µL) into a freshly prepared micro-chamber created by nail polish and continuously imaged the cells on 18 representative locations using DFOMS equipped with a CCD camera and a digital color camera every 25 min (7 min for the slide preparation and 18 min for imaging). We imaged the transport of single nanocarriers moving in and out of single cells in real time using DFOMS equipped with CCD camera (Micromax, Roper Scientific), digital color camera (Handycam, Sony) and multispectral imaging system (Nuance, Cambridge Research Inc.). [9, 14, 25, 58, 62] The design and construction of DFOMS have been fully described previously.[9, 13-14, 25-26, 28-29, 32-33, 43, 58-59, 61-62, 76, 80-82] Our dark-field optical microscope was equipped with a dark-field condenser (oil 1.43-1.20, Nikon) and a 100x objective (Nikon Plan fluor 100x oil, iris SL N.A. 0.5-1.3, W.D.0.20 mm) with a depth of field of 190 nm. Although we have achieved high temporal resolution up to 5 ms to continuingly image for tracking the transport of single NPs, we acquired images in every 1 min since we found that the transport of single NPs in and out of single living cells was

not a rapid process and a temporal resolution of minutes was sufficient to study transport of single NPs in real time.[9, 14]

We sampled the mixture and re-prepared a fresh micro-chamber every 25 min and imaged single cells for 18 representative locations for 2 h. By using this approach, we could acquire sufficient data from massive numbers of cells (1500 cells) for each sample for probing the accumulation rates of bulk cells at a single cell resolution. We quantified intracellular NPs and plotted them versus incubation time and determined the accumulation rates (slopes of the plots) of single NPs in the cells over time.

The viability of cells was characterized at a single cell resolution using LIVE/DEAD *Bac*Light viability and counting assay at the end of each experiment (2 h). We imaged cells in the micro-chamber using dark-field optical microscopy and epi-fluorescence microscopy and counted the green fluorescence cells stained by SYTO9 (λ_{max} = 520 nm) and the red fluorescence cells stained by propidium iodide (λ_{max} = 610 nm) as live and dead cells, respectively.

Data Analysis and Statistics

Cells were imaged for eighteen representative locations of each cell suspension containing 0.7 nM and 1.4 nM NPs in a presence or absence of orthovanadate every 25 min over 2 h and 5 min. Approximately fifteen cells were acquired in a single CCD image simultaneously. Therefore, approximately 300 cells were imaged every 25 min and 1500 cells were studied over 2 h and 5 min for each measurement. We repeated each experiment three times. Thus, we studied 4500 cells for each sample allowing us to gain sufficient statistics to study efflux function of bulk cells at a single cell resolution. We analyzed the numbers of intracellular NPs in 900 cells (300 cells per each measurement) at every 25 min and plotted them over time to determine the accumulation rates (slopes of the plots) of intracellular NPs of both AgMUNH-Oflx NPs and AgMUNH$_2$ NPs for the cells in the presence and absence of orthovanadate (25 µM) at 40.5 min incubation time when the accumulation of NPs reach a plateau and essentially remain stable. We performed statistical analysis (2-sample t-test) using

SPSS to compare means of intracellular NPs in the treated cells. We studied the viability of single cells at a minimum of 150 cells that were incubated with each type of NPs after each experiment (2 h). We repeated each measurement three times. Therefore, 450 cells were assayed for each sample.

CHAPTER V

STUDY OF SUBSTRATE- AND SIZE-DEPENDENT EFFLUX FUNCTION OF MULTIDRUG ABC MEMBRANE TRANSPORTERS IN SINGLE LIVE *ESCHERICHIA COLI* CELLS USING ANTIBIOTIC DRUG NANOCARRIER OPTICAL PROBES

INTRODUCTION

ATP-binding cassette (ABC) membrane transporters (efflux pumps) is a large protein family found in all prokaryotic and eukaryotic cells.[3, 7, 83] They mediate the uptake of nutrients and the export of a wide variety of substances across cellular membrane such as peptides, lipids and drugs.[3, 5, 7, 83] These efflux pumps protect cells (e.g., bacteria and cancer cells) from many cytotoxins such as antibiotics and anticancer drugs, conferring multidrug resistance (MDR).[3, 5, 7, 83-84] Efflux systems are currently thought to be responsible for MDR in bacteria and cancer cells which greatly causes ineffective treatments of infections and cancers.[4, 79, 84]

Despite a large number of structurally unrelated substrates, the ABC transporters have common four core domains: two transmembrane domains (TMDs) and two nucleotide-binding domains (NBDs).[3, 5, 7, 83] The TMDs consist of the large diversity of specific binding sites and multiple membrane-spanning proteins which together form the pathway through, which the transported substrate crosses the lipid bilayer, whereas the NBDs couple conformation changes induced by ATP binding and hydrolysis.[3, 5, 7, 83] MsbA is an essential ABC membrane transporters in Gram-negative bacteria (e.g., *Escherichia coli*) and play a key role in transport of lipid A and lipopolysaccharide (LPS) from the cytoplasmic leaflet (inward-facing) to the periplasmic leaflet (outward-facing) of bacterial inner membrane by utilizing ATP energy.[1-2, 83] Functional studies have reported that MsbA could recognize and extrude a wide spectrum of antibiotics causing resistance to certain antibiotics.[1, 10, 41]

Currently, the primary techniques to depict the structures of membrane transporters at the atomic resolution are X-ray crystallography and cryo-EM.[2, 71-73] Though the number of available X-ray crystal and cryo-EM structures of ABC membrane transporters is increasing, the molecular basis of efflux mechanisms, and how the similar structural membrane transporters could extrude diverse structurally unrelated substrates has not yet fully understood. These techniques cannot provide real-time dynamic insights into how the efflux pumps selectively detect and recognize various types of substrates before extruding them out of the cells.

Conventional methods to study MDR include measurements of the accumulation of radioisotopes (^{14}C and ^{3}H) or fluorescence dyes as they diffuse into the cells and are extruded by prokaryotic and eukaryotic cells over time.[9-12, 83] These approaches provide efflux kinetics of the bulk cells and they could mask any rare interesting event since individual cells behave differently emphasizing the importance to probe efflux kinetics of individual membrane transporters in single live cells in real time.[9, 14] Moreover, single radioisotopes and fluorophores themselves do not process distinctive size-dependent physiochemical properties. Therefore, these conventional probes could not serve as various size-dependent pump substrates for the study of efflux function of single membrane transporters in single live cells.

Nobel metal nanoparticles (e.g., Ag NPs) process distinctive plasmonic properties, which highly depend on their sizes, shapes, dielectric constant, and surrounding environments.[23-24] Single Ag NPs have high Rayleigh scattering enables us to image and characterize them under illumination of halogen lamps using dark-field optical microscopy and spectroscopy (DFOMS).[14, 25-27] We have demonstrated that we can use superior size-dependent LSPR and photostable single Ag NPs as optical probes to study the size-dependent efflux kinetics of multidrug membrane transporters in single live cells in real time.[9, 13-14, 28-29] In the previous studies, we have used bare Ag NPs and surface modified Ag NPs to study the dependence of transport kinetics and the accumulation of substrates on the sizes, charges, chemicals, and bacterial strains of Gram-positive bacteria (BmrA in *Bacillus subtilis*)[9, 13, 29-30] and Gram-negative bacteria (MexAB-OprM in *Pseudomonas aeruginosa*).[14, 31-33]

In this study, we explored substrate-dependent accumulation and efflux function of single MsbA membrane transporters in single live *E. coli* cells using size-dependent LSPR (color) AgMUNH-Oflx NPs with a diameter of 92.6 ± 4.4 nm containing 6.5 x 10^5 Oflx molecules/NP and AgMUNH$_2$ NPs (control NPs without Oflx). We previously reported substrate-dependent efflux function of MsbA using the small and medium sized AgMUNH-Oflx NPs (2.4 ± 0.7 and 13.0 ± 3.1 nm). Therefore, this study offers a possibility to compare efflux kinetics of MsbA membrane transporters interacting to different sized antibiotic optical probes to investigate whether types and sizes of substrates play an important role in the selective extrusion of efflux pumps. To our knowledge, systematic studies of the dependence of the accumulation rates of substrates and efflux function of MsbA membrane transporters on the sizes of antibiotic nanocarrier optical probes in single live cells have not yet been reported.

RESULTS AND DISCUSSION

Study of Efflux Kinetics of Membrane Transporters using Single Antibiotic Drug Nanocarriers Optical Probes

We used the distinctive LSPR spectra (color) of single 92.6 ± 4.4 nm AgMUNH-Oflx NPs and AgMUNH$_2$ NPs to probe efflux kinetics of MsbA multidrug membrane transporters. These distinctive properties allow us to distinguish the NPs from the cell membrane and other debris which do not process plasmonic properties and appear white under dark-field illumination. We suspended the cells in a PBS buffer (0.5 mM phosphate buffer saline with 1.5 mM, pH = 7.0), but not cell culture medium. The studies of efflux function of membrane transporters in bacterial cells have been conducted in the PBS buffer to maintain cell concentration and cellular growth stage over time making results comparable to other experiments. [9, 13-14, 29-33] We incubated the cells (OD$_{600\text{ nm}}$ = 0.7) with the AgMUNH-Oflx NPs or AgMUNH$_2$ NPs and tracked single NPs in and out of single live cells in real time using DFOMS. Representative dark-field optical images of the single live cells (MsbA, WT) that were incubated with 3.7 pM solution of AgMUNH-Oflx NPs (Figure 27A) and AgMUNH$_2$ NPs (Figure 28A) show cross-sections of single rod-shaped bacterial cells with 2 µm in length and 0.5 µm in

width. As explained previously, we can image the thin-layer section of single cells with single NPs using DFOMS since the membranes of single live cells above and below the focal plane (190 nm depth of field) are invisible under dark-field illumination. Thus, NPs on top or below membranes of the cells are out of the focal plane and do not appear under dark-field illumination.

The scattering intensity of single NPs was used to identify whether they are intracellular NPs or extracellular NPs. The intracellular NPs look blurry, dimmer, and exhibit lower scattering intensity. The cell membrane absorbs photons from the dark-field illumination that penetrates through the cells to radiate intracellular NPs, reducing the scattering intensity that can pass through the cells to reach a detector. In contrast, the extracellular NPs show higher scattering intensity because they include scattering intensity from both NPs and cell membrane. We have demonstrated the feasibility of using the distinctive properties and scattering intensity of NPs to distinguish intracellular NPs and extracellular NPs in the study efflux function of multidrug membrane transporters in single live cells in real time. [9, 13-14, 29-33] Moreover, single Ag NPs show superior photo-stability over fluorescence dyes, allowing us to probe efflux function of multidrug membrane transporters using AgMUNH-Oflx NPs and AgMUNH$_2$ NPs over time. We used this validated approach to determine the intracellular AgMUNH-Oflx NPs (Figure 27B: a) and AgMUNH$_2$ NPs (Figure 28B: a) which are blurry, dimmer and exhibit a lower scattering intensity than the extracellular AgMUNH-Oflx NPs (Figure 27B: b) and AgMUNH$_2$ NPs (Figure 28B: b), respectively. As mentioned in our previous studies, [9, 13-14, 29-33] we use their LSPR spectra (color) to characterize the size and determine the number of single NPs in real time as they are incubated with the cells and transport in and out across the cell membrane over time. The representative LSPR spectra of single AgMUNH-Oflx NPs (Figure 27C) and AgMUNH$_2$ NPs (Figure 28C) show the peak wavelength and full width at half maxima (FWHM) at 641 (172) and 629 (215) nm, respectively. Taken together, we have successfully used plasmonic features of AgMUNH-Oflx NPs and AgMUNH$_2$ NPs to characterize single NPs, determine their numbers, and monitor them *in situ* in real time as they transport in and out across the cellular membrane over time.
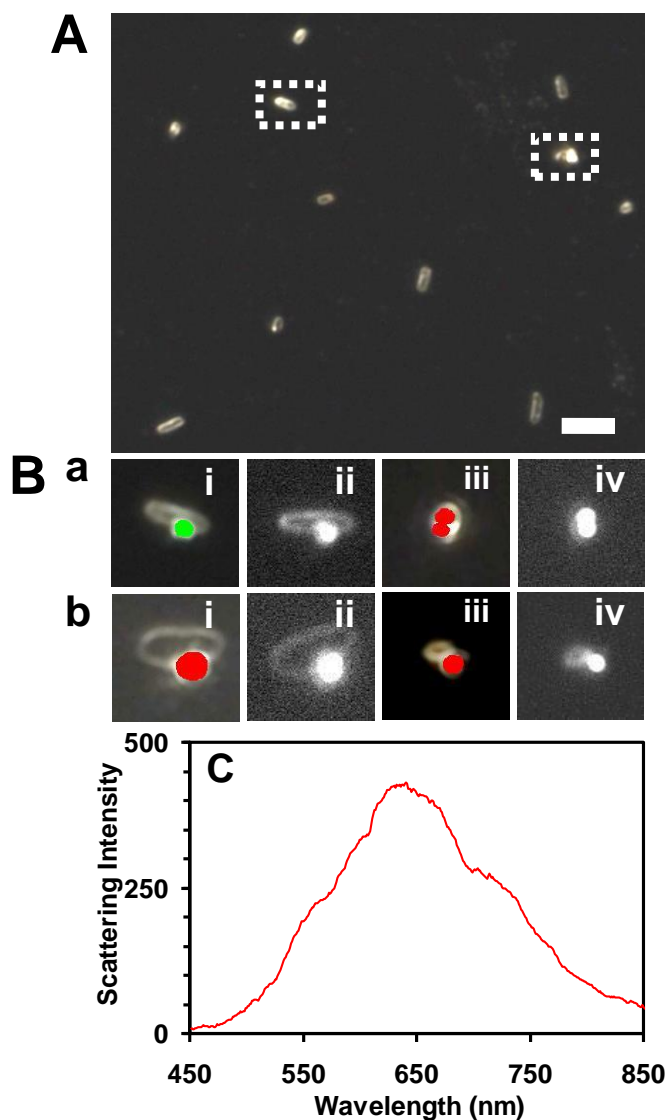
Figure 27. Imaging of single intracellular and extracellular 92.6 ± 4.4 nm AgMUNH-Oflx NPs in single living *E. coli* cells using DFOMS.

(A) The representative optical image of bacterial cells incubated with 3.7 pM AgMUNH-Oflx NPs showing intracellular and extracellular NPs as squared. (B) Zoom in optical color (i and iii) and CCD (ii and iv) images of single cells show (a) intracellular and (b) extracellular NPs which are pseudo colored in color images. The scale bar in A and B are 10 and 2 μm, respectively. (C) LSPR spectra of representative single 90nm AgMUNH-Oflx NPs show peak wavelengths and full width at half maxima (FWHM) at 641 (172) nm.
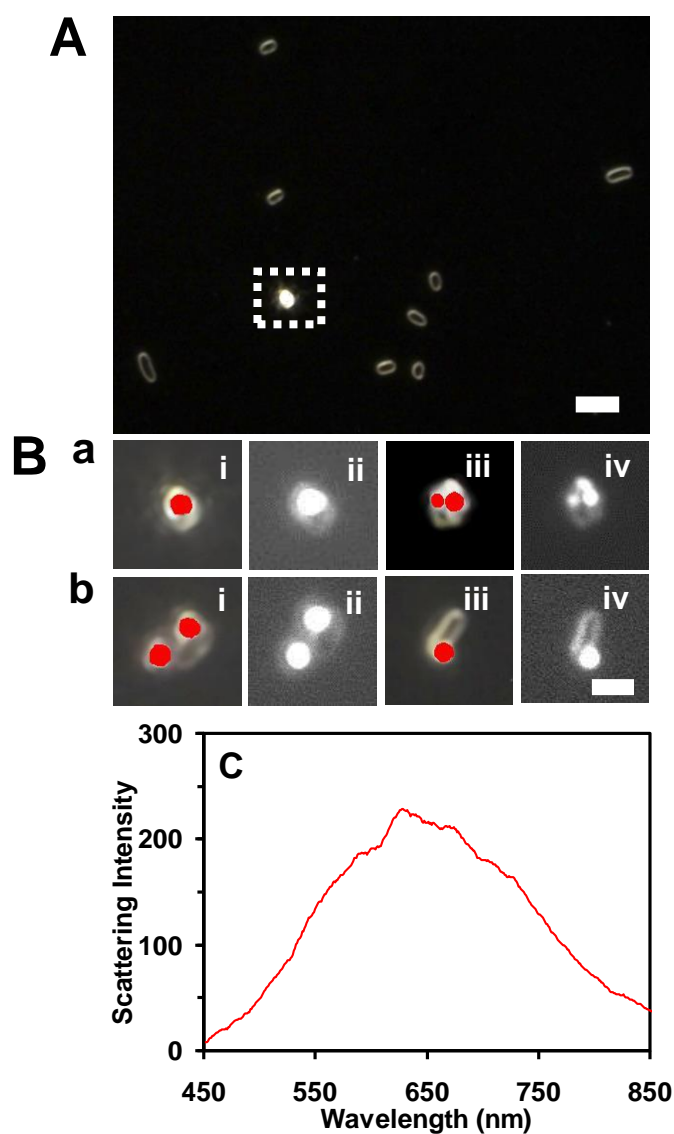
Figure 28. Imaging of single intracellular and 92.6 ± 4.4 nm AgMUNH$_2$ NPs in single living *E. coli* cells using DFOMS.

(A) The representative optical image of bacterial cells incubated with 3.7 pM AgMUNH$_2$ NPs showing intracellular NPs as squared. (B) Zoom optical color (i and iii) and CCD (ii and iv) images of single cells show (a) intracellular and (b) extracellular NPs which are pseudo colored in color images. The scale bar in A and B are 10 and 2 µm, respectively. (C) LSPR spectra of representative single 90nm AgMUNH$_2$ NPs show peak wavelengths and full width at half maxima (FWHM) at 629 (215) nm.

Study of the Dependence of Efflux Function of MsbA Membrane Transporters on the Pump Inhibitor

To study whether the membrane transporter (MsbA) is indeed responsible for the efflux out of the drug nanocarriers out of living cells, we studied the accumulation rates of the AgMUNH-Oflx NPs and AgMUNH$_2$ NPs in live *E. coli* (MsbA, WT) cells in the presence and absence of a pump (ATPase) inhibitor, orthovanadate (Na$_3$VO$_4$). The inhibitor interferes with ATP hydrolysis which is the important step of the MsbA (ABC) membrane transporters to extrude substrates out of the cells.[40, 83] Moreover, prokaryotes (bacterial cells) do not have endocytosis, pinocytosis and exocytosis so these processes are not involved in the transport of the NPs through cellular membranes. The results in Figure 29A, B: b and Table 5 show that the cells accumulate NPs over time. The accumulation rates of intracellular AgMUNH-Oflx NPs and AgMUNH$_2$ NPs during their incubation with 3.7 pM NPs over 41.5 min are 0.48 and 1.31 NPs/min, respectively. We further studied effects of the pump inhibitor on cellular efflux function and determine whether MsbA is responsible for the extrusion of NPs by incubating the cells with 3.7 pM NPs and orthovanadate (25 µM). The results in Figure 29A, B: a and Table 5 demonstrate that the accumulation rates of intracellular AgMUNH-Oflx NPs and AgMUNH$_2$ NPs is more rapidly in the presence of orthovanadate which the accumulation rate of intracellular NPs during their incubation with 3.7 pM NPs over 41.5 min increase from 0.48 to 1.10 and 1.31 to 2.21 NPs/min, respectively. Orthovanadate hindered efflux function of MsbA leading to a significant increasing of the number of intracellular NPs ($p < 0.005$).

The antibiotic nanocarrier optical probes used here are order of magnitude larger than the conventional antibiotic. However, the accumulation rates of the NPs shown in Figure 29 are very similar to those observed using a fluorescence probe (Hoechst 33342),[35] suggesting that the large sizes of NPs and conjugated Oflx did not disrupt their transport into the cells and their extrusion by the pumps. Thus, we can study the size-dependent transport kinetics of multidrug efflux pumps of single live cells in real time at a nanometer resolution using antibiotic drug nanocarrier optical probes.
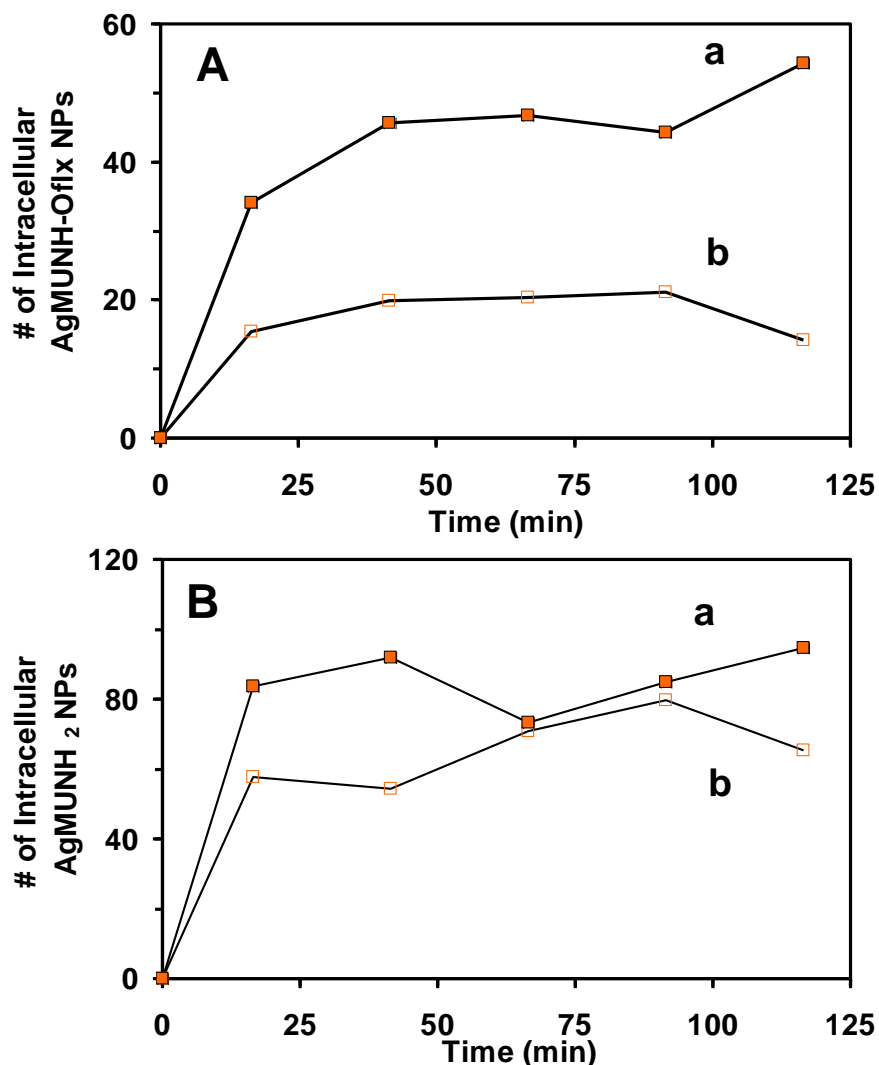
Figure 29. Study of effects of a pump (ATPase) inhibitor, orthovanadate on the accumulations of single 92.6 ± 4.4 nm AgMUNH-Oflx NPs and AgMUNH$_2$ NPs.

(A) Plots of number of intracellular AgMUNH-Oflx (A) and AgMUNH$_2$ (B) over time in the presence (a, solid) and absence (b, empty) of the inhibitor (25 μM). The points represent the experimental measurements and the lines are added to guide the trend. At each time point (25 min), 900 cells were analyzed. In (A) and (B), the number of intracellular NPs in (a) with the presence and (b) absence of orthovanadate are significantly different (p<0.0005) at 95% confidential interval, showing the dependence of efflux function of MsbA on the pump inhibitor.

Table 5. Summary of Accumulation Rates and Number of Intracellular Single 92.6 ± 4.4 nm NPs in Single Living *E. coli* Cells.

Types of NPs	C $_{Ag\,NPs}$ (pM)	Inhibitor [a] (µM)	Accumulation rate (NPs min^{-1}) [b]	Numbers of intracellular NPs [c]
AgMUNH-Oflx	1.85	0	0.22	9
	3.7	0	0.48	20
	3.7	25	1.10	46
AgMUNH$_2$	1.85	0	0.61	26
	3.7	0	1.31	54
	3.7	25	2.21	92

[a] Orthovanadate;

[b] Accumulation rates (slopes of the plots) at the 41.5 min incubation;

[c] Numbers of intracellular NPs accumulated in 900 live cells at the 41.5 min incubation.

Probing of the Dependence of Accumulation of Intracellular Antibiotic Drug Nanocarriers on Their Concentrations

We further studied the dependence of accumulation and efflux rates of antibiotic drug nanocarriers (AgMUNH-Oflx NPs) and control nanocarriers (AgMUNH$_2$ NPs) upon their concentrations (1.85 and 3.7 pM), aiming to determine how they enter the cells and compare the mechanism with those observed in conventional antibiotics. The results in Figure 30 show that the number of intracellular AgMUNH-Oflx NPs (Figure 30A) and AgMUNH$_2$ NPs (Figure 30B) significantly depends on NP concentrations (p < 0.0005). We summarize quantitative accumulation rates and the number of intracellular NPs in living cells (Figure 29 and 30) in Table 5, which increase with the concentration of NPs, vice versa. The accumulation rates of single AgMUNH-Oflx NPs and AgMUNH$_2$ NPs increased 2.2 times as the concentration of NPs increases from 1.85 to 3.7 pM, suggesting that NPs enter the cells via passive diffusion in which the NPs are driven by the concentration gradient across the membrane.

Study of the Dependence of Efflux Function of Membrane Transporters on Type and Size of NP Substrates in Single Live Cells

We further studied the dependence of the accumulation rates of intracellular NPs upon their types and sizes aiming to examine cellular mechanisms by which the ABC membrane transporters could selectively extrude a wide variety of structurally unrelated substances. In this study, we found the numbers of intracellular AgMUNH$_2$ NPs is significantly higher than those of the AgMUNH-Oflx NPs in both 1.85 and 3.7 pM (p < 0.0005) and the cells accumulated intracellular AgMUNH$_2$ NPs 2.8 time more rapidly than those of AgMUNH-Oflx NPs (Figure 30 and Table 5). Moreover, we previously reported that the accumulation rates of bare Ag NPs with a diameter of 93 ± 13 nm in Gram-positive bacteria (BmrA in *Bacillus subtilis*)[29] and 91.0 ± 9.7 nm in Gram-negative bacteria (MexAB-OprM in *Pseudomonas aeruginosa*)[14] were 6.8 NPs/min within 10.5 min and 1.65 NPs/min within 32.5 min, respectively. In comparison, the cells extruded AgMUNH-Oflx NPs much more rapidly than AgMUNH$_2$ NPs and bare Ag NPs, respectively.
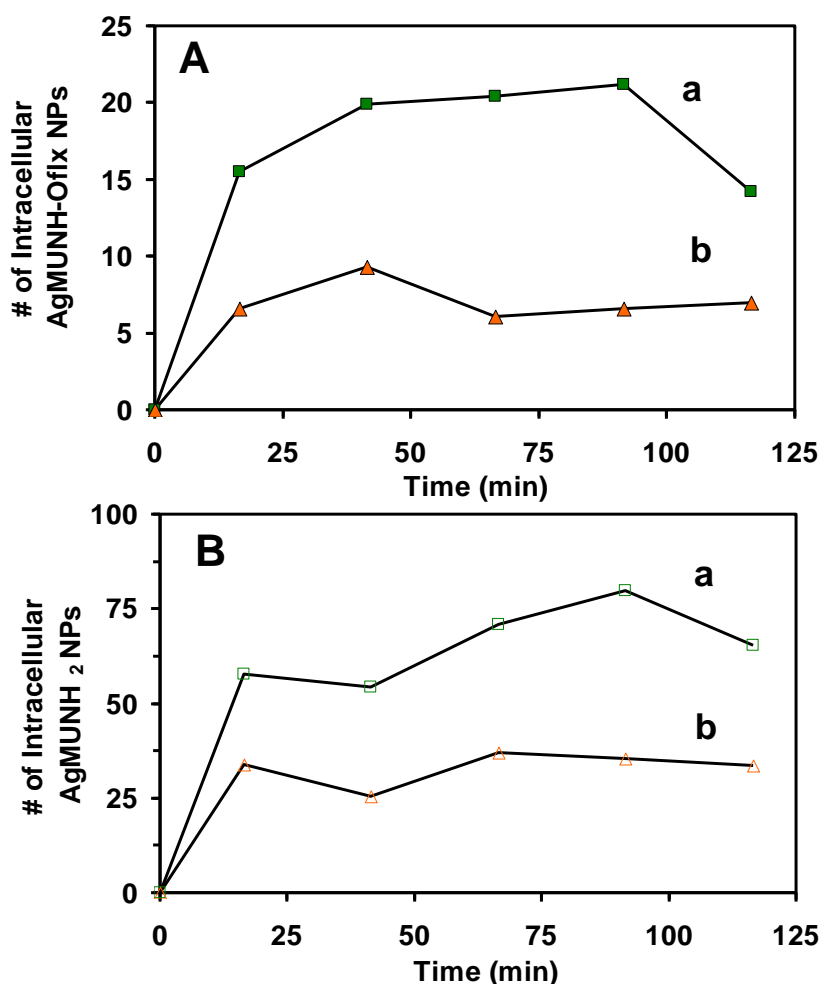
Figure 30. Study of the dependence of the accumulations of 92.6 ± 4.4 nm AgMUNH-Oflx NP and AgMUNH$_2$ NPs on NP concentrations in living *E. coli* cells.

(A) Plots of number of intracellular AgMUNH-Oflx NPs in MsbA incubated with 3.7 pM (a) and 1.85 pM (b) of the AgMUNH-Oflx NPs versus time. (B) Plots of number of intracellular Ag-MUNH$_2$ NPs in MsbA incubated with 3.7 pM (a) and 1.85 pM (b) of the AgMUNH$_2$ NPs versus time. The points represent the experimental measurements and the lines are added for trend projection. Note that 900 cells were analyzed at each point (every 25 min). In (A) and (B), data (a) and (b) are significantly different (p<0.0005) at 95% confidential interval, showing the dependence of accumulation of intracellular NPs on the NP concentration.

Interestingly, we have observed these phenomena in the studies of efflux function of MsbA membrane transporters using different sized antibiotic nanocarrier optical probes suggesting a strong dependence of efflux function on types of substrate which MsbA membrane transporters possibly be equipped with a sensing machinery for selectively detect and recognize noxious substrates (e.g., conjugated Oflx molecules) and then extrude them out of the cells.

Moreover, we compare the number of intracellular AgMUNH-Oflx NPs with a diameter of 92.6 ± 4.4 nm with those of 13.0 ± 3.1 and 2.4 ± 0.7 nm in the cells to study the size-dependent accumulation of single nanocarrier optical probes in single live cells. We found that the numbers of intracellular AgMUNH-Oflx NPs with a diameter of 2.4 ± 0.7 nm and 13.0 ± 3.1 nm are insignificantly different, and their accumulation rates of intracellular AgMUNH-Oflx NPs are 0.34 and 0.37 NPs/min, respectively. However, the accumulation rate of 92.6 ± 4.4 nm AgMUNH-Oflx NPs is 0.16 NPs/min and it is much lower than those of the smaller sized AgMUNH-Oflx NPs. These observations may be attributed to the low membrane permeability and the low concentration gradients across cell membrane of the largest nanocarriers (3.7 pM of 92.6 ± 4.4 nm nanocarriers versus 1.4 nM of 13.0 ± 3.1 and 2.4 ± 0.7 nm nanocarriers). We used the very low concentrations of 92.6 ± 4.4 nm nanocarriers in the study of efflux function because they are much more toxic than the other two smaller sized nanocarriers. As the accumulation rates of the nanocarriers increase with the concentration of NPs, we could have found a much higher number of intracellular 92.6 ± 4.4 nm drug nanocarriers if their concentrations are the same as the 13.0 ± 3.1 and 2.4 ± 0.7 nm drug nanocarriers (378 time higher). These results suggest size-dependent accumulation rates and efflux function of MsbA membrane transporters and the cells could not extrude the larger NPs out of single live cells as effectively as smaller NPs.

Characterization of the Viability of Single Cells

As reported previously, antibiotic drug nanocarriers with a diameter of 92.6 ± 4.4 nm inhibited bacterial growth in a dose-dependent manner.[46] It is important to study cellular viability as NPs could easily enter through disintegrated membrane of the dead

cells leading to inconclusive results. Therefore, we characterized the viability of the cells (MsbA WT) to ensure that the doses of the antibiotic drug nanocarriers (AgMUNH-Oflx NPs), the control nanocarriers (AgMUNH$_2$ NPs) and the pump inhibitor that we used to probe efflux function of *E. coli* did not kill cells and interfere with their pump function. At the end of each experiment, we characterized viability of the cells incubated with the antibiotic drug nanocarriers (AgMUNH-Oflx NPs) or the control nanocarriers (AgMUNH$_2$ NPs) throughout the duration of the experiment over 2 h using LIVE/DEAD *Bac*Light assay. We identify the live cells using the green SYTO9 fluorescence dye (λ_{max} = 520 nm) which penetrates to the cells and stains cellular nucleic acids while we detect the dead cells using red PI fluorescence dye (λ_{max} = 610 nm) which enter only the cells with disintegrated membrane.

Representative optical images of the cells incubated with 3.7 pM AgMUNH-Oflx NPs in the presence (Figure 31A: a) and absence (Figure 31B: a) of orthovanadate (25 µM) over 2 h show the cells with and without NPs. Their fluorescence images illustrate the green fluorescence but not the red fluorescence indicating that the cells are viable (Figure 31A, B: b). We determined percentage of live and dead cells by dividing the number of viable cells by the total number of cells. We found that more than 99 % of the cells incubated with 3.7 pM AgMUNH-Oflx NPs in the presence and absence of orthovanadate (25 µM) (Figure 31C) were viable. Similarly, representative optical images of the cells incubated with 3.7 pM AgMUNH$_2$ NPs in the presence (Figure 32A: a) and absence (Figure 32B: a) of orthovanadate (25 µM) over 2 h show the cells with and without NPs. The cells emitted green fluorescence but not red fluorescence suggesting that they were viable (Figure 32A, B: b). The results show that 99 % of the cells are alive (Figure 32C). As the cells with the NPs and orthovanadate are all alive, the accumulation rates of the NPs in single live cells are associated with NP passive diffusion and efflux function of the membrane transporters but not the compromised membrane integrity due to the cell death. The findings further demonstrate that the doses (1.85 and 3.7 pM) of the AgMUNH-Oflx NPs are suitable to use in study MDR and efflux function of multidrug membrane transporter using drug nanocarriers in *E. coli*.
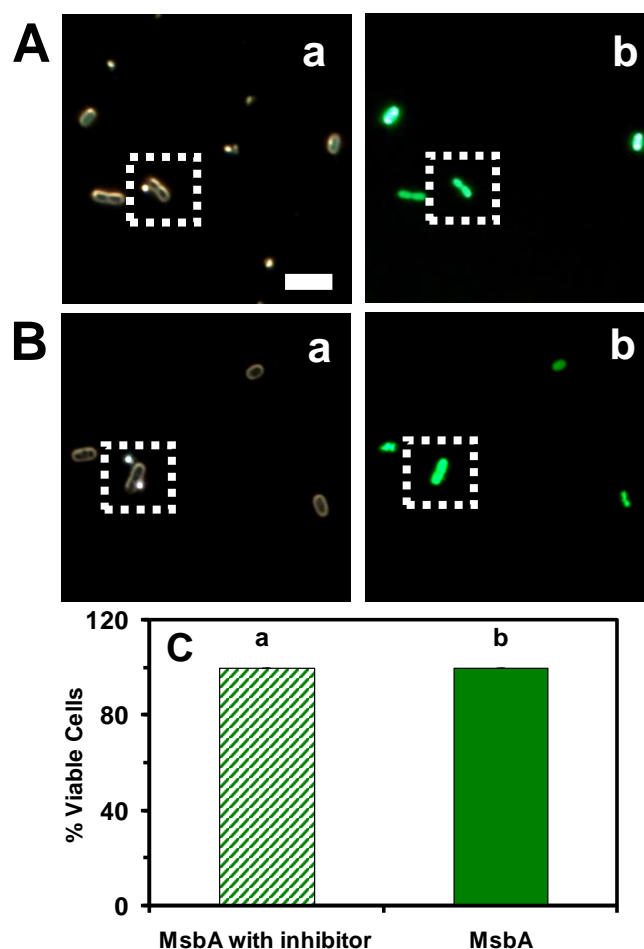
Figure 31. Characterization of viability of single bacterial cells incubated with 92.6 ± 4.4 nm AgMUNH-Oflx NPs using LIVE/DEAD *Bac*Light viability and counting assay.

In (A) and (B), representative dark field optical image (a) and fluorescence image (b) of single bacterial cells (MsbA), incubated with 3.7 pM Ag-MUNH$_2$-Oflx in the presence (A) and absence (B) of the inhibitor (25 µM) over the duration of each experiment for 2 h, show that the cells with NPs (as squared) or without NPs emit the green fluorescence (λ_{max} = 520 nm) of SYTO9, indicating that cells are viable. (C) Plots of percentage of viable cells (a) and dead cells (b) of MsbA incubated with 3.7 pM AgMUNH-Oflx with and without the inhibitor, indicate that 99-100% of the cells are alive. Minimum 300 cells were assayed and analyzed. The scale bar is 5 µm.
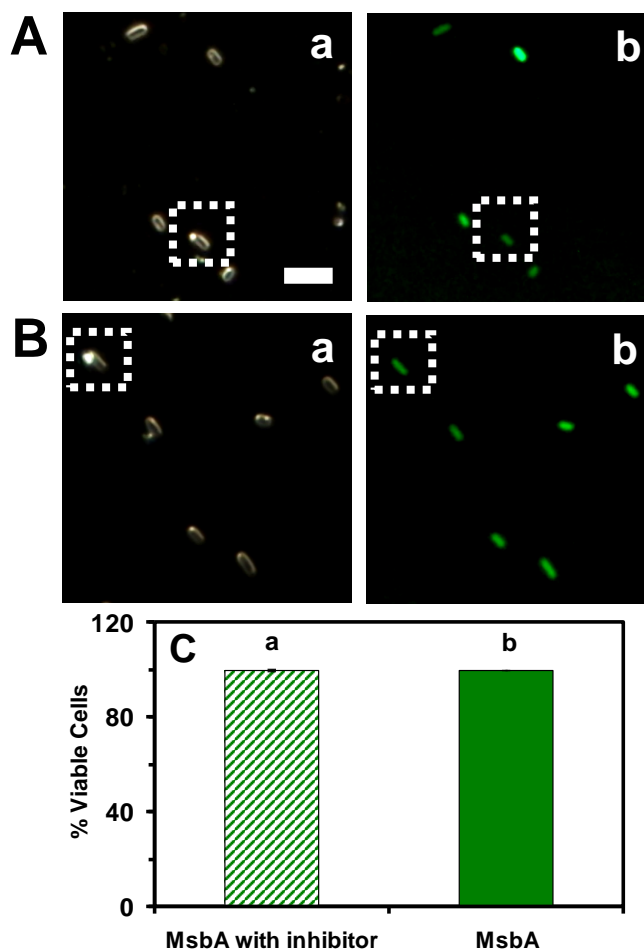
Figure 32. Characterization of viability of single bacterial cells incubated with 92.6 ± 4.4 nm AgMUNH₂ NPs using LIVE/DEAD *Bac*Light viability and counting assay.

In (A) and (B), representative dark field optical image (a) and fluorescence image (b) of single bacterial cells (MsbA), incubated with 3.7 pM AgMUNH₂ in the presence (A) and absence (B) of the inhibitor (25 µM) over the duration of each experiment for 2 h, show that the cells with NPs (as squared) or without NPs emit the green fluorescence (λ_{max} = 520 nm) of SYTO9, indicating that cells are viable. (C) Plots of percentage of viable cells (a) and dead cells (b) of MsbA incubated with 3.7 pM AgMUNH₂ with and without the inhibitor, indicate that 99-100% of the cells are alive. Minimum 300 cells were assayed and analyzed. The scale bar is 5 µm.

SUMMARY

We studied efflux kinetics of MsbA (ABC) membrane transporters in single live cells in real time using 92.6 ± 4.4 nm antibiotic drug nanocarrier optical probes (AgMUNH-Oflx NPs) containing 6.5 x10^5 Oflx molecules/NP. We found the accumulation rates of the AgMUNH-Oflx NPs and AgMUNH$_2$ NPs (control NPs without Oflx) increase with the concentration of NPs indicating that the passive diffusion driven by concentration gradients is the main mechanism for the NPs to transport into the cells, similar to conventional pump substrates (antibiotics). We found that the pump inhibitor (orthovanadate) affected the accumulation rates of intracellular AgMUNH-Oflx NPs and AgMUNH$_2$ NPs as the accumulation rates increased in the presence of orthovanadate. Notably, we observed that the numbers of intracellular AgMUNH$_2$ NPs are significantly higher than that of AgMUNH-Oflx NPs both in the presence and absence of orthovanadate, suggesting substrate-dependent efflux function of MsbA membrane transporters in which they could be equipped with a sensing machinery to selectively detect, recognize and extrude toxic substrates (e.g., antibiotics and chemotherapeutic agents). Notably, the accumulation rates and efflux kinetics of the AgMUNH-Oflx NPs show the dependence of NP's sizes which the accumulation rates of intracellular small- and medium-sized AgMUNH-Oflx NPs (2.4 ± 0.7 and 13.0 ± 3.1 nm) are higher than those of the large sized AgMUNH-Oflx NPs (92.6 ± 4.4 nm). These observations might be attributed to the higher membrane permeability and the higher concentration of the smaller nanocarriers. In summary, this study demonstrates that single AgMUNH-Oflx NPs and AgMUNH$_2$ NPs can serve as excellent optical probes for study of size- and substrate-dependent efflux function of MsbA (ABC) membrane transporters because of their distinctive size-dependent LSPR spectra and exhibit inhibitory effects in bacterial cells. Results from this study also suggest that multidrug membrane transporters could have a sensing machinery to screen for toxic substrates. Better understanding of molecular basis of efflux mechanisms will result in a feasibility of a better drug design that could potentially improve drug efficacy and avoid MDR in pathogenic bacterial cells, such as *E. coli*.

MATERIALS AND METHODS

Reagents and Cell Line

We purchased sodium chloride, sodium phosphate (Sigma-Aldrich), sodium phosphate monobasic monohydrate (Sigma-Aldrich), bacto-tryptone (Sigma-Aldrich), yeast extract (Sigma-Aldrich), orthovanadate (Sigma-Aldrich). We purchased Live/dead backlight viability assay (Life Technologies) and Hoechst 33342 (Life Technologies). We used all reagents as received. We used the nanopure deionized (DI) water (18 MΩ water, Barnstead) to rinse glassware and prepare all solutions including standard LB medium (1% tryptone peptone, 0.5% yeast extract, and 0.5% NaCl, pH = 7.2). We purchased cell line of *Escherichia coli*, wt w3110 (MsbA) from Coli Genetic Stock Center (CGSC).

Cell Culture and Preparation

We pre-cultured *E. coli* (MsbA) strain cells in an Erlenmeyer flask containing 10 mL of L-Broth (LB) medium (1% tryptone peptone, 0.5% yeast extract, and 0.5% NaCl, pH = 7.2) in an incubated floor shaker (Thermo Scientific, MaxQ5000; 160 rpm, 37 °C). After 12 h incubation, we inoculated 3 mL of pre-cultured cells into 10 mL of the LB medium in an Erlenmeyer flask. We then incubated the flask in the shaker (160 rpm, 37 °C) for another 8 h. We harvested the cultured cells using centrifugation (Beckman Model J2-21 Centrifuge, JA-14 rotor, at 7500 rpm, 23 °C, 10 min), washed the cells with the PBS buffer (0.5 mM phosphate buffer, 1.5 mM NaCl, pH 7.0) three times, and finally re-suspended the cells in the buffer. The final concentration of the cells was adjusted to $OD_{600\ nm}$ = 0.7 and used for the entire study.

Imaging of Single Intracellular and Extracellular NPs in Single Living Cells and Cellular Viability Characterization

The cell suspension ($OD_{600\ nm}$ = 0.7) containing 1.85 pM and 3.7 pM of AgMUNH-Oflx NPs and $AgMUNH_2$ NPs (control NPs without ofloxacin) in the presence and

absence of orthovanadate (25 µM) was prepared. The timer was simultaneously started to record the incubation time as NPs were added into the cell suspension. We sampled the mixture (1 µL) into a micro-chamber created by nail polish and imaged the cells on 18 representative locations using DFOMS equipped with a CCD camera and a digital color camera every 25 min (7 min for the slide preparation and 18 min for imaging) for 2 h and 5 min. Imaging of the transport of single nanocarriers moving in and out of single cells in real time using DFOMS allowed us to identify and locate positions of single NPs simultaneously.

The design and construction is fully explained in our previous studies.[9, 12-14, 25, 28-30, 42-43, 58-59, 61-62, 75, 78] In particularly, our dark-field optical microscope was equipped with a dark-field condenser (oil 1.43-1.20, Nikon), a 100x objective (Nikon Plan fluor 100x oil, iris SL N.A. 0.5-1.3, W.D.0.20 mm), a charge coupled device (CCD) camera (Micromax, Roper Scientific), a digital color camera (Handycam, Sony) and a multispectral imaging system (Nuance, Cambridge Research Inc.).[42-43] We have achieved high temporal resolution up to 5 ms to continuingly image of transport of single NPs in and out of single living cells.[9, 14] However, we acquired images in every 1 min as we found that the transport of single NPs in and out of single living cells was not a rapid process.[9, 14] Thus, a temporal resolution of minutes was sufficient to study transport of single NPs in real time.

We prepared a fresh micro-chamber every 25 min and imaged single cells for 18 representative locations. This approach allowed us to study transport of single NPs in massive numbers of cells (1500 cells) for each sample to make data adequate for probing the accumulation rates of bulk cells at a single cell resolution. We quantified intracellular NPs and plotted them versus incubation time and determined the accumulation rates (slopes of the plots) of single NPs in the cells over time.

Lastly, we characterized the viability of the cells at a single cell resolution using LIVE/DEAD *Bac*Light viability and counting assay at the end of each 2h-experiment. We imaged cells in the micro-chamber using dark-field optical microscopy and epi-fluorescence microscopy and counted the green fluorescence cells (peak wavelength of

fluorescence spectra of SYTO9, λ_{max} = 520 nm) and the red fluorescence cells (peak wavelength of fluorescence spectra of propidium iodide, λ_{max} = 610 nm) as live and dead cells, respectively.

Data Analysis and Statistics

Cells were imaged for eighteen representative locations of each cell suspension incubated with 1.85 pM and 3.7 pM NPs every 25 min over 2h and 5 min. Approximately fifteen cells were acquired in a single CCD image simultaneously. Therefore, approximately 300 cells were imaged every 25 min and 1500 cells were studied over 2 h and 5 min for each measurement. We repeated each experiment three times. Thus, we studied 4500 cells for each sample allowing us to gain sufficient statistics to study efflux function of bulk cells at single cell resolution. We analyzed the numbers of intracellular NPs in 900 cells (300 cells per each measurement) at every 25 min and plotted them over time to determine the accumulation rates (slope of the plot) of intracellular NPs of both AgMUNH-Oflx NPs and AgMUNH$_2$ NPs for the cells in the absence and presence of orthovanadate (25 µM). We determined accumulation of intracellular NPs at 41.5 min incubation. We performed statistical analysis (2-sample t-test) using SPSS to compare means of intracellular NPs in the treated cells.

The viability of single cells was characterized at a minimum of 150 cells that were incubated with each type of NPs after each experiment (2 h). We repeated each measurement three times. Therefore, 450 cells were assayed for each sample.

CHAPTER VI

CONCLUSION

This dissertation presents our development of Ag NP-based antibiotic drug nanocarriers to serve as powerful drug delivery vehicles and as superior photostable drug nanocarrier optical probes, aiming to improve drug efficacy and to study efflux function of multidrug ABC membrane transporters in single live cells for a better understanding of the molecular basis of MDR mechanisms. We have studied and found size-dependent inhibitory effects of antibiotic drug nanocarriers against bacterial cells (e.g., *Escherichia coli*). We have studied efflux kinetics of multidrug ABC membrane transporters (MsbA) in single live *E. coli* cells using different sized antibiotic drug nanocarriers. A summary of significant findings in each chapter is described below.

As described in Chapter II, we synthesized and characterized three different sized antibiotic drug nanocarriers (AgMUNH-Oflx NPs) by functionalizing three different sized Ag NPs (2.4 ± 0.7, 13.0 ± 3.1, and 92.6 ± 4.4 nm) with a monolayer of AUT to prepare AgMUNH$_2$ NPs, followed by covalently conjugating the amine group of the AgMUNH$_2$ NPs with the carboxyl group of an antibiotic (ofloxacin, Oflx). We determined the amount of conjugated Oflx molecules on each single NP (the conjugation ratios) of 2.4 ± 0.7, 13.0 ± 3.1, and 92.6 ± 4.4 nm as 8.6×10^2, 9.4×10^3, and 6.5×10^5 molecules/NP, respectively. We studied the dependence of inhibitory effects of free Oflx and conjugated Oflx attached on the surface of the nanocarriers on the dose of Oflx and the size of nanocarriers in *E. coli*. We found that the inhibitory effects of Oflx significantly depend on the dose of Oflx and the size of nanocarriers. The largest nanocarriers (92.6 ± 4.4 nm) show the highest inhibitory effects with the lowest MIC$_{50}$ (0.026 ± 0.003 µM) of Oflx while the smallest nanocarriers (2.4 ± 0.7 nm) exhibit the lowest bactericidal inhibitory with the highest MIC$_{50}$ (0.314 ± 0.010 µM) of Oflx against *E. coli*. These results demonstrate that the same amount of Oflx generates a substantially higher bactericidal potency when it is carried and delivered by the larger nanocarriers. The findings suggest that the densely loaded Oflx molecules (multivalence) enhance their

binding affinity to the targets and the higher drug payload could raise local drug concentrations and their bactericidal effects. Thus, an optimal size of nanocarriers is required to create maximum inhibitory effects against pathogenic bacteria. Notably, the inhibitory effects of drug nanocarriers are dose dependence but not linearly proportional to their sizes indicating that an interplay among several factors, such as the multivalence effects, their intracellular distribution (pharmacodynamics) and the extrusion by multidrug membrane transporters could contribute to their inhibitory effects. Therefore, we further used these antibiotic drug nanocarriers to study efflux function of multidrug ABC (MsbA) membrane transporters in single live cells (*E. coli*), as presented in Chapter III – V.

In Chapter III, we used the smallest antibiotic drug nanocarriers (2.4 ± 0.7 nm AgMUNH-Oflx NPs) and the same sized control nanocarriers (AgMUNH$_2$ NPs) to probe efflux kinetics of ABC (MsbA) membrane transporters of single live *E coli* cells. We developed an imaging method including DFOMS which uses LSPR spectra of single AgMUNH-Oflx NPs and AgMUNH$_2$ NPs to identify and track transport of single NPs in and out of single live cells over time. We found a high dependence of the accumulation of intracellular AgMUNH-Oflx NPs and AgMUNH$_2$ NPs upon a presence of a pump (ATPase) inhibitor (25 µM orthovanadate) and the concentration of NPs (0.7 and 1.4 nM). These results suggest that the NPs are substrates of MsbA transporters and more likely enter the cells via passive diffusion, which are driven by concentration gradient across the cellular membrane similarly to fluorescence dye (Hoechst 33342) and conventional antibiotics. Interestingly, the accumulation of the AgMUNH$_2$ NPs is twice that of the AgMUNH-Oflx NPs in single live cells. These findings suggest substrate-dependent efflux kinetics of MsbA, showing that the efflux pumps can extrude noxious substrates (e.g., conjugated Oflx) more effectively and rapidly out of the cells than AgMUNH$_2$ NPs because the AgMUNH-Oflx NPs consist of conjugated Oflx which exhibits inhibitory effects while the AgMUNH$_2$ NPs are biocompatible to the cells as we reported in Chapter II. This provides an evidence that multidrug membrane transporters might have a sensing machinery to selectively detect, recognize toxic substances (e.g.,

antibiotics and anticancer drugs), and then extrude them out as cellular defense mechanisms.

Furthermore, in Chapter IV, we used slightly larger antibiotic drug nanocarriers (13.0 ± 3.1 nm AgMUNH-Oflx NPs) and the same sized control nanocarriers (AgMUNH$_2$ NPs) to probe efflux kinetics of ABC (MsbA) membrane transporters of single live *E coli* cells using DFOMS. We found that the accumulation rates and efflux kinetics depend on the concentration of NPs, suggesting that they most likely enter the cells through passive diffusion. Interestingly, we found that the pump inhibitor (orthovanadate) only caused an increasing of the accumulation rate of intracellular AgMUNH-Oflx NPs. The accumulation rates of intracellular AgMUNH$_2$ NPs in the presence and absence of orthovanadate are essentially the same (9 NPs/min) during the first 90 min incubation and much higher than those of the AgMUNH-Oflx NPs at any given time points. These results confirm the dependence of efflux function of MsbA membrane transporters on types of substrates, and that the efflux pumps can effectively extrude harmful substances, similarly to results previously reported in Chapter III. Moreover, we found that the efflux pumps might be able to extrude the smaller nanocarriers (2.4 ± 0.7 nm) more effectively than the larger nanocarriers (13.0 ± 3.1 nm) as the number of intracellular 2.4 ± 0.7 nm AgMUNH-Oflx NPs become significantly higher than those of 13.0 ± 3.1 nm AgMUNH-Oflx NPs when the efflux pumps were blocked by the inhibitor (p = 0.004).

Finally, as we described in Chapter V, we studied efflux kinetics of ABC (MsbA) membrane transporters of single live *E coli* cells using the largest antibiotic drug nanocarriers (92.6 ± 4.4 nm AgMUNH-Oflx NPs) and the same sized of blank control nanocarriers (AgMUNH$_2$ NPs). We found that the accumulation rates of intracellular NPs and efflux kinetics of MsbA membrane transporters depend on the concentration of NPs, suggesting that such large NPs could passively diffuse into the cells. Moreover, the pump inhibitor (orthovanadate) interrupt efflux function of MsbA membrane transporters leading to the increase of accumulation rates of intracellular AgMUNH-Oflx NPs and AgMUNH$_2$ NPs. Interestingly, similarly to the small drug nanocarriers (2.4 ± 0.7 and 13.0 ± 3.1 nm), we found that the accumulation rates of intracellular AgMUNH$_2$ NPs

in the presence and absence of orthovanadate are higher than those of the AgMUNH-Oflx NPs, emphasizing the dependence of the accumulation rates on the type of NPs. Notably, we found that the accumulation rates of the larger NPs (92.6 ± 4.4 nm) are slower than those of the smaller NPs (2.4 ± 0.7 nm and 13.0 ± 3.1 nm). These findings could be attributed to the low membrane permeability and much low concentration gradients of 92.6 ± 4.4 nm nanocarriers. As the accumulation rates of the nanocarriers increase with the concentration of NPs, we could have found a much higher number of intracellular 92.6 ± 4.4 nm drug nanocarriers if their concentrations are the same as the 13.0 ± 3.1 and 2.4 ± 0.7 nm drug nanocarriers (378 time higher). These results suggest size-dependent accumulation rates and efflux function of MsbA membrane transporters and the cells could not extrude the larger NPs out of single live cells as effectively as the smaller NPs.

Taken together, this dissertation demonstrated that Ag NPs can serve as not only powerful drug nanocarriers, but also photostable size-dependent optical imaging probes for the study of ABC (MsbA) transporters in single live cells (*E. coli*). Drug therapeutic effects increase substantially when they are delivered by the larger nanocarriers. We can study the efflux function of multidrug ABC membrane transporters using the drug nanocarriers as superior photostable plasmonic optical probes. We found that the smaller nanocarriers could be effectively extrude out of the cells by the ABC (MsbA) membrane transporters more effectively than the larger nanocarriers, and therefore, they are less toxic than the larger nanocarriers, making them well suited as excellent imaging probes. In contrast, the larger nanocarriers show higher potent inhibitory effects than the smaller nanocarriers, enabling them to server as powerful drug delivery vehicles. All these findings offer a possibility of designing antibiotic drug nanocarriers that could generate the most potent bactericidal effects and overcome MDR.

REFERENCES

1.   Reyes, C. L.; Ward, A.; Yu, J.; Chang, G., The structures of MsbA: Insight into ABC transporter-mediated multidrug efflux. *FEBS Letters* **2006,** *580*, 1042-1048.

2.   Ward, A.; Reyes, C. L.; Yu, J.; Roth, C. B.; Chang, G., Flexibility in the ABC transporter MsbA: Alternating access with a twist. *Proceedings of the National Academy of Sciences* **2007,** *104* , 19005-19010.

3.   Orelle, C. J., J. M., Structures and Transport Mechanisms of the ABC Efflux Pumps. In *Efflux-Mediated Antimicrobial Resistance in Bacteria*, Li, X. E., C. A.; Zgurskaya, H. I., Ed. Springer: Switzerland, 2016; pp 73-98.

4.   Nikaido, H.; Pagès, J.-M., Broad-specificity efflux pumps and their role in multidrug resistance of Gram-negative bacteria. *FEMS Microbiology Reviews* **2012,** *36* (2), 340-363.

5.   Chang, G., Multidrug resistance ABC transporters. *FEBS Lett* **2003,** *555*, 102-5.

6.   Chang, G.; Roth, C. B., Structure of MsbA from E. coli: a homolog of the multidrug resistance ATP binding cassette (ABC) transporters. *Science* **2001,** *293*, 1793-1800.

7.   Higgins CF, L. K., The ATP switch model for ABC transporters. *Nat. Struct. Mol. Biol.* **2004,** *11*, 918-926.

8.   Davidson, A. L.; Dassa, E.; Orelle, C.; Chen, J., Structure, Function, and Evolution of Bacterial ATP-Binding Cassette Systems. *Microbiology and Molecular Biology Reviews : MMBR* **2008,** *72*, 317-364.

9.   Lee, K. J.; Browning, L. M.; Huang, T.; Ding, F.; Nallathamby, P. D.; Xu, X.-H. N., Probing of multidrug ABC membrane transporters of single living cells using single plasmonic nanoparticle optical probes. *Anal. Bioanal. Chem.* **2010,** *397*, 3317-3328.

10.   Woebking, B.; Reuter, G.; Shilling, R. A.; Velamakanni, S.; Shahi, S.; Venter, H.; Balakrishnan, L.; van Veen, H. W., Drug-Lipid A Interactions on the *Escherichia coli* ABC Transporter MsbA. *Journal of Bacteriology* **2005,** *187*, 6363-6369.

11.   Kaur, H.; Lakatos-Karoly, A.; Vogel, R.; Nöll, A.; Tampé, R.; Glaubitz, C., Coupled ATPase-adenylate kinase activity in ABC transporters. *Nature Communications* **2016,** *7*, 13864.

12.   Xu, X.-H. N.; Brownlow, W. J.; Huang, S.; Chen, J., Real-time measurements of single membrane pump efficiency of single living pseudomonas aeruginosa cells using fluorescence microscopy and spectroscopy. *Biochem. Biophys. Res. Commun.* **2003,** *305*, 79-86.

13.   Browning, L. M.; Lee, K. J.; Cherukuri, P. K.; Huang, T.; Warren, S.; Xu, X.-H. N., Single nanoparticle plasmonic spectroscopy for study of charge-dependent efflux function of multidrug ABC transporters of single live *Bacillus subtilis* cells. *J. Phys. Chem. C* **2016,** *120*, 21007-21016.

14.   Nallathamby, P. D.; Lee, K. J.; Desai, T.; Xu, X.-H. N., Study of multidrug membrane transporters of single living pseudomonas aeruginosa cells using size-dependent plasmonic nanoparticle optical probes. *Biochemistry* **2010,** *49*, 5942-5953.

15.   Pelgrift, R. Y.; Friedman, A. J., Nanotechnology as a therapeutic tool to combat microbial resistance. *Advanced drug delivery reviews* **2013,** *65*, 1803-1815.

16.   Skwarecki, A. S.; Milewski, S.; Schielmann, M.; Milewska, M. J., Antimicrobial molecular nanocarrier-drug conjugates. *Nanomedicine* **2016,** *12*, 2215-2240.

17.   Austin, L. A.; Mackey, M. A.; Dreaden, E. C.; El-Sayed, M. A., The optical, photothermal, and facile surface chemical properties of gold and silver nanoparticles in biodiagnostics, therapy, and drug delivery. *Archives of toxicology* **2014,** *88*, 1391-1417.

18.   Gatoo, M. A.; Naseem, S.; Arfat, M. Y.; Mahmood Dar, A.; Qasim, K.; Zubair, S., Physicochemical Properties of Nanomaterials: Implication in Associated Toxic Manifestations. *BioMed Research International* **2014**, 8.

19.   Yu, X.; Trase, I.; Ren, M.; Duval, K.; Guo, X.; Chen, Z., Design of Nanoparticle-Based Carriers for Targeted Drug Delivery. *Journal of Nanomaterials* **2016**, 15.

20.   Siarheyeva, A.; Sharom, F. J., The ABC transporter MsbA interacts with lipid A and amphipathic drugs at different sites. *Biochem J* **2009,** *419*, 317-28.

21.   Mulder, A.; Huskens, J.; Reinhoudt, D. N., Multivalency in supramolecular chemistry and nanofabrication. *Organic & Biomolecular Chemistry* **2004,** *2* (23), 3409-3424.

22.   Vigderman, L.; Zubarev, E. R., Therapeutic platforms based on gold nanoparticles and their covalent conjugates with drug molecules. *Advanced Drug Delivery Reviews* **2013,** *65*, 663-676.

23.   Klar, T.; Perner, M.; Grosse, S.; von Plessen, G.; Spirkl, W.; Feldmann, J., Surface-plasmon resonances in single metallic nanoparticles. *Phys. Rev. Lett.* **1998,** *80*, 4249-4252.

24.   Kelly, K. L.; Coronado, E.; Zhao, L. L.; Schatz, G. C., The optical properties of metal nanoparticles: the influence of size, shape, and dielectric environment. *J. Phys. Chem. B* **2003,** *107*, 668–677.

25.   Nallathamby, P. D.; Huang, T.; Xu, X.-H. N., Design and characterization of optical nano rulers of single nanoparticles using optical microscopy and spectroscopy. *Nanoscale* **2010,** *2*, 1715-1722.

26.   Huang, T.; Nallathamby, P. D.; Gillet, D.; Xu, X.-H. N., Design and synthesis of single nanoparticle optical biosensors for imaging and characterization of single receptor molecules on single living cells. *Anal. Chem.* **2007,** *79*, 7708-7718.

27.   Nallathamby, P. D.; Lee, K. J.; Xu, X.-H. N., Design of stable and uniform single nanoparticle photonics for in vivo dynamics imaging of nanoenvironments of zebrafish embryonic fluids. *ACS Nano* **2008,** *2*, 1371-1380.

28.   Xu, X.-H. N.; Brownlow, W. J.; Kyriacou, S. V.; Wan, Q.; Viola, J. J., Real-time probing of membrane transport in living microbial cells using single nanoparticle optics and living cell imaging. *Biochemistry* **2004,** *43*, 10400-10413.

29.   Browning, L. M.; Lee, K. J.; Cherukuri, P. K.; Nallathamby, P. D.; Warren, S.; Jault, J.-M.; Xu, X.-H. N., Single nanoparticle plasmonic spectroscopy for study of efflux function of multidrug ABC membrane transporters of single live cells. *RSC Advances* **2016,** *6*, 36794-36802

30.   Ding, F.; Lee, K.; Vahedi-Faridi, A.; Huang, T.; Xu, X.-H. N., Design and probing of efflux function of EGFP fused ABC membrane transporters in live cells using fluorescence spectroscopy. *Anal. Bioanal. Chem.* **2011,** *400*, 223-235.

31.   Kyriacou, S. V.; Brownlow, W. J.; Xu, X. H. N., Using nanoparticle optics assay for direct observation of the function of antimicrobial agents in single live bacterial cells. *Biochemistry* **2004,** *43*, 140-147.

32.   Kyriacou, S. V.; Nowak, M. E.; Brownlow, W. J.; Xu, X.-H. N., Single live cell imaging for real-time monitoring of resistance mechanism in pseudomonas aeruginosa. *J. Biomed. Opt.* **2002,** *7*, 576-586.

33.   Ding, F.; Lee, K. J.; Vahedi-Faridi, A.; Yoneyama, H.; Osgood, C. J.; Xu, X. H. N., Design and study of the efflux function of the EGFP fused MexAB-OprM membrane

transporter in Pseudomonas aeruginosa using fluorescence spectroscopy. *Analyst* **2014,** *139*, 3088-3096.

34.   Songkiatisak, P.; Ding, F.; Cherukuri, P. K.; Xu, X.-H. N., Study of Size-dependent Inhibitory Effects of Drug Nanocarriers on *Escherichia coli.* **in preparation**.

35.   Songkiatisak, P.; Cherukuri, P. K.; Xu, X.-H. N., Single Antibiotic Nano-Optical Probes for Study of Substrate-Dependent Efflux Function of Multidrug ABC Membrane Transporters in Single Live *Escherichia coli* Cells **in preparation**.

36.   Songkiatisak, P.; Cherukuri, P. K.; Xu, X.-H. N., Study of Efflux Mechanisms of Multidrug ABC Membrane Transporters in Single Live *Escherichia coli* Cells Using Size-Dependent Plasmonic Antibiotic Nano-Optical Probes. **in preparation**.

37.   Songkiatisak, P.; Cherukuri, P. K.; Xu, X.-H. N., Study of Substrate- and Size-Dependent Efflux Function of Multidrug ABC Membrane Transporters in Single Live Escherichia coli Cells Using Antibiotic Nano-Optical Probes. **in preparation**.

38.   Flores-Mireles, A. L.; Walker, J. N.; Caparon, M.; Hultgren, S. J., Urinary tract infections: epidemiology, mechanisms of infection and treatment options. *Nature reviews. Microbiology* **2015,** *13*, 269-284.

39.   Olsvik, Ø.; Wasteson, Y.; Lund, A.; Hornes, E., Pathogenic Escherichia coli found in food. *International Journal of Food Microbiology* **1991,** *12*, 103-113.

40.   Doerrler, W. T.; Raetz, C. R., ATPase activity of the MsbA lipid flippase of Escherichia coli. *J Biol Chem* **2002,** *277*, 36697-705.

41.   Eckford, P. D.; Sharom, F. J., Functional characterization of Escherichia coli MsbA: interaction with nucleotides and substrates. *J Biol Chem* **2008,** *283*, 12840-50.

42.   Huang, T.; Browning, L. M.; Xu, X.-H. N., Far-field photostable optical nanoscopy (PHOTON) for real-time super-resolution single-molecular imaging of signaling pathways of single live cells. *Nanoscale* **2012,** *4*, 2797-2812.

43.   Huang, T.; Nallathamby, P. D.; Xu, X.-H. N., Photostable single-molecule nanoparticle optical biosensors for real-time sensing of single cytokine molecules and their binding reactions. *J. Am. Chem. Soc.* **2008,** *130*, 17095-17105.

44.   Huang, T.; Xu, X.-H. N., Synthesis and characterization of tunable rainbow colored silver nanoparticle solutions using single-nanoparticle plasmonic microscopy and spectroscopy. *J. Mater. Chem.* **2010,** *20*, 9867-9876

45.   Huang, T.; Xu, X.-H. N., Multicolored nanometer-resolution mapping of single protein-ligand binding complex using far-field photostable optical nanoscopy (PHOTON). *Nanoscale* **2011,** *3*, 3567-3572.

46.   Ding, F.; Songkiatisak, P.; Cherukuri, P. K.; Huang, T.; Xu, X.-H. N., Size-Dependent Inhibitory Effects of Antibiotic Drug Nanocarriers against *Pseudomonas aeruginosa. ACS Omega* **2018,** *3*, 1231-1243.

47.   Cosa, G.; Focsaneanu, K.-S.; McLean, J. R. N.; McNamee, J. P.; Scaiano, J. C., Photophysical properties of fluorescent DNA-dyes bound to single- and double-stranded DNA in aqueous buffered solution. *Photochemistry and Photobiology* **2001,** *73*, 585–599.

48.   Hochman, Y.; Carmeli, S.; Carmeli, C., Vanadate, a Transition State Inhibitor of Chloroplast CFI-ATPase. *J. Biol. Chem.* **1993,** *268*, 12373-1237.

49.   Urbatsch, I. L.; Tyndall, G. A.; Tombline, G.; Senior, A. E., P-glycoprotein catalytic mechanism: studies of the ADP-vanadate inhibited state. *J. Biol. Chem.* **2003,** *278*, 23171-23179.

50.   McCaffrey, C.; Bertasso, A.; Pace, J.; Georgopapadakou, N. H., Quinolone accumulation in Escherichia coli, Pseudomonas aeruginosa, and Staphylococcus aureus. *Antimicrobial Agents and Chemotherapy* **1992,** *36*, 1601-1605.

51.   Petri, W. A. J., Sulfonamides, trimethoprim-sulfamethoxazole, quinolones and agents for urinary tract infections. In *Goodman & Gilman's The phamacological basis of therapeutics*, 12 ed.; Brunton, L. L., Ed. The McGraw-Hill: 2011; pp 1463-1476.

52.   Vincent, S.; Glauner, B.; Gutmann, L., Lytic effect of two fluoroquinolones, ofloxacin and pefloxacin, on Escherichia coli W7 and its consequences on peptidoglycan composition. *Antimicrobial Agents and Chemotherapy* **1991,** *35*, 1381-1385.

53.   Piddock, L. J.; Walters, R. N.; Diver, J. M., Correlation of quinolone MIC and inhibition of DNA, RNA, and protein synthesis and induction of the SOS response in Escherichia coli. *Antimicrobial Agents and Chemotherapy* **1990,** *34*, 2331-2336.

54.   Dörr, T.; Lewis, K.; Vulić, M., SOS Response Induces Persistence to Fluoroquinolones in *Escherichia coli. PLOS Genetics* **2009,** *5*, e1000760.

55.   Horii, T.; Kobayashi, M.; Sato, K.; Ichiyama, S.; Ohta, M., An in-vitro study of carbapenem-induced morphological changes and endotoxin release in clinical isolates of gram-negative bacilli. *J Antimicrob Chemother* **1998,** *41*, 435-42.

56.   Mirelman, D.; Yashouv-Gan, Y.; Schwarz, U., Regulation of murein biosynthesis and septum formation in filamentous cells of Escherichia coli PAT 84. *Journal of Bacteriology* **1977,** *129*, 1593-1600.

57.   Huang, T.; Cai, W.; Elsayed-Ali, H. E.; Xu, X. H. N., High-throughput ultrasensitive characterization of chemical, structural and plasmonic properties of EBL-fabricated single silver nanoparticles. *Nanoscale* **2012,** *4*, 380 - 385.

58.   Lee, K. J.; Nallathamby, P. D.; Browning, L. M.; Osgood, C. J.; Xu, X.-H. N., In vivo imaging of transport and biocompatibility of single silver nanoparticles in early development of zebrafish embryos. *ACS Nano* **2007,** *1*, 133-143.

59.   Browning, L. M.; Lee, K. J.; Nallathamby, P. D.; Xu, X.-H. N., Silver nanoparticles incite size and dose-dependent developmental phenotypes and nanotoxicity in zebrafish embryos. *Chem. Res. Toxico.* **2013,** *26*, 1503-1513.

60.   Xu, X.-H. N.; Chen, J.; Jeffers, R. B.; Kyriacou, S. V., Direct measurement of sizes and dynamics of single living membrane transporters using nano-optics. *Nano Lett.* **2002,** *2*, 175-182.

61.   Browning, L. M.; Lee, K. J.; Huang, T.; Nallathamby, P. D.; Lowman, J.; Xu, X.-H. N., Random walk of single gold nanoparticles in zebrafish embryos leading to stochastic toxic effects on embryonic developments. *Nanoscale* **2009,** *1*, 138-152.

62.   Nallathamby, P. D.; Xu, X.-H. N., Study of cytotoxic and therapeutic effects of stable and purified silver nanoparticles on tumor cells. *Nanoscale* **2010,** *2*, 942-952.

63.   Berney, M.; Hammes, F.; Bosshard, F.; Weilenmann, H. U.; Egli, T., Assessment and Interpretation of Bacterial Viability By Using The LIVE/DEAD Baclight Kit In Combination With Flow Cytometry. *Appl. Environ. Microbiol.* **2007,** *73*, 3283-3290.

64.   Xu, X.-H. N.; Wan, Q.; Kyriacou, S. V.; Brownlow, W. J.; Nowak, M. E., Direct observation of substrate induction of resistance mechanism in Pseudomonas aeruginosa using single live cell imaging. *Biochem. Biophys. Res. Commun.* **2003,** *305*, 941-949.

65.   Reuter, G.; Janvilisri, T.; Venter, H.; Shahi, S.; Balakrishnan, L.; van Veen, H. W., The ATP Binding Cassette Multidrug Transporter LmrA and Lipid Transporter MsbA Have Overlapping Substrate Specificities. *Journal of Biological Chemistry* **2003,** *278*, 35193-35198.

66.   Chen, J.; Sharma, S.; Quiocho, F. A.; Davidson, A. L., Trapping the transition state of an ATP-binding cassette transporter: Evidence for a concerted mechanism of

maltose transport. *Proceedings of the National Academy of Sciences* **2001,** *98*, 1525-1530.

67.   Sharma, S.; Davidson, A. L., Vanadate-Induced Trapping of Nucleotides by Purified Maltose Transport Complex Requires ATP Hydrolysis. *Journal of Bacteriology* **2000,** *182*, 6570-6576.

68.   Fox, E.; Widemann, B. C.; Pastakia, D.; Chen, C. C.; Yang, S. X.; Cole, D.; Balis, F. M., Pharmacokinetic and pharmacodynamic study of tariquidar (XR9576), a P-glycoprotein inhibitor, in combination with doxorubicin, vinorelbine, or docetaxel in children and adolescents with refractory solid tumors. *Cancer Chemotherapy and Pharmacology* **2015,** *76*, 1273-1283.

69.   Chène, P., ATPases as drug targets: learning from their structure. *Nature Reviews Drug Discovery* **2002,** *1*, 665.

70.   Spadaccini, R.; Kaur, H.; Becker-Baldus, J.; Glaubitz, C., The effect of drug binding on specific sites in transmembrane helices 4 and 6 of the ABC exporter MsbA studied by DNP-enhanced solid-state NMR. *Biochimica et Biophysica Acta (BBA) - Biomembranes* **2017**.

71.   Gottesman, M. M.; Ambudkar, S. V.; Xia, D., Structure of a multidrug transporter. *Nat. Biotechnol.* **2009,** *27*, 546-547.

72.   Higgins, C. F., ABC transporters: physiology, structure and mechanism--an overview. *Res. Microbiol.* **2001,** *152*, 205-210.

73.   Dawson, R. J.; Locher, K. P., Structure of a bacterial multidrug ABC transporter. *Nature* **2006,** *443*, 180-185.

74.   Mie, G., Beiträg zur optik trüber medien, speziell kolloidaler metrallősungen. *Annu. Phys.* **1908,** *25*, 377-445.

75.   Xu, X.-H. N.; Song, Y.; Nallathamby, P. D., Probing Membrane Transport of Single Live Cells Using Single Molecule Detection and Single Nanoparticle Assay. In *New Frontiers in Ultrasensitive Bioanalysis: Advanced Analytical Chemistry Applications in Nanobiotechnology, Single Molecule Detection, and Single Cell Analysis*, Xu, X.-H. N., Ed. Wiley: New Jersey, 2007; pp 41-65.

76.   Lee, K. J.; Browning, L. M.; Nallathamby, P. D.; Xu, X. H. N., Study of charge-dependent transport and toxicity of peptide-functionalized silver nanoparticles using zebrafish embryos and single nanoparticle plasmonic spectroscopy. *Chem Res Toxicol.* **2013,** *26*, 904-917.

77.   Browning, L. M.; Lee, K. J.; Cherukuri, P. K.; Huang, T.; Songkiatisak, P.; Warren, S.; Xu, X.-H. N., Single gold nanoparticle plasmonic spectroscopy for study of chemical-dependent efflux function of single ABC transporters of single live Bacillus subtilis cells. *Analyst* **2018,** *143*, 1599-1608.

78.   Nallathamby, P. D. Design and synthesis of photostable nanoparticle probes for molecular imaging and sensing in life science. Old Dominion University, Norfolk, VA, 2010.

79.   Li, X. Z.; Plesiat, P.; Nikaido, H., The challenge of efflux-mediated antibiotic resistance in Gram-negative bacteria. *Clin. Microbiol. Rev.* **2015,** *28*, 337-418.

80.   Lee, K. J.; Browning, L. M.; Nallathamby, P. D.; Xu, X.-H. N., Silver nanoparticles induce developmental stage-specific embryonic phenotypes in zebrafish. *Nanoscale* **2013,** *5*, 11625-11636.

81.   Lee, K. J.; Nallathamby, P. D.; Browning, L. M.; Desai, T.; Cherukuri, P.; Xu, X.-H. N., Single nanoparticle spectroscopy for real-time in vivo quantitative analysis of transport and toxicity of single nanoparticles in single embryos. *Analyst* **2012,** *137*, 2973-2986

82.   Lee, K. J.; Browning, L. M.; Nallathamby, P. D.; Desai, T.; Cherukuri, P.; Xu, X.-H. N., In vivo quantitative study of size-dependent transport and toxicity of single silver nanoparticles using zebrafish embryos. *Chem. Res. Toxico.* **2012,** *25*, 1029-1046.

83.   Davidson, A. L.; Chen, J., ATP-binding cassette transporters in bacteria. *Annu. Rev. Biochem.* **2004,** *73*, 241-268.

84.   Higgins, C. F., Multiple molecular mechanisms for multidrug resistance transporters. *Nature* **2007,** *446*, 749.

APPENDIX

This dissertation follows the procedures and guidelines how to work safely and handle biohazard materials in the protocol number 16-009 approved by the Institutional Biosafety Committee. Personnel who works with biohazard materials such as bacteria and nanoparticles must wear cloth lab coats, disposable gloves and safety goggles. Appropriate personal clothing is required in all laboratories. Long pants and closed toed shoes are required. Hand washing facilities are provided in all labs and hand washing must be performed after handling bacterial cells and nanomaterials. All solutions are disposed of as hazardous waste following established guidelines of the Environmental Health and Safety Office. All personnel must complete all applicable CITI trainings and pass all the requirements.

VITA

Preeyaporn Songkiatisak

Dept. of Chemistry and Biochemistry
Alfriend Chemistry Building
Old Dominion University
Norfolk, VA 23529

Education

May, 2018: Ph.D. Biomedical Sciences, Old Dominion University, Norfolk, VA 23529

December, 2009: M.S. Sciences, James Madison University, Harrisonburg, VA 22807

March, 2002: B.S. Pharmaceutical Sciences, Chulalongkorn University, Thailand

Publications

1. Ding, F. [†]; **Songkiatisak, P.** [†]; Cherukuri, P. K. [†]; Huang, T.; Xu, X. N.*, "Size-Dependent Inhibitory Effects of Antibiotic Drug Nanocarriers against *Pseudomonas aeruginosa*", *ACS Omega* **2018,** *3* , 1231-1243 ([†] Equal first co-authorship).

2. Browning, L. M.; Lee, K. J.; Cherukuri, P. K.; Huang, T.; **Songkiatisak, P.**; Warren, S.; Xu, X. N.*, "Single Gold Nanoparticle Plasmonic Spectroscopy for Study of Chemical-Dependent Efflux Function of Single ABC Transporters of Single Live *Bacillus subtilis* Cells" *Analyst* **2018**.

Presentations

1. **Songkiatisak, P.**; Johnson, M.; Browning, L.; Cherukuri, P. K.; Xu, X. N.*, "*In Vivo* Study of Toxic Effects of Silver Ions on Embryonic Development", Pittcon, Chicago, 2014.

2. **Songkiatisak, P.**; Cherukuri, P. K.; Huang, T.; Xu, X. N.*, "Real-Time Imaging and Sensing of Single Cancer Stem Cells", ACS National Meeting and Expo, Washington DC, 2017.